Doctoral Thesis

Study on the Pharmacological Effects of Organogermanium Compound THGP on RIG-I-Mediated Viral Sensing and Viral Replication during Influenza a Virus Infection

（インフルエンザウイルス感染時における RIG-I を介したウイルス認識およびウイルス複製に対する有機ゲルマニウム化合物 THGP の薬理学的効果に関する研究）

Sunanda Baidya

Graduate School of Chemical Sciences and Engineering,

Institute for Genetic Medicine,

Division of Signaling in Cancer and Immunology,

Hokkaido University

December 2021

Acknowledgements

Firstly, I would like to express my gratitude to gracious, most powerful, creature of this heavenlier universe the Almighty God, without the blessing from whom we cannot think of breathing to learn and has kept me healthy, strong, and energetic to complete this hard but successful research work.

I would like to convey my profound gratitude to my honorable supervisor Professor Akinori Takaoka. I am extremely grateful to him for giving me the opportunity to participate in this great research area, and thanks for his inspiration, guidance, constructive criticism, great support, and kind suggestion throughout this research. For all this and more, I am deeply indebted to him. I thank him for believing in me. I am happy to learn from him so many things, not only his exceptional scientific knowledge but also his extraordinary human qualities of kindness, hearty, humour and understanding. Additionally, I would also like to thank my sub-advisers Professor Mutsumi Takagi and Professor Yota Murakami for their kind presence and constructive suggestions, which were essential for the accomplishment of my doctoral study.

I am very much thankful, grateful and indebted to Dr. Seiichi Sato for supporting me at every step of the way, showing me every step of the way and also teaching me how to do experiments and to improve my analytic power, interpretation skills, problem-solving and decision-making skills throughout the entire research study from celebrating every small research success, to consoling and encouraging me every single time and so on. I would like to express my deepest sense of gratitude to him for the great support not only on research but also my accommodation in Hokkaido. His take-the bull-by the horns approach to research and hard work will always be an inspiration for me. Thanks a lot also for the constructive comments during the writing of the thesis.

Thanks to all the collaboration partners of this work, T. Yamada Y. Nishimoto, N. Sakurai, H. Nonaka, K. Noguchi, M. Kido, S. Tadano, K. Ishikawa, K. Li, A. Okubo, Y. Orba, M. Sasaki, H. Sawa, H. Miyamoto, A. Takada, from Hokkaido University; Y. Shimada and T. Nakamura from Asai Germanium Research Institute Co., Ltd. Japan.

My sincere thanks also goes to H. Kida (Hokkaido University) for VSV; A. Takada (Hokkaido University) for FluV; T. Fujita (Kyoto University) for the luciferase reporter plasmid p-125Luc; Y. Kawaoka (University of Tokyo) for the plasmids for FluV polymerase; T. Seya.

(Hokkaido University) for pIRM-3HA-TRIF vector; and T. Kubota (National Institute of Infectious Diseases Tokyo) for pcDNA3.1(-)IRF-3/5D-FLAG vector.

I gratefully acknowledge the financial support provided by the Ministry of Education, Culture, Sports, Science and Technology (MEXT), Japan to pursue my doctoral endeavor.

Finally, I am highly grateful to my little son who had sacrificed a lot and gave me great support and encouragement at every step of my thesis work. Words cannot express my love and gratitude for my parents who given their all for their children. Their innumerable sacrifices, their selfless love and their keep interest in my success are what have gotten me to this point. I am also thankful to my brother for his support during my thesis work.

Abstract

During microbial infections, microbes-associated molecular patterns (MAMPs) are mainly recognized by pattern recognition receptors (PRRs), including transmembrane-type Toll-like receptors (e.g., TLR3 and TLR9) and cytoplasmic sensors, such as RIG-I (retinoic acid-inducible gene I), MDA5 (melanoma differentiation-associated protein 5) and cGAS (cyclic GMP-AMP synthetase) to trigger antiviral immune responses. In addition to the interactions, the recognition of viral nucleic acids by viral polymerase is a crucial event during viral replication. It has previously been reported that, a hydrolysate of Ge-132, 3-(trihydroxygermyl) propanoic acid (THGP) shows a modulatory effect on microbial infections, inflammation, and immune responses. However, the detailed mechanism by which THGP can modify these processes during viral infections remained unknown. The results of this study demonstrated that THGP can specifically downregulate type I interferon (IFN) production in response to stimulation with a cytosolic RNA sensor RIG-I ligand 5′-triphosphate RNA (3pRNA) but not double-stranded RNA, DNA or lipopolysaccharide, which are ligands for MDA5, cGAS and TLR-4 respectively. Consistently, treatment with THGP resulted in dose-dependent suppression of type I IFN induction upon infections with influenza virus (FluV) and vesicular stomatitis virus that are known to be mainly sensed by RIG-I but not EMCV, recognized by MDA5. Mechanistically, detailed molecular analyses displayed that, THGP directly binds to the 5′-triphosphate moiety of viral RNA and 3pRNA and competes with RIG-I-mediated recognition, resulting in decreased type I interferon production. Furthermore, it has been observed that, THGP can directly counteract replication of FluV but not EMCV, by inhibiting the interaction of viral polymerase with RNA genome. Moreover, THGP treatment restored the body weight loss and improved the survival rate of FluV-infected mice, whereas the treatment with THGP itself did not show any toxic effect on survival or the body-weight curves of uninfected mice. Finally, FluV nucleoprotein RNA levels were significantly reduced in the lung tissues of THGP-treated mice, as compared with untreated mice. These results suggest a possible therapeutic implication of THGP that shows direct antiviral action together with a suppressive activity of innate inflammation.

Acronyms and Abbreviations

5’-pppRNA/3pRNA	5′-triphosphorylated RNA
ATP	adenosine triphosphate
AIM	absent in melanoma
ALRs	AIM-like receptors
AGS	Aicardi-Goutieres syndrome
ARF	ADP-ribosylation factor
CARD	caspase recruitment domain
CDNs	cyclic dinucleotides
COPII	coat protein complex II
cGAMP	cyclic guanosine monophosphate-adenosine monophosphate
cGAS	cyclic GMP-AMP synthase
CLRs	C-type lectin receptors
cRNA	complementary RNA
cRNP	complementary ribonucleoprotein
CTT	C-terminal tail domain
CTL	cytotoxic T lymphocytes
DAI	DNA-dependent activator of interferon regulatory factor.
DCs	dendritic cells
DAMPs	damage-associated molecular patterns
DDX41	DEAD (Asp-Glu-Ala-Asp) Box Polypeptide 41
dsRNA/DNA	double-stranded RNA/DNA
DNA-PK	DNA-dependent protein kinase
EBOV	ebola virus
EBV	Epstein–Barr virus
ELISA	enzyme-linked immunosorbent assay
ER	endoplasmic reticulum
EMCV	encephalomyocarditis virus
FADD	FAS-associated death domain-containing protein
Ge	Germanium
HA	hemagglutinin
HCV	hepatitis C virus
HCMV	human cytomegalovirus

HPV	human papillomaviruses
HIV	human immunodeficiency virus
HT-DNA	herring testis DNA
hnRNPA2B1	heterogeneous nuclear ribonucleoprotein A2B1
HSV	herpes simplex virus
IAV	influenza A virus
IFI16	interferon, gamma-inducible protein 16
IFN	interferon
IKK	inhibitor-κB kinase
IL	interleukin
IRAK	interleukin-1 receptor-associated kinase
IRF	interferon-regulatory factor
ISGs	IFN stimulated genes
ISRE	IFN stimulated genes interferon-sensitive response element
IRES	internal ribosome entry site
JEV	Japanese encephalitis virus
JAK	janus tyrosine kinase
JNK	c-Jun N-terminal kinase
KSHV	Kaposi's sarcoma herpesvirus
LGP2	laboratory of genetics and physiology 2
LACV	La Crosse virus
LPS	lipopolysaccharide
LBD	ligand-binding domain
L-DOPA	L-3,4-Dihydroxyphenylalanine
M1	matrix 1
M2	matrix 2
mRNAs	messenger RNAs
MAPK	mitogen-activated protein kinase
MAVS	mitochondrial antiviral signaling protein
MDA5	melanoma differentiation associated protein-5
MYD88	myeloid differentiation primary-response protein 88 neutralizing antibody
NA	neuraminidase
NP	nucleoprotein

NSP1	non-structural protein 1
NS2	non-structural protein 2
NEP	nuclear export protein
NF-κB	nuclear factor- kappa-B
NK cells	natural killer cells
NLRs	NOD-like receptors
NDV	newcastle disease virus
NOD	nucleotide-binding oligomerization domain
NTase	nucleotidyltransferase
NTD	N-terminal domain
OAS	oligoadenylate synthetase
ORF	Open reading frame
PA	polymerase acidic protein
PB1	polymerase basic protein 1
PB2	polymerase basic protein 2
PAMPs	pathogen-associated molecular patterns
PBMCs	peripheral blood mononuclear cells
PI3K	phosphatidylinositol 3-kinase
PKR	protein kinase R
Pol III	RNA polymerase III
poly I:C	polyriboinosinic polyribocytidylic acid
PRRs	pattern recognition receptors
RBD	receptor-binding domain
RNase L	ribonuclease L
RIG-I	retinoic acid inducible gene 1
RIP	receptor-interacting protein
RHIM	RIP homotypic interaction motif
RIP assay	RNA-binding protein immunoprecipitation assay
RLRs	RIG-I-like receptors
RNAi	RNA interference
RdRp	RNA dependent RNA polymerase
RVFV	Rift Valley fever virus
RSV	respiratory syncytial virus
SeV	sendai virus

SARS-CoV-2	severe acute respiratory syndrome coronavirus 2
SFV	Semliki Forest virus
SLE	systemic lupus erythematosus
SKIV2L	super killer viralicidic activity 2
SNPs	Single nucleotide polymorphisms
SMS	Singleton-Merten syndrome
STIM1	stromal interaction molecule 1
STAT	signal transducers and activators of transcription
STING	stimulator of interferon genes protein
TAK1	transforming growth factor-*β*-activated protein kinase 1
TBK1	TANK-binding kinase 1
TIRAP	Toll/IL-1 receptor (TIR) domain containing adaptor protein
THGP	3-(trihydroxygermyl)propanoic acid
TLRs	Toll-like receptors
TRAM	TRIF-related adaptor molecule
TRIF	TIR domain-containing adapter protein inducing IFN-β
TRAF	tumor necrosis factor receptor-associated factors
TRADD	TNFR-associated death domain protein
THES	tricho-hepato-enteric syndrome
TTC37	tetratricopeptide repeat domain-containing protein 37
vRNPs	viral ribonucleoproteins
VSV	vesicular stomatitis virus
VACV	Vaccinia virus
WNV	west nile virus
WT	wild type

List of figures

List of tables

Table of contents

1. Introduction

1.1 Our Immune system

Our immune system is a complex network of cells and proteins that defends the body against microbial infections. The immune system keeps a memory of every microbe it has ever defeated in case of repeated infection, it can recognize and destroy the microbe quickly if it enters the body again [1]. This is achieved by an array of cells and molecules, distributed through-out the body. Most of the major immune cells derived from progenitors in the bone marrow and develop into mature cells through a series of changes [2, 3]. Many of the mature cells circulate in the bloodstream and are dispersed through-out tissues, while some also congregate in specialized lymphoid tissues.

Beyond, the structural and chemical barriers which protect us from infections, the immune system consitsts of two distinct parts, innate and adaptive immunity (Figure 1.1). Innate immunity constitutes the first line of defense to an intruding pathogen. It is an antigen-independent defense mechanism that is generated immediately or within hours of encountering an antigen [4]. This non specific response has no immunologic memory. Adaptive immunity, on the other hand, is an antigen-dependent immune response and therefore, responds in a slower but specific manner, with the generation of long-lived immunological memory [5]. Through, innate immunity is able to eradicate the pathogens efficiently, initial clearance of infection can fail due to the high number or virulence of invading pathogens. In these settings, adaptive immune mechanisms are in action, which permits specific recognition and elimination of the pathogen [6]. Although, the innate and adaptive immune systems are often considered as contrasting, they usually act together, with the innate response representing the first line of host defense, and with the adaptive response becoming dominent after several days. Components of the innate system contribute to the activation of antigen-specific cells and by recruiting innate effector mechanisms those cells amplify their responses to control invading microbes. Thus, while the mechanisms of actions of innate and adaptive immune responses are fundamentally different, synergy between them is crucial for an intact, fully effective immune response [7-9].

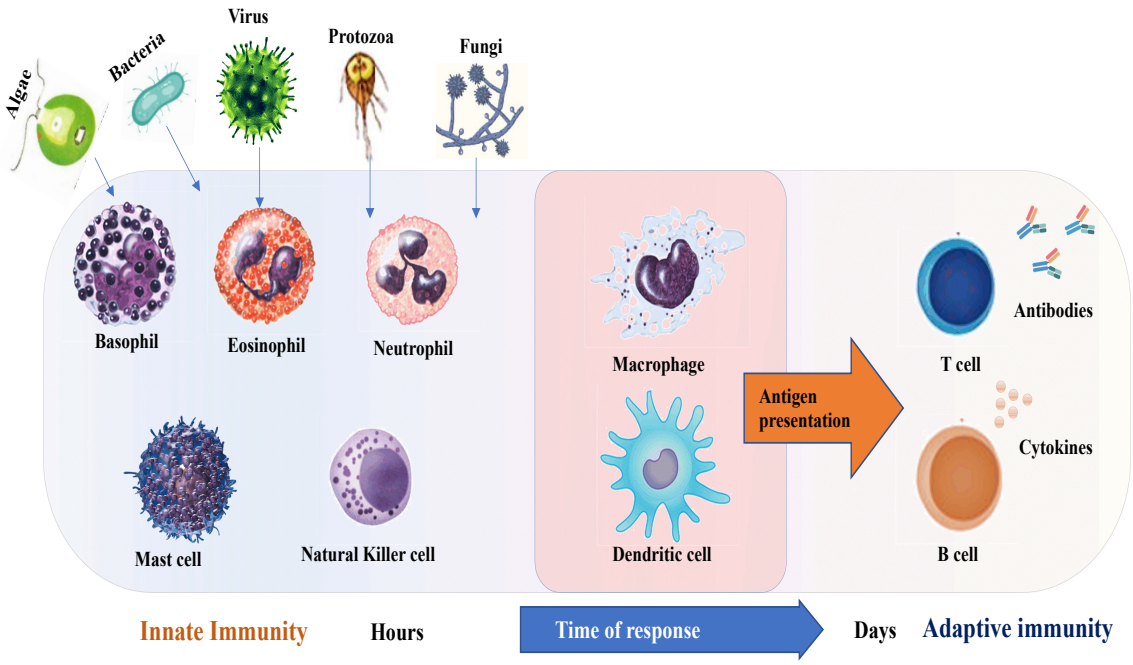

Figure 1.1 Innate and adaptive immunity. During the first hours and days of an infection, influx by pathogens induces activation of innate immune cells such as macrophages, monocytes, or NK-cells. These pathways strongly activate an inflammatory reaction and eliminate the pathogens. But when infection is not fully eliminated, pathogens are ingested and processed by antigen-presenting cells, followed by antigen presentation and stimulation of T- and B-lymphocytes. Innate and adaptive immunity are not mutually exclusive mechanisms of host defense, but rather are complementary, with defects in either system resulting in host vulnerability or inappropriate responses.

1.2 Pattarn Recognition Receptors (PRRs)

Innate immunity permits a limited range of immune cells to detect and respond rapidly to a wide range of pathogens that share common structures, known as pathogen-associated molecular patterns (PAMPs), which are recognized by germline encoded pattern recognition receptors (PRRs). PRRs are also capable of sensing endogenous molecules released from damaged cells, termed damage-associated molecular patterns (DAMPs) [10]. PRRs are proteins, which are expressed mainly by dendritic cells, macrophages, monocytes, neutrophils, and epithelial cells and also mediate the initiation of antigen-specific adaptive immune response and release of inflammatory cytokines [11, 12]. PRRs can be classified into membrane bound PRRs and cytoplasmic PRRs according to their localization in cells. Membrane-bound PRRs include Toll like receptors (TLRs) and C-type lectin receptors (CLRs), whereas

cytoplasmic PRRs include NLRs (nucleotide-binding oligomerization domain (NOD)-like receptors), ALRs (absent in melanoma (AIM)-like receptors), RLRs (retinoic acid inducible gene 1 (RIG-I)-like receptors) and a range of cytosolic nucleic acid sensors, including DAI (DNA-dependent activator of interferon regulatory factor), cGAS (Cyclic GMP-AMP synthase), DDX41 (DEAD (Asp-Glu-Ala-Asp) Box Polypeptide 41), etc. (Figure 1.2) [13].

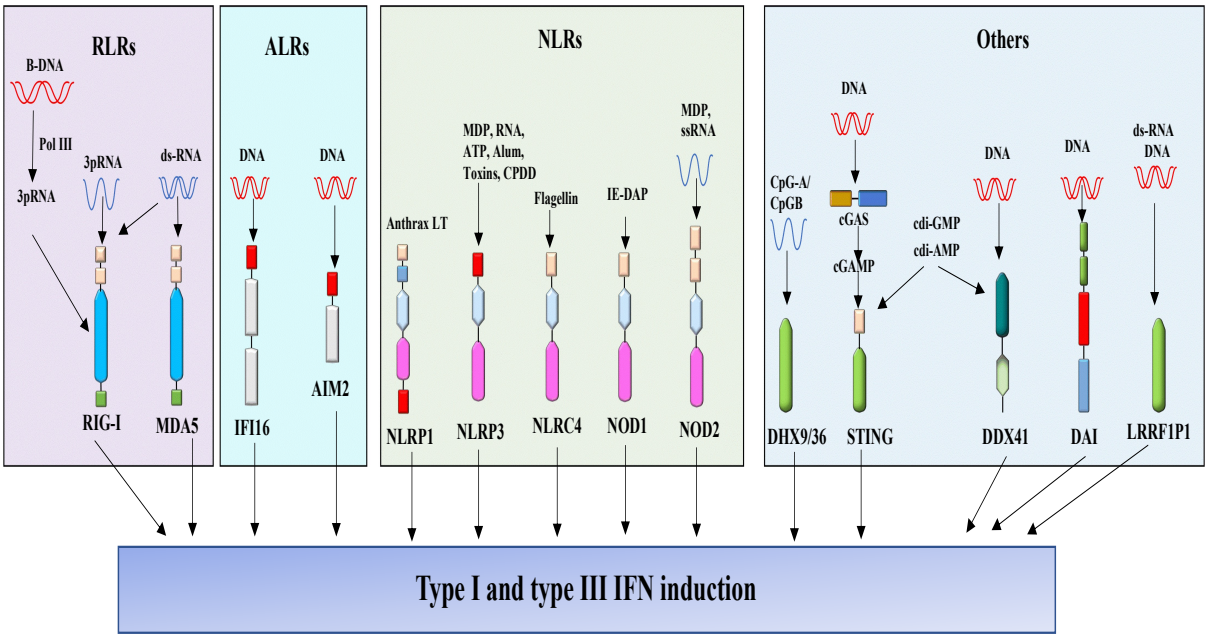

Figure 1.2 Cytoplasmic pattern recognition receptors. RLRs family members RIG-I and MDA5 recognize ssRNA and dsRNA and ALRs family members IFI16 and AIM2 detect cytosolic DNA. NLRs family members detect different types of PAMPs from bacteria or virus. Other sensors like DAI and cGAS identify cytosolic DNA, LRRFIP1 detects both cytosolic dsDNA and dsRNA, DDX41 detects CDNs or B-form DNA. All the sensors lead to the activation of IFN signaling.

Pathogen-associated molecular patterns (PAMPs) that are sensed by PRRs include bacterial carbohydrates (such as lipopolysaccharide or LPS, mannose), nucleic acids (such as bacterial or viral DNA or RNA), bacterial peptides (flagellin, microtubule elongation factors), peptidoglycans and lipoteichoic acids (from Gram-positive bacteria), N-formylmethionine, lipoproteins and fungal glucans and chitin [14]. A list of different PRRs and their ligands is appear in Table 1.1.

Table 1.1 PRRs and Their Ligands

PRRs	Localization in Cell	Ligand
TLR		
TLR1	Plasma membrane	Triacyl lipoprotein
TLR2	Plasma membrane	Lipoprotein
TLR3	Endolysosome	dsRNA
TLR4	Plasma membrane	LPS
TLR5	Plasma membrane	Flagellin
TLR6	Plasma membrane	Diacyl lipoprotein
TLR7 (human TLR8)	Endolysosome	ssRNA
TLR9	Endolysosome	CpG-DNA
TLR10	Endolysosome	Unknown
TLR11	Plasma membrane	Profilin-like molecule
RLR		
RIG-I	Cytoplasm	Short dsRNA, 5′-triphosphate dsRNA
MDA5	Cytoplasm	Long dsRNA
ALR		
IFI16	Cytoplasm	DNA
AIM2	Cytoplasm	DNA
NLR		
NOD1	Cytoplasm	iE-DAP
NOD2	Cytoplasm	MDP
CLR		
Dectin-1	Plasma membrane	β-Glucan
Dectin-2	Plasma membrane	β-Glucan
MINCLE	Plasma membrane	SAP130
MR	Plasma membrane	mannose
DC-SIGN	Plasma membrane	Mannose, fucose

1.3 Immune signaling by RIG-I-like receptors

The RIG-I-like receptor (RLR) family members include retinoic acid-inducible gene I (RIG-I), melanoma differentiation-associated gene 5 (MDA5), and laboratory of Genetics and Physiology 2 (LGP2) [15]. Both RIG I and MDA5 contain two N-terminal caspase recruitment domains (CARDs) but LGP2 lacks one CARD domain, a central DEAD box helicase domain with ATPase activity, and a C-terminal regulatory domain. RLRs are localized in the cytoplasm and detect the genomic RNA of dsRNA viruses and dsRNA generated as the replication intermediate of ssRNA viruses. Researchers have found that RIG-I and MAD5 can recognize many different kinds of virus for example, RIG-I can recognize viruses including Paramyxoviridae, such as newcastle disease virus (NDV); sendai virus (SeV); vesicular stomatitis virus (VSV); rabies virus; influenza virus (IAV); Japanese encephalitis virus (JEV); Flaviviridae, such as hepatitis virus. In contrast, MDA5 primarily recognizes picornavirus families such as encephalomyocarditis virus (EMCV); and coronaviruses such as murine hepatitis virus. Moreover, both RIG-I and MDA5 recognize dengue virus, new Nile virus, and reovirus [16]. The production of type I IFNs is positively regulated by LPG2 in response to RNA viruses recognized by both RIG-I and MDA5 [17]. RIG-I recognizes relatively short

dsRNA (up to 1 kb), It has been found that 5′ triphosphate ssRNA synthesized by in vitro transcription is a RIG-I ligand [18, 19]. A minimum length of 19-mer or 21-mer dsRNA with a 5′ triphosphate end is required for the activation of RIG-I as chemically synthesized 5′ triphosphate ssRNA failed to induce RIG-I. MDA5 detects long dsRNA (more than 2 kb) such as poly I:C, relative to RIG-I. CARDs domains of RLRs are madiators of triggering signaling cascades by interacting with the N-terminal CARD-containing adaptor mitochondrial antiviral signaling proteins (MAVS) (also known as IPS-1, CARDIF, or VISA) [20] (Figure 1.3). RLRs catalyze ATP via the DExD/H helicase domain, and the ATP hydrolysis involved conformational changes, which is essential for type I IFN induction [21-23]. This domain along with the adjacent C-terminal domain is required for RNA binding.

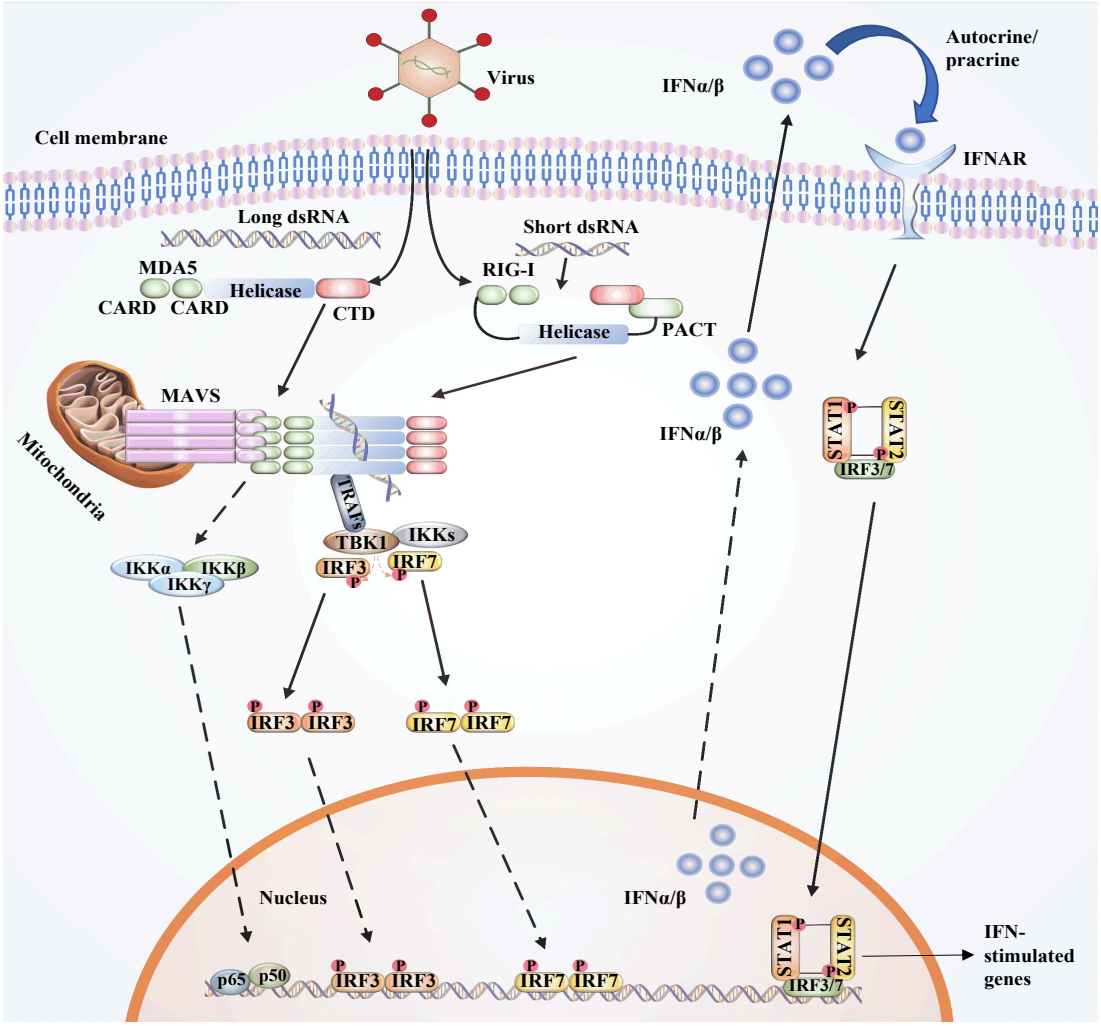

Figure 1.3 Virus detection and induction of antiviral signaling pathways by RIG-I-like receptors RLR. The recognition of PAMP by RIG-I and MDA5 causes them to activate and interact with MAVS. Activated MAVS then initiate a molecular cascade by transducing the

signal to the downstream TRAFs, TBK1 kinase and IKK complex, which is followed by the phosphorylation of the transcription factors IRF3 and IRF7. Phosphorylated p-IRF3 and p-IRF7 then transfer into the nucleus and bind to transcription factor binding sites of the IFNα and IFNβ genes to activate their transcriptions. Expression and exportation of these genes trigger the IFN1 signaling cascade in an autocrine or paracrine fashion to induce expression of hundreds of interferon stimulated genes (ISGs) and inflammatory genes to confer antiviral resistance. RIG-I and MDA5 also activate the NF-κB pathway to promote the production of pro-inflammatory factors and inflammatory chemokines.

During infections, upon binding to PAMP, the activated RIG-I and MDA5 oligomerize and interact with the MAVS, through CARD–CARD-mediated interactions [24], which forms a multilayered protein complex contain several different proteins [25] that mediate the bifurcation of signaling into two branches. One branch involves tumor necrosis factor receptor-associated factors (TRAF)-2/6 and the receptor-interacting protein 1 to subsequently activate the inhibitor of nuclear factor kappa-B kinase (IKK) complex, leading to NF-κB activation [26]. The other branch acts through TRAF3 and activates the serine/threonine-protein kinase 1 (TBK1), leading to the phosphorylation and dimerization of interferon regulatory factors (IRF)-3 and -7 [27]. Phosphorylated p-IRF7 and p-IRF3 then dimerize and translocate into the nucleus and activate the expression of the type 1 interferon genes (IFNα and IFNβ). Type I interferon proteins are then exported out of the cell to activate the JAK–STAT pathway by binding to their receptor (IFNAR) in an autocrine or paracrine fashion either on the same cells or neighboring cells. This leads to the production of more type I IFNs in a positive feedback loop and a variety of interferon-stimulated genes (ISGs), which mediate vasodilation near the site of the pathogen infection and uptake of fluid, recruitment of innate immune cells, to the site of the infection to mediate the killing of the infected cells [28].

1.4 Cyclic GMP-AMP synthase (cGAS) and DNA sensing pathway

DNA is normally localized in the nucleus of our cells and the existence of DNA in the cytoplasm is a major indication of tumorigenesis, cellular damage or infection which leads to the activation of genes associated with the immune response. During infections, pathogenic DNA as a key PAMP, alerts cytosolic DNA sensors to trigger downstream innate immune responses [29]. Among identified multiple DNA sensors so far, cyclic guanosine monophosphate-adenosine monophosphate (cGAMP) synthase (cGAS) is an essential one [30, 31]. cGAS is an enzyme of the nucleotidyltransferase family and senses the aberrant

expression of dsDNA with viral, bacterial, mitochondrial, micronuclei, and retroelement origins within the cytosol in a sequence-independent manner. The C-terminal lobe of cGAS harboring the nucleotidyltransferase domain (the catalytic part) contains a conserved zinc-ion-binding module which binds the sugar–phosphate backbone of DNA and mediates cGAS dimerization [32, 33]. DNA binding to the primary site, induces conformational changes around the catalytic site in the protein that rearrange the catalytic pocket of the enzyme to allow for an optimal interaction with the substrates ATP and GTP [34]. In addition to the primary DNA-binding site, there is an additional site located beside the primary site, which is a helix formed between strands β7-β8 and several surface-exposed loops [35]. The proximity of the two DNA-binding sites leads to the formation of a 2:2 cGAS:DNA complex assembly, in which two cGAS molecules embrace two dsDNA molecules [36, 37]. Next to DNA, cGAS dimers are arranged in "head-to-head" alignment [38] and form stable "ladder-like" networks between one long curved dsDNA helix or two independent dsDNA strands phase-separated organelles [39, 40]. Moreover, long DNA is more efficient than short DNA in driving the liquid-liquid phase separation of cGAS, and the formation of liquid-like droplets is dependent on the concentration of cGAS and DNA in the cytoplasm [41]. The formation of these spatially restricted cGAS–DNA assemblies on longer DNA is essential for inducing immune responses [42, 43]. This way of activation offers an inbuilt safeguard mechanism for living cells in a mode, that cGAS signaling can only be initiated when longer dsDNAs are available to exceed a certain threshold level.

Once cGAS and dsDNA interacts, cGAS catalyzes the synthesis of 2′3′-cyclic GMP-AMP (2′3′-cGAMP), with ATP and GTP as substrates. The primary step is the formation of a linear dinucleotide 5′-pppG (2′-5′)pA with ATP serving as the donor and 2′-OH on GTP serving as the acceptor. Then, by placing GTP at the donor position and AMP at the acceptor position, the intermediate product flips over in the catalytic pocket, to form a second 3′-5′ phosphodiester bond [30, 44]. cGAMP is then recognized by the endoplasmic reticulum (ER) membrane protein, stimulator of interferon genes (STING) (~ 40 KD), also known as MITA, MPYS, ERIS and TMEM173 [45, 46] (Figure 1.4). STING is composed of a short cytosolic N-terminal segment, a four-span transmembrane domain, a connector region, and a cytosolic ligand-binding domain (LBD) on which a C-terminal tail (CTT) is affixed. In the absence of a ligand, STING is retained in the ER by interacting with the Ca^{2+} sensor stromal interaction molecule 1 (STIM1) [47]. The cytosolic ligand-binding domain of STING can interact with 2′3′- cGAMP or CDNs (cyclic dinucleotides) such as c-di-AMP, c-di-GMP or 3′3′-cGAMP from bacteria.

Upon interaction, the ligand binding pocket in the LBD closes and activates STING, which next transforms into a tetramer and translocate from the ER to the perinuclear area mediated by cytoplasmic coat protein complex II (COPII) and ADP-ribosylation factor (ARF) GTPases [48-50]. In the Golgi, STING palmitoylates at two cysteine residues (Cys88 and Cys91), which is necessary for its activation [51, 52]. Modified STING recruits TANK-binding kinase 1 (TBK1); promoting TBK1 autophosphorylation, STING phosphorylation at Ser366 and recruitment of interferon regulatory factor 3 (IRF3), which is also phosphorylated by TBK1 and dimerized. Ultimately, dimerized IRF3 enters the nucleus and exerts its function in the transcription of type I IFNs, interferon-stimulated genes (ISGs) and several other inflammatory mediators, pro-apoptotic genes, and chemokines. [53].

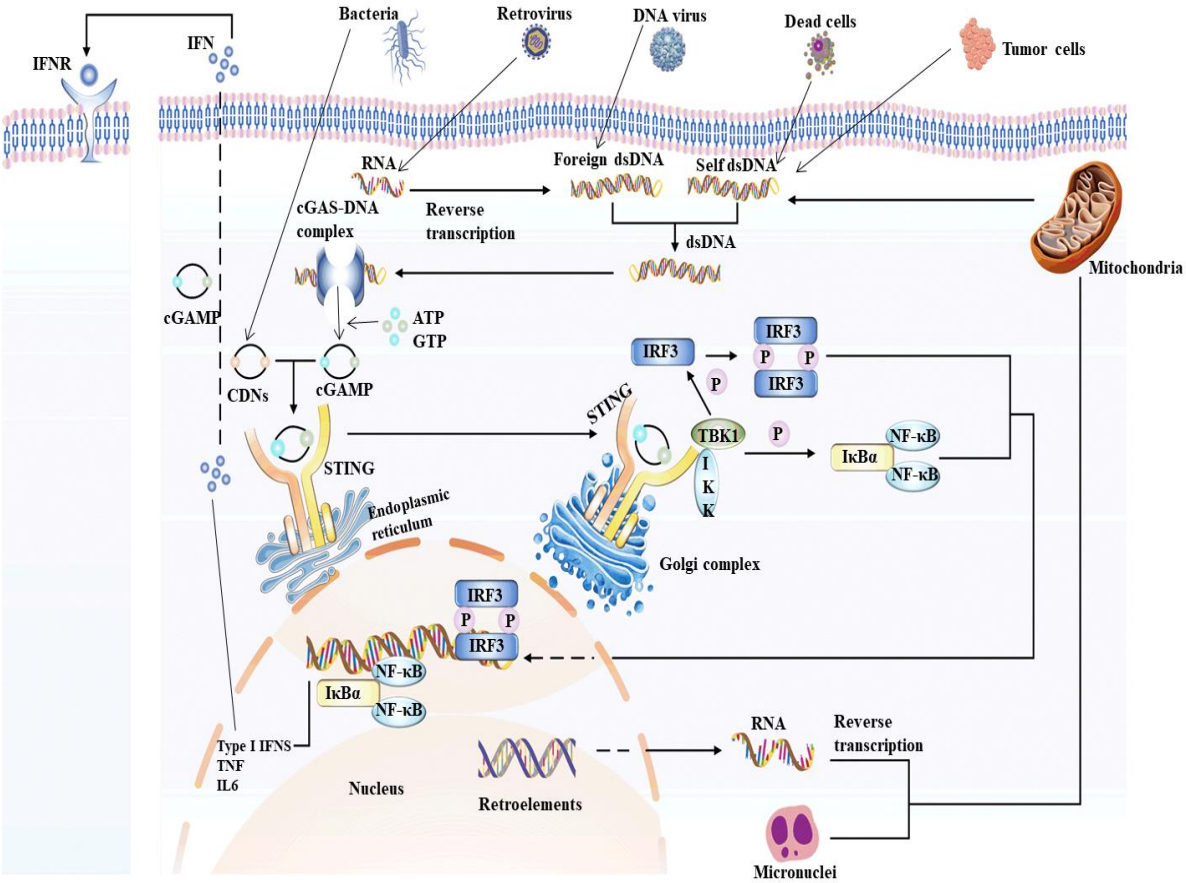

Figure 1.4 Sensing of cytosolic DNA through cGAS-STING pathway. Once DNA derived from virus, dying tumor cells or nucleus and mitochondria are located in the cytoplasm, they can be sensed by cGAS, and a 2:2 cGAS:dsDNA complex is produced to catalyze the synthesis of 2′3′-cGAMP in the presence of ATP and GTP. Then 2′3′-cGAMP and bacteria-derived CDNs induce the ER adaptor STING activation. Upon activation, STING translocate from ER

to Golgi compartments, where it activates TBK1 and IKK, which phosphorylate IRF3 and IκBα respectively. Then IRF3 and IκBα dimerize and enter nucleus, start the transcription of type I IFNs and other pro-inflammatory cytokines. The whole process shows that the dsDNA-cGAS-STING axis can lead to the activation of both innate and adaptive immunity.

Simultaneously, STING can also bind to and stimulate IκB kinase (IKK) to produce nuclear factor-κB (NF-κB)-driven inflammatory genes. Upon signal transduction termination, STING is degraded in endolysosomes [54]. Furthermore, newly synthesized type I IFNs activate interferon receptors (IFNAR1 and IFNAR2) through paracrine signaling and induce the transcription of ISGs [55]. Beside cGAS, other DNA sensors, namely IFNγ-inducible protein 16 (IFI16), DEAD-box helicase 41 (DDX41), DNA-dependent protein kinase (DNA-PK), and heterogeneous nuclear ribonucleoprotein A2B1 (hnRNPA2B1), can also mediate downstream signaling through STING [56-59]. In some extents, the presence of various DNA sensors seems to be a supplement to cGAS for pathogen detection [60].

1.5 Toll-like receptors (TLRs) signaling pathway

Toll-like receptors (TLRs) family is firstly identified and best characterized among PRRs family and recognize the external pathogen-associated molecular patterns (PAMPs) like bacterial lipopeptides, flagellin, lipopolysaccharides, double-stranded DNA (dsDNA), double-stranded RNA (dsRNA) derived from various microbes [61] and the internal damage-associated molecular patterns (DAMPs) released from injured cells [62]. Until now, 10 human (TLR1–TLR10) and 13 murine (TLR1–TLR9, TLR11–TLR13) subtypes of TLR have been identified, but TLR10 is non-functional in the mouse [63]. TLRs can localize to the cell membrane or to intracellular compartments such as the ER, endosome, lysosome, or endolysosome. TLR1, TLR2, TLR4, TLR5, and TLR6 are localized in the plasma membrane, and TLR3, TLR7, TLR8, and TLR9 are expressed within endosomes [64]. Each TLR is type I transmembrane glycoprotein which is structurally characterized by an extracellular domain, leucine-rich repeats (LRRs) that mediate ligands recognition, a transmembrane domain, and a cytoplasmic Toll/IL-1 receptor (TIR) domain that initiates downstream signaling [65]. Leucine rich repeat (LRR) is composed of 19–25 tandem copies of the "xLxxLxLxx" motif and forms a horseshoe-like structure [66]. Structural and biochemical analysis represent that all TLRs form hetero- or homodimers (e.g., TLR1/TLR2, TLR2/TLR6, TLR3/TLR3, and TLR4/TLR4), which assists dimerization of the cytoplasmic TIR domain to activate intracellular signaling [66]. In the case of TLR3 or TLR4 homodimers, direct or indirect interactions by ionic and

hydrogen bonds with their ligands are required for recognition [67, 68] whereas, TLR2 forms a heterodimer with either TLR1 or TLR6 through hydrophilic interactions [69, 70]. Upon ligands recognition, TLR recruits TIR domain-containing adaptor proteins like Myeloid differentiation primary-response protein 88 (MyD88), TIR domain-containing adaptor protein (TIRAP or MAL), TIR domain-containing adaptor protein inducing IFN-β (TRIF) and TRIF-related adaptor molecule (TRAM) [71]. Thus, depending on the adaptors, TLR signaling is largely divided into two pathways: the MyD88-dependent and TRIF-dependent pathways. Most members of TLRs depend on MyD88 pathway except TLR3. TIRAP activation is MyD88-dependent and is associated with TLR2 and 4 [72], TRIF acts independently of MyD88 following TLR3 and 4 activation [73] and TRAM operates TLR4 signaling in a TRIF-dependent way [74].

After TLR engagement, MyD88 recruits members of the interleukin-1 receptor-associated kinase (IRAK) family composed of IRAK1, IRAK2, IRAK4 and IRAK-M. In response to stimuli, IRAK4 and IRAK1 are sequentially auto-phosphorylated at several sites [75] and dissociated from MyD88 [76], results in the activation of tumor necrosis factor receptor-associated factor 6 (TRAF6) containing an N-terminal RING domain E3 ubiquitin protein ligase. TRAF6, along with ubiquitin-conjugating enzyme UBC13 and UEV1A, activates transforming growth factor-*β*-activated protein kinase 1 (TAK1), a member of the MAP kinase kinase family, in a ubiquitin-dependent manner [77]. TAK1 then activates IKK complex by binding to it that leads to NF-κB pathway and MAPK pathway activation [78]. The IKK complex is composed of two catalytic subunits IKKα and IKKβ and the regulatory subunit NEMO (also called IKKγ). The IKK complex then phosphorylates the NF-κB inhibitory protein IκBα and allows NF-κB to translocate into the nucleus to induce proinflammatory cytokines. TAK1 activation also phosphorylates members of MAPK kinase family such as MKK3 and MKK6 or MKK4 and MKK7, which mediates the activation of p38 and JNK respectively to regulate inflammatory responses [79].

On the other hand, to govern the expression of inflammatory cytokines and type I IFNs TLR3 initiates a TRIF-dependent pathway. TRIF interacts with TRAF3 and TRAF6 through TRAF-binding motifs present in its N-terminal portion [80]. TRIF also have a C-terminal receptor-interacting protein (RIP) homotypic interaction motif (RHIM), through which it interacts with RIP1 and RIP3. An essential adaptor for TNFR signaling, TNFR-associated death domain protein (TRADD), has also been involved in the TRIF-dependent signaling pathway [81]. TRADD forms a complex with FAS-associated death domain-containing protein

(FADD) and RIP1, and mediates ubiquitination of RIP1, which is required for NF-κB activation. In the presence of stimuli, TRAF3 activates two IKK-related kinases, TANK-binding kinase 1 (TBK1) and IKK-i (also known as IKK-ε) [82, 83]. Next, TBK1 and IKK-i mediate the phosphorylation of IRF3 and IRF7; IRF3 and IRF7 dimers translocate to the nucleus, resulting in induction of type I IFNs and expression of IFN-inducible genes. IKK-i also phosphorylates STAT1 to facilitate the induction of a set of IFN-inducible genes including Adar1, Ifit3, and Irf7 [84].

1.6 3-(trihydroxygermyl)propanoic acid (THGP) and its biological significance

Germanium (Ge), a chemical element in Group (IVa) of the periodic table, between silicon and tin, which is a silvery-gray metalloid, intermediate in properties between the metals and the nonmetals [85]. It was first discovered by Clemens Winkler in 1886 and became economically significant in 1945, when its properties as a semiconductor were recognized. Germanium is widely distributed in nature but is too reactive to occur free. This element is brittle and the atoms in its crystals are arranged as are the carbon atoms in diamond [86]. In addition to its applications in electronic devices, also used as a component of alloys and in phosphors for fluorescent lamps [87]. Properties of germanium has been listed in Table 1.2.

Table 1.2 Properties of Germanium

Property	Germanium Winkler discovery (1886)
atomic mass	72.63
density (g/cm^3)	5.35
melting point (°C)	947
color	Gray
oxide type	refractory dioxide
oxide density (g/cm^3)	4.7
oxide activity	feebly basic
chloride boiling point (°C)	86 ($GeCl_4$)
chloride density (g/cm^3)	1.9

Germanium can be found in soil, animals, and plants as a natural compound, and is also available in mushrooms, garlic, onion, and ginseng [88]. It can occur as both in organic and inorganic form. The inorganic germanium compound GeO_2 is insoluble in water, has been reported as hazardous and excessive GeO_2 intake can lead to lethal nephropathy via

accumulation in the nephrons of kidneys, neurotoxicity and even death [89]. Organogermanium compounds are organometallic compounds containing a carbon to germanium chemical bond. Organogermanium is advocated as a non-toxic alternative to many toxic organotin reagents, while metallic germanium is widely used in semiconductor devices, infrared light sensors, etc. The biological activity of Ge compounds was discovered long ago, this area began to develop vigorously when the first water-soluble organogermanium compounds, Ge sesquioxides, were synthesized. Germanium sesquioxides were first discovered by Russian researchers in 1965 via hydrolysis of the addition products of HGeCl3 to 1,3-enones, in particular, methyl methacrylate [90]. This reaction was expanded further to incorporate other compounds with a double bond. Numerous organogermanium compounds have been synthesized, among them, the most well-known example was bis(2-carboxyethylgermanium) sesquioxide, $[(GeCH_2CH_2COOH)_2O_3]n$, the addition product of HGeCl3 and propionic acid that was subsequently hydrolyzed [91]. This organogermanium compound also known as Poly-trans-[(2-carboxyethyl) germasesquioxane], Ge-132, repagermanium or 2-carboxyethyl-germasesquioxane, was first synthesized by Oikawa et al. in 1967, and its structure was reported in 1976 [92, 93]. In water this compound is hydrolyzed to 3-(trihydroxygermyl)propanoic acid (THGP) monomer, and this monomer can be neutralized with cations to yield its salt form, which has an extremely high solubility in aqueous solutions [94]. The structures of Ge-132 and THGP are shown in Figure 1.5.

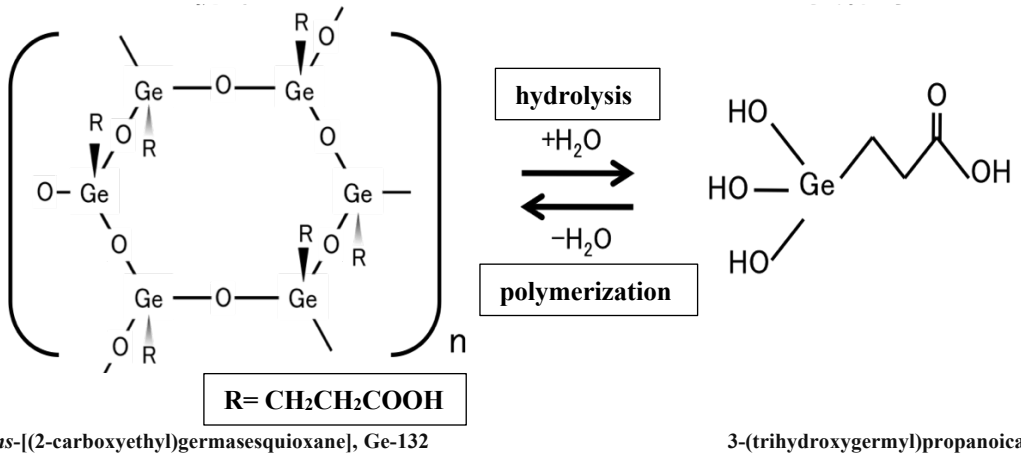

Figure 1.5 Structure of Ge-132 and 3-(trihydroxygermyl)propanoic acid (THGP). In the presence of water, Ge-132 is hydrolyzed to 3-(trihydroxygermyl)propanoic acid (THGP) monomer.

In vivo, Ge-132 exists in a hydrolyzed form (i.e.,THGP) as it undergoes dilution under neutral conditions. Previously nuclear magnetic resonance (NMR) analysis demonstrated that THGP interacts with the diol groups of saccharides via ^{1}H [95]. Moreover, it has been reported that THGP interacts with the cis-diol moiety of sugar structures even forms stronger complexes with the cis-diol of furanose, where the dihedral angle is narrower, than with pyranose [94]. Therefore, nucleosides and nucleotides structures, with a ribose skeleton, meet the conditions for interaction with THGP and ^{1}H NMR analysis proofed that, THGP formed a complex with AMP, containing a cis- diol structure, but not with dAMP or cAMP, which lack this structure [96]. In addition, Nakamura et al. [97] reported that, the THGP mediated mechanism of pain relief depends on the formation of a complex between THGP and ATP. THGP also forms a complex with L-DOPA (L-3,4-Dihydroxyphenylalanine) [98] along with catecholamine, ATP, and adenosine. So, the physiological activities of THGP are mediated by binding to cis-diol structures. THGP was developed for medical use and has undergone various animal experiments and multiple clinical evaluations which reported that it is safe [99-102]. Thus, in Japan, China, South Korea, and the United States Ge-132 is currently used as a supplement in health foods and cosmetics [98]. There are many different studies, which have been reported various biological activities of THGP. In vitro studies showed that it can induce interferon γ production [103], activate natural killer cells [104] and macrophages [105] by modulating the immune system. Further, in vivo studies suggested that it has antiviral [106], antimicrobial [107], analgesic [108], antitumorigenic activity, and inhibits cancer metastasis [109, 110]. Oxidative stress induced by hydrogen peroxide is reported to be associated with many chronic diseases such as cancer, diabetics, cardiovascular disease, inflammation, aging, and other neurodegenerative diseases in humans. It has been reported that THGP is also effective against hydrogen peroxide induced oxidative stress [88]. When a peripheral burn damages skin tissue, large quantities of ATP are leaked from the injured cells. The treatment of Ge-132 as a medical cream, decreases pain very quickly due to the interaction between Ge-132 and leaked ATP. It has been reported that the interaction of THGP and cis-diol neurotransmitters, such as adrenaline may regulate homeostasis and neurotransmission through the adjustment of receptor binding activity [97]. Moreover, the symbiotic immunological effects of Ge-132 in combination with lactobacilli and oligosaccharide can stimulate intestinal immunity [111]. Oral intake of Ge-132 can increase α-tocopherol transfer protein (Ttpa) gene expression by 1.62-fold and can also modulate hepatic gene expression profiles to promote immune activation in mice [112]. Injection of THGP were found to inhibit tumor growth remarkably in the mice

bearing solid Meth-A tumors by the continued augmentation of NK activity in peripheral blood, which was followed by the induction of specific killer cells appearing in the spleen [113, 114].

1.7 Role of THGP in viral infections

There are some investigations regarding effect of THGP during viral infections. The oral intake of THGP in influenza virus (FluV) infected mice demonstrated a significant protective effect. Compared to control group there was indication of an increase of survivors, a prolongation of mean survival days, an inhibition of the development of lung consolidation, and a decrease of virus titer in lung tissues of influenza virus (FluV) infected mice. Natural killer (NK) cell activity in the spleens and lungs of the infected mice was also significantly augmented after the oral administration of THGP [106]. In addition, THGP stimulated NK cells in vivo showed killing activity against NK-insensitive Meth-A cells infected with influenza virus. This protective effect in mice against influenza virus infection may be displayed through immunomodulating activities of THGP such as the augmentation of NK cell activity [115]. A controlled pilot study of 16-week treatment with Ge 132 for chronic hepatitis B patients with moderate and mild grades on hepatic histology disclosed a sustained clearance of hepatitis B e (HBe) antigen and a favorable biochemical response at week 16 of treatment and at week 48 post-treatment [116]. Mice infected with herpes simplex virus type I (HSV-1) showed significantly prolonged the mean survival days after oral administration of THGP by inducing cytotoxic T lymphocytes (CTL) against HSV-1 antigen. Oral doses of Ge-132 ranging from 0.2 to 10 mg/kg suppressed the number of pocks on the tail of mice which were induced by vaccinia virus [117].

1.8 PRRs mediated innate immune responses

The innate immune system represents the first line of defense that detects the presence of PAMPs from various microbes, mediated by different pattern recognition receptors (PRRs) and initiates downstream signaling to eliminate potential threats. In the case of microbeial infections, microbes-derived nucleic acids (RNA or DNA) are mainly recognized by certain PRRs, such as retinoic acid-inducible gene-I (RIG-I), melanoma differentiation-associated gene 5 (MDA5), and cyclic GMP-AMP synthase (cGAS) and Toll-like receptors (TLRs) [13]. The first group of characterized PRRs were TLRs and they recognize PAMPs in the extracellular compartment or within endosomes of macrophages and DCs. So far, 13 members of TLR family have been identified and TLR ligands are generally categorized into three groups: proteins, nucleic acids and lipid-based elements. The ligand specificities and

expression of TLRs in different cell types are described as follows: TLR2 is expressed on monocytes, mature macrophages and DCs, and mast cells and along with TLR1 or TLR6 recognizes wide variety of PAMPs including lipoproteins, peptidoglycans, lipotechoic acids, zymosan, mannan, and tGPI-mucin [79]. TLR3 is an endosomal TLR expressed in dendritic cells and recognizes double stranded RNA, small interfering RNAs, self-RNAs and the synthetic ligand polyriboinosinic polyribocytidylic acid (poly I:C) [118, 119]. TLR4 recognizes LPS and is expressed mainly on monocytes, mature macrophages and DCs, mast cells and the intestinal epithelium. TLR5 binds bacterial flagellin and is expressed primarily on cell surface of the intestinal epithelium and in monocytes, macrophages and DCs [120]. TLR7 and TLR8 are found in endosomes of monocytes and macrophages and plasmacytoid DCs and both recognize ssRNA from viruses [121]. TLR9 is expressed in endosomes of monocytes, macrophages and plasmacytoid dendritic cells, and recognizes bacterial and viral DNA rich in unmethylated CpG-DNA motifs. Synthetic oligonucleotides that contain unmethylated CpG motifs are used to activate TLR9. TLR10 is expressed in endosomes of macrophages and DCs, TLR10 is pseudogene in mouse due to an insertion of a stop codon. Both of mouse TLR11 and TLR12 are localized in endolysosomes of DCs and macrophages and recognize a profilin-like molecule derived from the parasite Toxoplasma gondii. TLR12 is predominantly expressed in myeloid cells, whereas TLR11 is mostly expressed in epithelial tissue [122]. TLR13 recognizes bacterial rRNAs, specifically the conserved CGGAAAGACC motif of 23S rRNA [123, 124]. Following ligands recognition, TLR4 induces inflammatory cytokines and IFN-β production by TRIF mediated pathway through IRFs (interferon-regulatory factors) signaling.

Mammalian RLRs are composed of three family members, RIG-I, MDA5 and LPG2. RIG-I and MDA 5 are major cytosolic sensors, RIG-I preferentially recognizes 5′-triphosphorylated RNA (5'-pppRNA or 3pRNA) and short dsRNA while MDA5 detects mainly long dsRNA [125]. RNA polymerase III (Pol III) can also function as a sensor of B-form DNA [poly(dA:dT)] by converting it into dsRNA. RIG-I is auto-suppressed in the absence of ligands, the second CARD domain interacts with helicase domain which ensures the prevention of direct access of any RNA to the helicase domain. During infections, the viral RNA is recognized by CTD and ATP-dependent conformational change forms a packed complex of the helicase domain/CTD with dsRNA, the CARDs are released from auto-repression. The active RIG-I then interacts with downstream adaptor molecule MAVS. Consequently, activated MAVS stimulates downstream signaling effectors TBK1 and IKK which activates transcription

factor IRFs (mainly IRF-3 and IRF-7) and NF-κB pathway respectively. MDA5 signaling pathway is activated through a similar mechanism as RIG-I.

The first identified cytosolic DNA sensor is DAI (also known as ZBP1, Z-DNA binding protein 1) which detects DNA and play a role in HSV-1 (herpes simplex virus 1) and HCMV (human cytomegalovirus) infections [126, 127]. DAI interacts with TBK1 and IRF-3, and with RIP1 and RIP3 to activate NF-κB, leading to type I IFN and inflammatory cytokine productions [128-130]. It is likely that the DAI pathway also involves STING-TBK1-IRF-3 pathway to induce type I IFN production. 2′, 3’-cGAMP synthase (cGAS) which belongs to the nucleotidyltransferase (NTase) family and exhibits structural and sequence homology to the catalytic domain of OAS (oligoadenylate synthetase) is also a sensor for cytosolic DNA. Upon binding to DNA, cGAS catalyzes the production of cGAMP from ATP and GTP. cGAMP functions as an endogenous second messenger to activate STING and sequentially recruit TBK1 to phosphorylate IRF-3 and promote IRF-3 nuclear trans-localization and binding to IFNs promoter, and STING also can activate NF-κB pathway via TRAF6-TBK1 signaling [131]. Although STING is thought to function as an adaptor protein, which links upstream PRRs to IRF-3 and NF-κB pathway activation, it also directly senses bacterial CDNs (cyclic dinucleotides), including c-di-GMP, c-di-AMP and 3′,3′-cGAMP [132, 133]. Innate immune responses mediated by different PRRs has been illustrated in Figure 1.6.

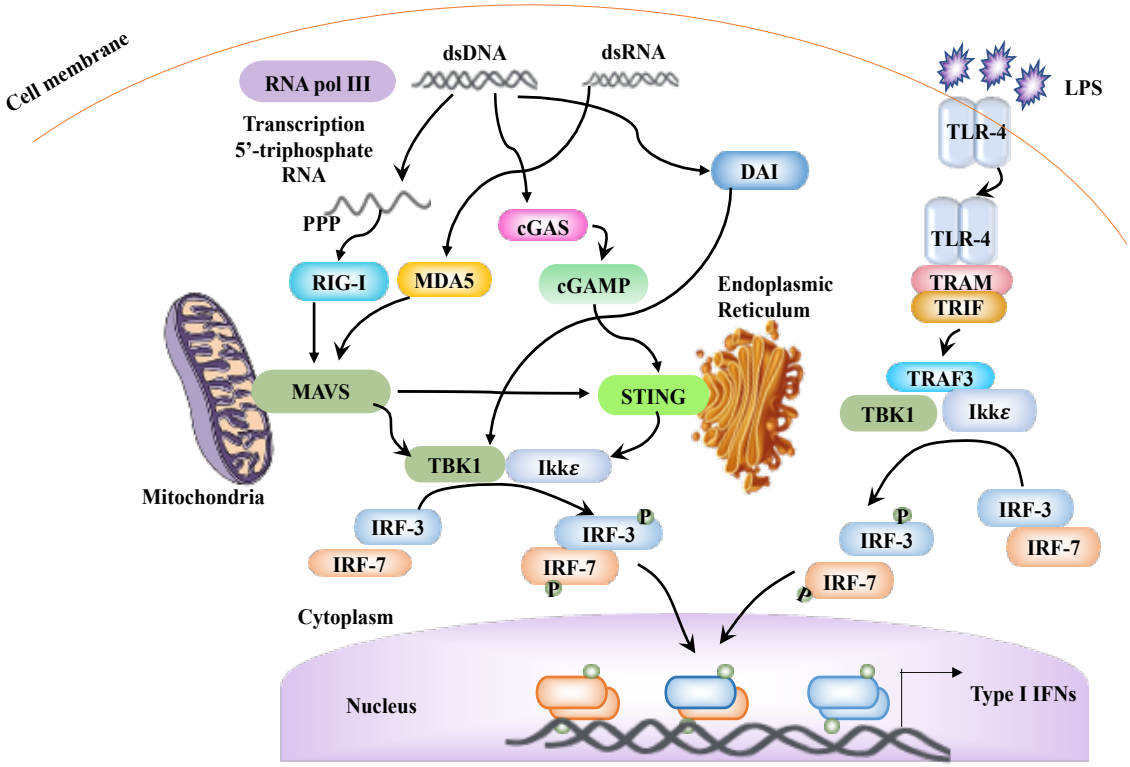

Figure 1.6 Innate immune responses through different PRRs. Upon binding to the corresponding ligands, different immune sensors such as RIG-I, MDA5, cGAS, DAI, TLR4 activate their downstream signaling pathways by interacting with different adaptor molecules like IPS-1, STING, TRIF, TRAF3 lead to the induction of the IFN-regulatory factor-3 (IRF-3) and NF-κB-dependent gene expression and subsequent production of type I IFNs and inflammatory cytokines through TBK1-IRF3 signaling pathways.

1.9 Inflammatory diseases caused by RIG-I hyperactivation

Nucleic acid sensor RIG-I senses viral invasion by the recognition of non-self-motifs and the proper induction of antiviral interferons (IFN) is essential to eliminate invading viruses. Recently several evidence have shown that aberrant antiviral signaling from RIG-I can result in the excess production of IFN, leading to disorders such as type I interferonopathies. Single nucleotide polymorphisms (SNPs) and mutations in the RNA helicase domains of RIG-I may lead to the susceptibility to autoimmune diseases such as systemic lupus erythematosus (SLE), Aicardi-Goutieres syndrome (AGS), and Singleton-Merten syndrome (SMS), all of which exhibit a type I IFN signature. Plasmacytoid dendritic cells (pDC) is the professional IFN-producing cells in antiviral innate immunity. Type I IFNs have pleiotropic effects, including the maturation of dendritic cells into antigen-presenting cells and activation and differentiation of B cell and T cell, in turn promoting further IFN production from pDCs [134-136]. Dysregulation of these self-amplifying loops is a hallmark of SLE and other IFN-driven diseases. Hyperactivation of RIG-I may lead to another kind of inflammatory disease tricho-hepato-enteric syndrome (THES) also known as syndromic diarrhoea (SD) or phenotypic diarrhoea (PD). Syndromic diarrhoea/tricho-hepato-enteric syndrome (SD/THE) is a rare congenital syndrome which is characterized by the combination of 9 signs: intractable diarrhea of infancy, hair abnormalities, facial dysmorphism, immune system abnormalities, intrauterine growth restriction, liver abnormalities, skin abnormalities, congenital heart defect and platelet abnormalities [137, 138]. It is an autosomal recessive genetic disease with an estimated prevalence of 1:100,000. It was first described in 1982 by Stankler et al. and explored more in 1994 by D Girault et al. [139, 140]. The etiology of this disease linked to pathogenic variants mutation in super killer viralicidic activity 2 (SKIV2L) or tetratricopeptide repeat domain-containing protein 37 (TTC37), both constituting the putative human ski complex [141]. The ski complex is a heterotetrametric cofactor of the cytoplasmic RNA exosome which ensures aberrant mRNAs decay. The diagnosis is primarily based on clinical findings and confirmed by direct sequencing of TTC37 and SKIV2L. Recently, it has been reported that SKIV2L is a

negative regulator of the RIG-I mediated antiviral responses and humans with deficiency in SKIV2L have a type I IFN signature in their peripheral blood [142]. Therefore, regulation of RIG-I mediated immune responses could be a possible therapeutic option to treat this disease.

1.10 Genomic organization of Influenza virus (FluV), Vesicular stomatitis virus (VSV), Encephalomyocarditis virus (EMCV) and Severe acute respiratory syndrome coronavirus 2 (SARS-CoV-2)

Influenza viruses (FluVs) are single-stranded negative sense RNA viruses that compose a major threat to human health and responsible for common respiratory infection in human, spreading as seasonal epidemics and sporadic pandemics. The name "influenza" is derived from the Latin word for "influence," and the pathogens that cause this disease are RNA viruses belong to the Orthomyxoviridae family. Every year seasonal influenza epidemics cost the lives of about 30,000 people and cause hospitalization of more than 100,000 in USA [143]. The genome of FluV is organized in eight, negative-sense RNA segments. The segments are assembled into viral ribonucleoprotein (vRNP) complexes in which the termini of the viral RNA (vRNA) associate with the viral RNA-dependent RNA polymerase and the rest of the vRNA is bound to oligomeric arginine rich nucleoprotein (NP) in virions [144]. The influenza capsid is studded with antigenic glycoprotein spikes of hemagglutinin (HA) and neuraminidase (NA), in a ratio of approximately four to one and to form the capsid several hundred molecules of HA and NA are needed [145] (Figure 1.7).

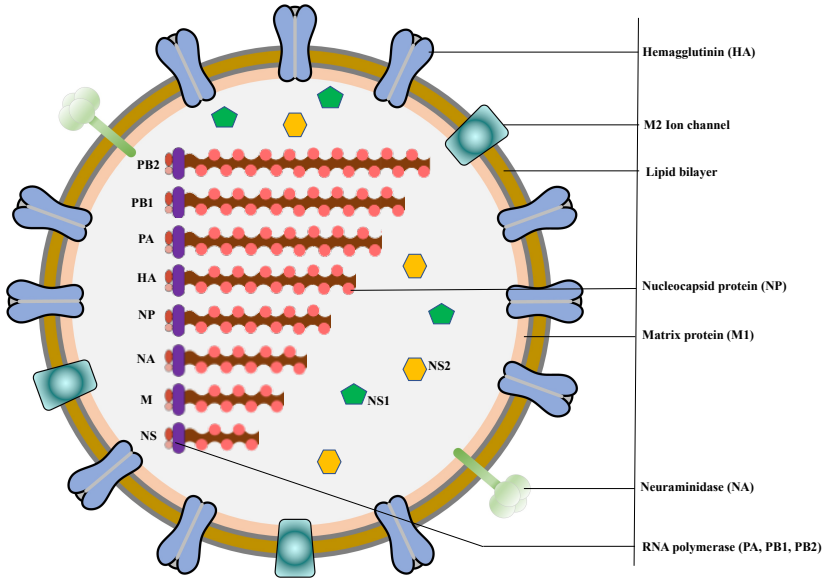

Figure 1.7 Schematic representation of FluV. FluV contains eight RNA segments, which encode RNA polymerase subunits (PB2, PB1 and PA), viral glycoproteins (haemagglutinin (HA), with its distinct globular 'head' and 'stalk' structures, which facilitate viral entry, and neuraminidase (NA), which facilitates viral release), viral nucleoprotein (NP), matrix protein (M1) and membrane protein (M2), the nonstructural protein NS1 and nuclear export protein (NEP).

As many different subtypes of HA and NA proteins exit, our immune system is challenged frequently with new antigens. The size of vRNA ranges from ~0.9 to 2.3 kb, while the total genome is about 13.5 kb. All vRNAs are organized as: a central open reading frame that encodes one or more protein (in the antisense orientation) flanked by two short untranslated regions (UTRs). Segments 1–8 are numbered in order of decreasing length and the encoded proteins are polymerase basic protein 2 (PB2), polymerase basic protein 1 (PB1), polymerase acidic protein (PA), hemagglutinin (HA), nucleoprotein (NP), neuraminidase (NA), matrix protein (M), and nonstructural protein (NS). Segments 1, 3, 4, and 5 encode just one protein per segment: the PB2, PA, HA and NP proteins, PB1 is encoded by segment 2, segment 6 encodes NA protein. Segment 7 codes for the M1 matrix protein and for M2 ion channel by RNA splicing [146], finally segment 8 expresses the interferon-antagonist NS1 protein [147] and by mRNA splicing, NEP/NS2, involved in viral RNP export from the host cell nucleus [148]. The genomic segments of influenza A/Puerto Rico/8/1934 (H1N1) virus and their encoded proteins are listed in Table 1.3.

Table 1.3 The genomic segments of influenza A virus and their encoded proteins

Segment	Segment length In nucleotide.	Encoded Protein(s)	Protein length in Amino acids	Protein function
1	2341	PB2	759	Polymerase subunit; mRNA cap recognition
2	2341	PB1	757	Polymerase subunit; RNA elongation, endonuclease activity
3	2233	PA	716	Polymerase subunit; protease activity
4	1778	HA	550	Surface glycoprotein; major antigen, receptor binding and fusion activities
5	1565	NP	498	RNA binding protein; nuclear import regulation
6	1413	NA	454	Surface glycoprotein; sialidase activity, virus release
7	1027	M1	252	Matrix protein; vRNP interaction, RNA nuclear export regulation, viral budding
		M2	97	Ion channel; virus uncoating and assembly
8	890	NS1	230	Interferon antagonist protein; regulation of host gene expression
		NS2	121	Nuclear export of RNA

Each segment of influenza virus forms a partially double-stranded promoter structure through base-pairing of the highly conserved 13 nucleotides at the 5' end and 12 at 3' end, which undergoes substantial structural rearrangements at certain stages of the viral replication cycle to perform distinct functions [149, 150]. To produce complete infectious progeny virions eight vRNPs (containing each of vRNA segments) are required. This genome architecture not only provides evolutionary advantages to influenza virus but also complicates the process of genome packaging. Genome segmentation provides a major evolutionary advantage, it allows for the exchange of segments, when at least two viruses co-infect the same cell. This process is a source of genetic variability leading to the production of new pandemic viral strains. However, virus propagation can also be ensured by segmentation which imposes a specific and precise mechanism of genome packaging [151].

Vesicular stomatitis virus (VSV) belongs to the family Rhabdoviridae, and Vesiculovirus genus. The viral genome constitutes of a linear, single-stranded, non-segmented negative-sense RNA molecule of approximately 11 kb encoding five genes in the following order from 3′ to 5′: the nucleocapsid protein (N), phosphoprotein (P), matrix protein (M), glycoprotein (G) and polymerase (L) (Figure 1.8). Each of these proteins has multiple binding partners, thus can mediate multiple functions. This virus is characterized a unique fact that its genome does not exist as naked RNA, rather encapsidated by nucleocapsid proteins in the entire replication cycle. To encapsidate the genomic RNA, N forms a cavity by its 2 lobes angled together. Each monomer of N can accommodate 9 bases of RNA and interacts with 3 neighboring N molecules across the nucleocapsid. For RNA encapsidation interaction between the elongated N terminus and an extended loop (C loop) within the C-terminal lobe is essential [152]. Residues within this loop are also involved in binding to the P. Thus, the N protein alone contains all the information for the assembly of a capsid structure of VSV.

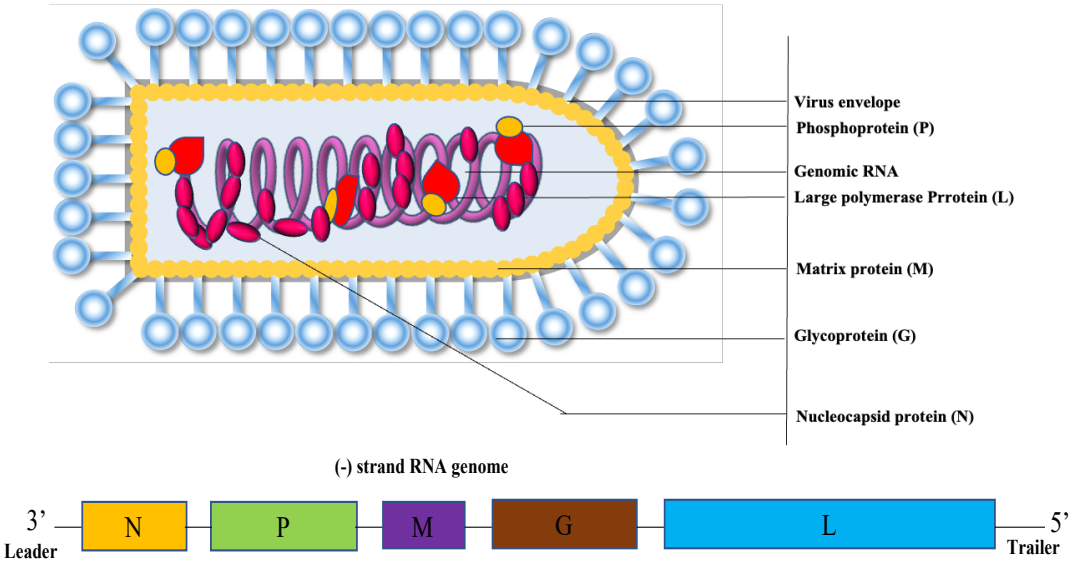

Figure 1.8 Virion and genome of Vesicular stomatitis virus. The viral RNA dependent RNA polymerase binds the encapsidated genome at the leader region, then sequentially transcribes each gene by recognizing start and stop signals flanking viral genes. mRNAs are capped and polyadenylated by the L protein during synthesis.

VSV polymerase transcribes the viral genes sequentially leading to a protein gradient from N to L [153]. P protein of VSV functions as a 265-aa nonenzymatic cofactor of the viral polymerase. The N-terminal domain of P protein contains the first 106 residues and among them 3 residues (Ser-60, Thr-62, and Ser-64) are indispensable because they are required for transcription [154]. The L-protein of VSV is a single-chain multi-domain RNA-dependent RNA polymerase, which catalyzes mRNA 5′-capping, cap methylation, and mRNA 3′ polyadenylation [155]. Replication mediated by a replicase complex formed by the N, P, and L-proteins, whereas the transcription complex is formed by P and L without N [156].

In 1945 Helwig and Schmidt first isolated the encephalomyocarditis virus (EMCV), which belongs to the Picornaviridae. It is a small non-enveloped, positive sense single-stranded RNA virus, of approximately 7.8 kb that allows direct translation of the RNA into a polyprotein. The virus genome consists of 5′- and 3′-untranslated regions (UTRs), and a single open reading frame (ORF) encodes a polyprotein [157]. In case of EMCV viral proteins are not required to initiate viral gene expression, therefore transfection of viral RNA can produce infectious viral particles and can act as a mRNA during translation and as template during genome replication. The 3′ UTR (120 nucleotides long) composed of short stem-loop structures followed by a

poly(A) tail while the 5′ UTR is about 800 to 1,200 nucleotides long. The viral RNA is capped with a 7-methyl-guanosine, covalently linked at the 5′ end to a 20 amino acid protein called virion protein, genome-linked (VPg) [158]. It encodes a large polyprotein (L-1ABCD-2ABC-3ABCD) that is co- and post translationally processed into approximately 13 mature proteins. Proteins and precursors of EMCV were named from their position within the polyprotein, that is, the leader protein (L), the precursor P1, comprising capsid proteins VP4, VP2, VP3 and VP1once integrated into the virion. The P2 and P3 are precursors of the non-structural proteins: 2A, 2B and 2C, and 3A, 3B (also called VPg), 3C protease and the RNA-dependent RNA polymerase 3D (Figure 1.9) [159]. The 5′ UTR also contains a type II internal ribosome entry site (IRES) of about 450 structure made up of hairpin loops. The IRES allows ribosome binding, and the translation initiation of the open reading frame encoding a polyprotein of 2,292 amino acids.

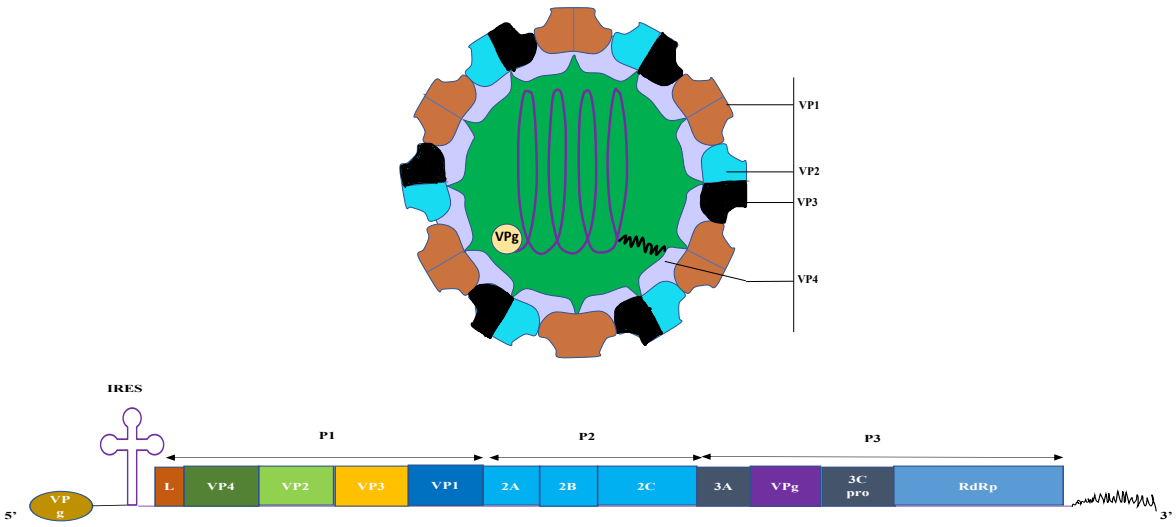

Figure 1.9 Virion and genomic representation of encephalomyocarditis virus (EMCV). The capsid consists of a densely packed icosahedral arrangement of 60 protomers, each consisting of 4 polypeptides, VP1, VP2, VP3 and VP4. VP4 is located on the internal side of the capsid. The genomic RNA has a viral protein (VPg) at its 5' end and the 5' long UTR contains a type II internal ribosome entry site (IRES). The P1 region encodes the structural polypeptides. The P2 and P3 regions encode the nonstructural proteins associated with replication. The leader (L) protein is thought to exert important functions in virus-host interactions. The shorter 3' UTR is important in (-) strand synthesis.

Different viral proteins of EMCV and their associated functions are listed in Table 1.4.

Table 1.4 Proteins of EMCV

Proteins	Functions
Leader protein	Counteracts host defenses to promote spread within the infected host.
Capsid protein VP1	Forms an icosahedral capsid with capsid proteins VP2 and VP3.
Capsid protein VP2	Forms an icosahedral capsid with capsid proteins VP1 and VP3.
Capsid protein VP3	Forms an icosahedral capsid with capsid proteins VP1 and VP2.
Capsid protein VP4	Lies on the inner surface of the capsid shell formed by VP1, VP2 and VP3.
Protein 2A	Involves in host translation shutoff by inhibiting cap-dependent mRNA translation.
Protein 2B:	Affects membrane integrity and causes an increase in membrane permeability.
Protein 2C	Induces structural rearrangements of intracellular membranes.
Protein 3A	Serves as membrane anchor via its hydrophobic domain.
VPg	Forms a primer, VPg-pU, which is utilized by the polymerase for the initiation of RNA chains.
Protease 3C	Generates mature viral proteins from the precursor polyprotein, it also binds to viral RNA, and thus influences viral genome replication.
RNA-directed RNA polymerase	Replicates the genomic and antigenomic RNAs by recognizing replications specific signals.

Severe Acute Respiratory Syndrome Coronavirus 2 (SARS-CoV-2) has been declared as a pandemic, with 8 million confirmed cases and 0.44 million deaths globally by WHO on 14th April 2020. Structurally, SARS-CoV-2 is a non-segmented, double-layered lipid enveloped virus with a diameter of 50–200 nm. The SARS-CoV-2 is comprised of a single stranded positive RNA of approximately ~29.9 kB in size [160]. It has 13-15 open reading frames (ORFs), encoding about 7096 residues long polyprotein, that consists of many structural and non-structural proteins (nsps) [161]. The genome contains a cap structure at the 5′ untranslated region (UTR) of 265 nucleotides, replication complex (ORF1a and ORF1b), Spike (S) gene, Envelope (E) gene, Membrane (M) gene, Nucleocapsid (N) gene, 3′ UTR of 358 nucleotides, several unidentified non-structural ORFs and a poly (A) tail [162] (Figure 1.10). These gene products are important for viral entry, fusion, and survival in host cells. The first ORF (ORF1a and ORF1b) comprises approximately 67% of the genome encoding 16 nonstructural proteins, whereas the remaining ORFs encode for accessory and structural proteins. Polyprotein pp1a encoded by the ORF1a gene at the 5′UTR, which contains 10 nsps. Next to ORF1a, the ORF1b gene is located and encodes for polyprotein pp1ab which contains 16 nsps [163]. Although polyprotein pp1a can translate directly from the genomic RNA; expression of ORF1b requires a − 1 ribosomal frameshift near the end of ORF1, resulting in a single polyprotein pp1ab. pp1ab and pp1a proteins undergo autoproteolytic cleavage into multiple enzymes that form replicase-

transcriptase machinery including the papain-like protease (NSP3), the main protease (NSP5), the NSP7–NSP8 primase complex, the primary RNA-dependent RNA polymerase (NSP12), a helicase–triphosphatase (NSP13), an exoribonuclease (NSP14), an endonuclease (NSP15) and N7- and 2′O-methyltransferases (NSP10 and NSP16), essential to viral genome replication and nucleic acid metabolism [164]. The 3′UTR contains the four structural genes encoding Spike glycoprotein (S), Envelope protein (E), Membrane glycoprotein (M), and Nucleocapsid protein (N) and eight accessory genes, whose functions are mostly unknown [165]. S glycoprotein is a fusion viral protein comprising signal peptide, N-terminal domain (NTD), and receptor-binding domain (RBD), which is mainly responsible for interaction with the ACE2 receptor [166]. The Envelope protein is involved in pathogenesis as it interacts with the tight junction related protein PALS1 [167]. The M glycoprotein comprising three domains, a long C-terminal cytoplasmic domain, three transmembrane domains, and N-terminal glycosylated ectodomain, responsible for the assembly of viral particles [168]. The nucleocapsid, a phosphoprotein packs the viral genome into a ribonucleoprotein complex [169] (Figure 1.10).

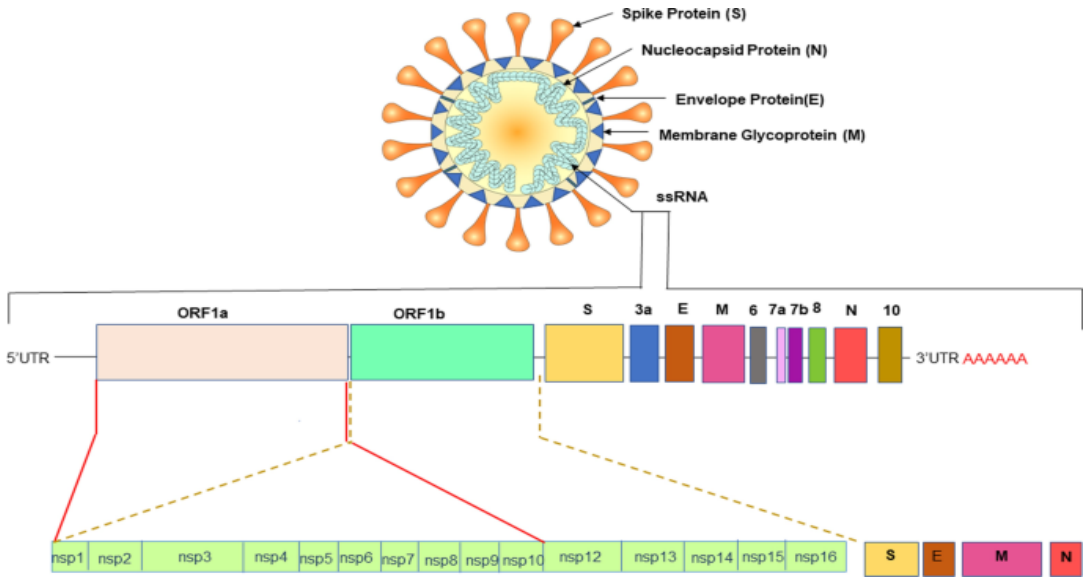

Figure 1.10 Schematic presentation of the SARS-CoV-2 genome Structure. SARS-CoV-2 has a spherical structure covered with spike glycoprotein (S), which mediates interaction with cell surface receptor ACE2. The viral membrane glycoprotein (M) and envelope (E) proteins are embedded in host membrane-derived lipid bilayer encapsulating the helical nucleocapsid comprising viral RNA. The full-length RNA genome consists of approximately 29,903 nucleotides and has a 5′ capped replicase complex (comprised of ORF1a and ORF1b) at the 5′UTR. The ORF1a encodes for nsp1–nsp10, while ORF1b encodes for nsp1–nsp16. The nsps includes two viral cysteine proteases, including papain-like protease (nsp3), chymotrypsin-like,

3C-like, or main protease (nsp5), RNA-dependent RNA polymerase (nsp12), helicase (nsp13), and others likely to be involved in the transcription and replication. Four genes that encode for the structural proteins: Spike gene, Envelope gene, Membrane gene, Nucleocapsid gene and a poly (A) tail at the 3′UTR. The accessory genes are distributed in between the structural genes.

1.11 Viral schemes to evade host innate immune responses

For the maintenance of life, distinguishing between self and non-self is very essential. Non-self-recognition of an invading virus is a first and critical step of defense in programming the host innate immune response for control of infection. Viruses, in turn, have evolved sophisticated programs of their own to escape from the innate immune system, evasion of the host innate immune responses permit the virus to gain an early footrail during infection, replicating to a high titer before an effective adaptive immune response can be launched. Initiation of innate immune responses begins with the recognition of PAMPs by PRRs. Many RNA viruses replicate in the cytoplasm where they are detected by the cytoplasmic PRRs, MDA5 and RIG-I, on the other hand most DNA viruses replicate within the nucleus and can be sensed in the nucleus or in the cytoplasm by IFI16 or cGAS, respectively. Viruses recognized by different PRRs are listed in Table 1.5.

Table 1.5 Viruses sensed by different PRRs

pattern-recognition receptors (PRRs)	Viruses
RIG I	Influenza viruses, Measles virus, Japanese encephalitis virus (JEV), Hepatitis C virus, Vesicular stomatitis virus (VSV), Rift Valley fever virus (RVFV) and La Crosse virus (LACV), Newcastle disease viruses (NDV), Ebola virus (EBOV), Sendai virus (SenV), Arenaviruses, West Nile virus (WNV), Dengue virus (DENV), Grass carp reovirus (GCRV), Rabies virus, Epstein–Barr virus (EBV), Kaposi's sarcoma herpesvirus (KSHV), Respiratory Syncytial virus (RSV), Hepatitis B virus (HBV) etc.
MDA5	Encephalomycarditis virus (EMCV), Poliovirus, Measles virus, Hepatitis D virus, Semliki Forest virus (SFV), Porcine respiratory and reproductive syndrome virus (PRRSV), Thrombocytopenia syndrome virus (SFTSV), West Nile virus (WNV), Dengue virus (DENV), Sindbis virus (SINV), Borna disease virus (BDV), Hantaviruses, SARS coronavirus, Mengo virus, Theiler's virus, Zika virus, Rhinovirus; Coxsackie B virus etc.
cGAS	Herpes simplex virus-1 (HSV-1), Herpes simplex virus 2 (HSV2) Adenoviruses, Murine gammaherpesvirus 68 (MHV68), Vaccinia

virus (VACV), Ectromelia virus (ECTV), Human cytomegalovirus (HCMV) and Human papillomaviruses (HPV), Human immunodeficiency virus (HIV), Hepatitis B virus (HBV), Varicella zoster virus, Merkel cell polyomavirus etc.

There are many different immune evasion strategies of various viruses including: (i) interference with the functions of the host innate immune response via physical interactions with viral antagonistic proteins targeted to sensors, adaptors, related intracellular kinases and transcription factors; (ii) inducing degradation or specific cleavage at the protein level; and (iii) sequestration of signal transduction molecules targeting the post translational modification (PTM) systems. For example, the positive-sense single-stranded RNA virus, dengue virus (DenV), replicates in ER-derived membrane structures called vesicle packets and convoluted membranes, and induces membrane modifications that sequester the DenV RNA away from RIG-I and MDA5, thus, limits triggering the innate response via PRRs [170]. Like DenV, hepatitis C virus (HCV) -induced membrane rearrangement to house its replication machinery prevents recognition of HCV RNA by RIG-I [171]. During replication, SARS-CoV-2 uses its own capping machinery composed of nsp10, nsp13 and the dedicated enzyme nsp16 to generate 2′-o-methyltransferase caps to protect the 5′ ends of RNA, which in turn limits degradation and importantly blocks recognition by cytosolic PPRs [172]. In addition, SARS-CoV uses its endoribonuclease (nsp15) to cleave its own viral RNA in the cytosol that would otherwise act as PAMPs, thus evading MDA-5, protein kinase R (PKR) and OAS/RNAse L [173]. Hepatitis B virus may evade recognition by shielding the DNA within the viral capsid. Another strategy of innate immune evasion is modifying or degrading viral PAMPs. For example, to avoid recognition by RIG-I some virus can hide or remove 5'tri-phosphate. Influenza virus RNA polymerase complexes with PB1, an endonuclease with cap binding activity that captures a N7 methylguanosine 5' cap from host cellular pre-mRNA known as 'cap snatching' and utilize these caps to mask viral RNA PAMPs [174]. Viral peptide linked to the genome (VPg) of poliovirus is covalently attached to the 5' end of viral RNA, thus lacking 5'-triphosphate [175]. Hantaan virus (HTNV) and Borna disease virus (BDV) do not trigger RIG-I-mediated IFN responses, as the 5'-triphosphate structure of these viral genomic RNA is removed by processing [176]. Human immunodeficiency virus type 1 (HIV-1) uses host exonuclease TREX1 to degrade HIV DNA generated during HIV-1 infection and avoid detection by nucleic acid sensors [177]. Lassa virus encodes an exonuclease, nucleoprotein that hydrolyses RNA, thus Lassa virus evades immune recognition by digesting its own PAMPs by an exonuclease

[178]. Poliovirus (PV), coxsackievirus B3 (CVB3), and enterovirus 71 (EV-D71), are positive-sense ssRNA viruses encode two proteases, 2Apro and 3Cpro, which can cleave MDA5 and RIG-I respectively [179]. Hepatitis C virus (HCV) non-structural (NS) proteins NS3-4A protease complex cleaves MAVS and TRIF, thus, inhibit further innate signaling [180, 181]. Herpes simplex virus 1 (HSV1) encoded protein γ34.5 can inactivate STING through disrupting the trafficking of STING from the endoplasmic reticulum to the Golgi apparatus [182]. The oncogene E1A from adenovirus and E7 from human papillomavirus (HPV) inhibit the cGAS/STING pathway by directly binding to STING. Vaccinia virus produces poxins, which cleave CDNS, thus suppresses cGAS/STING pathway. Packaging of relaxed-circular HBV DNA into the viral capsid protein blocks direct recognition by cGAS [183]. Zika virus-encoded NS1 protein promotes proteolysis of cGAS by stabilizing caspase-1 [184]. Human cytomegalovirus (HCMV) encoded tegument protein UL83 binds to cGAS and blocks downstream signaling [185]. NS1 protein of IAV binds to the regulators of RIG-I, TRIM25 and Riplet in a species-specific manner leading to a decreased induction of IFN [186]. The NS2B3 protease of DenV cleaves the mitofusins, MFN1 and MFN2, known to be positive (MFN1) or negative (MFN2) regulators of MAVS function [187]. Further, ebola virus Vp35 protein inhibits both TBK1 and IKKε to prevent their interactions with the transcription factors IRF3 and IRF7 [188]. Enterovirus 68 (EV-D68) 3Cpro cleaves IRF7 to evade IFN induction during infection [189] and additionally, the HCV core protein dysregulates STAT1 signaling by increasing the levels of non-phosphorylated STAT1 in the cell [190].

1.12 Life cycle, replication mechanism and pathophysiology of FluV

Influenza (FluV) is an infectious respiratory disease can be caused by influenza A and influenza B, influenza virus C and influenza virus D. All influenza viruses are negative-sense single-strand RNA viruses with a segmented genome and have a pleiomorphic envelope with a diameter of 50–120 nm. The life cycle of influenza viruses generally involves the following stages: entry into the host cell; entry of viral ribonucleoproteins (vRNPs) into the nucleus; transcription and replication of the viral genome; export of the vRNPs from the nucleus; and assembly and budding at the host cell plasma membrane (Figure 1.11). Influenza virus replication mainly takes place in epithelial cells of the respiratory tract in humans and other mammals and in epithelial cells of the intestinal tract in birds. The first step in the FluV life cycle starts with the binding to host cells, mediated by viral hemagglutinin (HA) protein since it binds to sialic acids on the surface of the host cell's membrane. The HA proteins of human FluVs preferentially recognize sialic acid linked to galactose by an α2,6-linkage (Siaα2,6Gal),

whereas avian virus HA proteins preferentially bind to Siaα2,3Gal [191–194]. Upon binding to the host cell's sialic acid residues, receptor-mediated endocytosis internalized the virus in an endosome. The endosome has a low pH of around 5 to 6 which triggers a conformational change in the viral HA, exposing the HA2 fusion peptide which inserts itself into the endosomal membrane, bringing both the viral and endosomal membranes into contact with each other [195]. Once virions have undergone endocytosis, the virion-associated M2 ion channel opens and acidifies the viral core, leading to the dissociation of the acid-labile viral matrix protein (M1)-viral ribonucleoprotein (vRNP) complex interactions [196]. Dissociation from M1 allows vRNP release into the host cell's cytoplasm and subsequent import into the nucleus, mediated by cellular nuclear import factors importin-α and importin-β [197-199]. The viral proteins that make up the vRNP have nuclear localization signals (NLSs) that bind to the nuclear import machinery and, thus, enter the nucleus, where transcription and replication of the viral RNA takes place. Viral RNA dependent RNA polymerase (RdRp) starts replication with the synthesis of a positive sense copy of the vRNA, termed complementary RNA (cRNA). Nascent cRNAs are encapsidated by newly synthesized NP and viral polymerases, leading to the formation of complementary ribonucleoprotein (cRNP) complex. cRNPs are then generate large amounts of vRNAs, which form progeny vRNPs [200]. Transcription of viral RNA is initiated by the binding of PB2 to the 5′-cap structure of host mRNAs and the endonuclease activity of PA then 'snatches' the cap structure and cleaves the cellular mRNAs 10 to 15 nucleotides 3' to the cap structure. This cellular capped RNA fragment is used by the viral RdRp to prime viral transcription [201]. Transcription proceeds until the polymerase complex stalls at a polyadenylation signal near the end of the viral RNA [202] and results in positive-strand mRNAs that are capped and polyadenylated and exported into the cytoplasm for translation into viral proteins by the host cell translation machinery. During infection IAV mRNAs are preferentially translated compared to host cell protein [203]. To further increase the rate of viral RNA synthesis, newly synthesized viral polymerases (PB1, PB2 and PA) and viral NP are imported to the nucleus, whereas virus membrane proteins HA, NA and M2, following their synthesis by the cellular translation machinery, traffic to and get inserted into the endoplasmic reticulum (ER) where they are glycosylated (HA and NA) or palmitoylated (HA and M2) [204]. Cytoplasmic vRNPs finally migrate to the plasma membrane where virus assembly and budding take place. At the plasma membrane, HA and NA associate with lipid rafts which are the site of influenza virus budding [205]. The assembly and virion incorporation of the eight vRNPs requires segment-specific packaging signals in the viral RNAs [206].

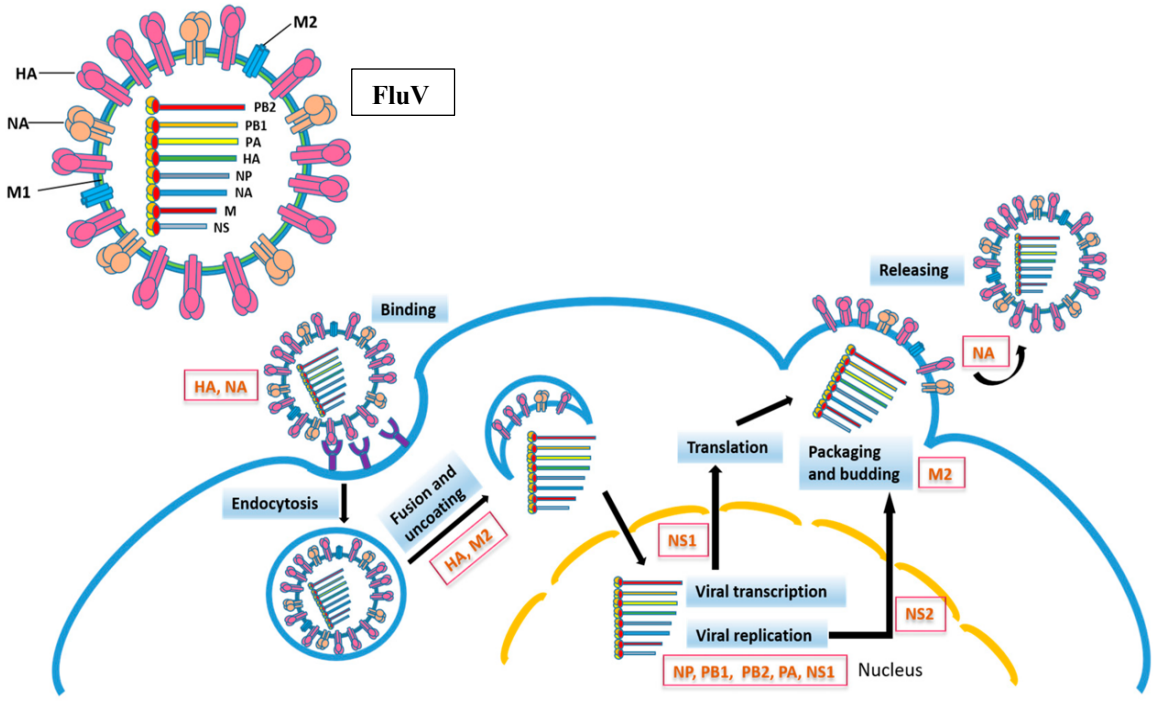

Figure 1.11 Scheme of the influenza virus life cycle. Influenza virus (FluV) enters the cell by endosomal uptake and release, and its negative-sense genetic material in the form of viral ribonucleoproteins (vRNPs) is imported to the nucleus for transcription and replication. Viral mRNA is translated into viral proteins in the cytoplasm, and these are assembled into new virions together with the newly synthesized vRNPs. HA, haemagglutinin; M2, membrane protein; NA, neuraminidase; NEP/NS2, nuclear export protein; NP, nucleoprotein; NS1, nonstructural protein; PB1, PB2 and PA, viral RNA polymerases.

Human influenza viruses are transmitted through the respiratory route and target epithelial cells of the respiratory tract for infection and productive replication. Severe infection arises while the virus replicates in the lower respiratory tract, accompanied by severe inflammation leading to immune cell infiltration. The respiratory epithelium is the only site where the hemagglutinin (HA) molecule can effectively cleave to generate infectious virus particles. Virus transmission occurs when an individual comes into contact with aerosols or respiratory fomites from an infected individual [207]. In most healthy individuals the acute symptoms persist for seven to ten days and able to infect other people beginning 1 day before symptoms develop and up to 5 to 7 days after becoming sick. The immune reactions specifically interferon responses are responsible for the viral syndrome including high fever, coryza, and body aches. High-risk groups having chronic lung diseases, cardiac disease, and pregnancy are more prone

to severe complications that can lead to acute respiratory distress syndrome, primary viral pneumonia, secondary bacterial pneumonia, hemorrhagic bronchitis, and death. Infected persons can transmit the virus to other individuals before knowing they are sick, as symptoms start 1 to 4 days after the virus enters the body. Asymptomatic persons may still spread the virus to others. Influenza pathophysiology involves lung inflammation caused by immune responses recruited to handle the spreading virus (Table 1.6). This inflammation can spread systemically and manifest as a multiorgan failure [208].

Table 1.6 Host and viral mechanisms of influenza-associated pathology

Direct viral induced pathology	Innate immune responses	Adaptive immune responses
• Epithelial cell death (apoptosis and necrosis) • Alveolar compromise • Denudation of the airways	• Local and systemic cytokine production • Innate immune cellular infiltration (neutrophils, inflammatory monocytes) • Extracellular matrix degradation	• Exuberant T cell responses (CD4 and CD8) • Excess cytokine production • Immune cell mediated epithelial denudation • Amplification of inflammation and local and systemic cytokine production

There are some associations between influenza virus infection and cardiac sequelae, including increased risk of myocardial disease in the weeks following influenza virus infection, but the mechanisms of this are still unresolved [209, 210]. The interactions between influenza virus and alveolar macrophages of lung airways and the epithelial lining are an important determinant for alveolar disease progression [211]. After that viral antigen expose to the endothelial layer causing amplification of inflammation as endothelial cells work as a major source of pro-inflammatory cytokines that will increase the magnitude and subsequent activation of innate and adaptive immune responses [212]. Ultimately, this involvement leads to a physiological failure and lung becomes unable to perform gas exchange results from multiple mechanisms, including obstruction of the airways, loss of alveolar structure, loss of lung epithelial integrity from direct epithelial cell killing, and degradation of the critical extracellular matrix that maintains the structure of the lung [213]. Approximately 30–40% of the hospitalized patients with laboratory-confirmed influenza are diagnosed with acute pneumonia. The immune response to influenza shares many common pathways with the response to bacteria, thus in some cases virus infection can have a very similar clinical presentation to bacterial sepsis [214]. Central nervous system complications associated with influenza include encephalitis, acute disseminated encephalomyelitis, transverse myelitis,

aseptic meningitis, and Guillain-Barre syndrome [215, 216]. Influenza virus can change in two different ways, the antigenic drift, and the antigenic shift. Antigenic drift can be demonstrated as small genetic changes that happen continually over time as the virus replicates. These small changes produce viruses that are closely related, sharing the similar antigenic properties. But over time these small genetic changes can accumulate and result in antigenically different viruses, thus the flu vaccine composition needs to be updated each year to keep up with evolving viruses [217]. In contrast to antigenic drift, antigenic shift refers to drastic changes in the antigenicity of circulating influenza A viruses, resulting in new hemagglutinin and/or new hemagglutinin and neuraminidase proteins associated with influenza A pandemics. The HA — and sometimes the NA — molecules of pandemic viruses are derived from antigenically diverse animal strains of influenza virus, which can be acquired by human influenza strains through reassortment. While viruses are changing by antigenic drift all the time, antigenic shift happens only occasionally.

1.13 Innate immune responses against Influenza virus (FluV) infection

Influenza virus infections trigger multiple host antiviral responses and innate responses are the only weapons that the host can use to prevent or slow down viral replication early during infection. First few days are most critical in the development of the disease and, without a vigilant system capable of immediately detecting the presence of the pathogen, the virus would spread from the initial focus of upper respiratory tract to the lower airways and deeper tissues, thereby impairing respiratory functions and threatening the host life. A vigorous innate response is essential not only to mount immediate defensive responses, but also to trigger the subsequent production of antibodies and T cells. Pattern recognition receptors (PRRs) recognize infecting agents and trigger cellular antiviral responses, As a major host defense mechanism [218]. Three groups of PRRs: 1) Toll-like receptors (TLRs); 2) RIG-I-like receptors (RLRs); 3) NOD-like receptors (NLRs) play a role in the defense against FluV infections. Among different TLRs, IAV infection recognized by TLR3 [219, 220], which binds to the adaptor molecule TRIF (TIR-domain-containing adapter-interferon-beta) to stimulate IFN-regulated factor 3 and NFκB (nuclear factor-kappa beta); TLR7 [221, 222], which acts through the adaptor protein MYD88 (myeloid differentiation factor 88) and induces IRF7 (interferon regulatory factor 7) and NFκB; and RIG-I [223-225] (Figure 1.12). Upon interaction with viral RNA, the RIG-I helicase domain binds to ATP and then forms a complex with the mitochondrial antiviral signaling protein (MAVS) through its caspase-recruitment domains, leads to the stimulation of IRF3, IRF7, and NFκB. IAV infection can also activate the

inflammasome [226-229], leading to the cleavage and activation of pro-caspase-1, interleukin-1 beta (IL-1β), and IL-18. Activation of diverse PRRs results in the synthesis of IFNα/β, which binds to the IFNα/β (IFNAR) receptor and upregulates JAK/STAT (janus kinase/signal transducer and activator of transcription) pathway. JAK/STAT signaling then stimulates the formation of a transcription factor complex, composed of STAT1, STAT2, and IRF-9, leading to the expression of a number IFN-stimulated genes (ISGs) such as PKR (protein kinase R), OAS (2′-5′-oligoadenylate synthetase), RNaseL (ribonuclease L), Mx, ISG15, IFITM family members, and viperin.

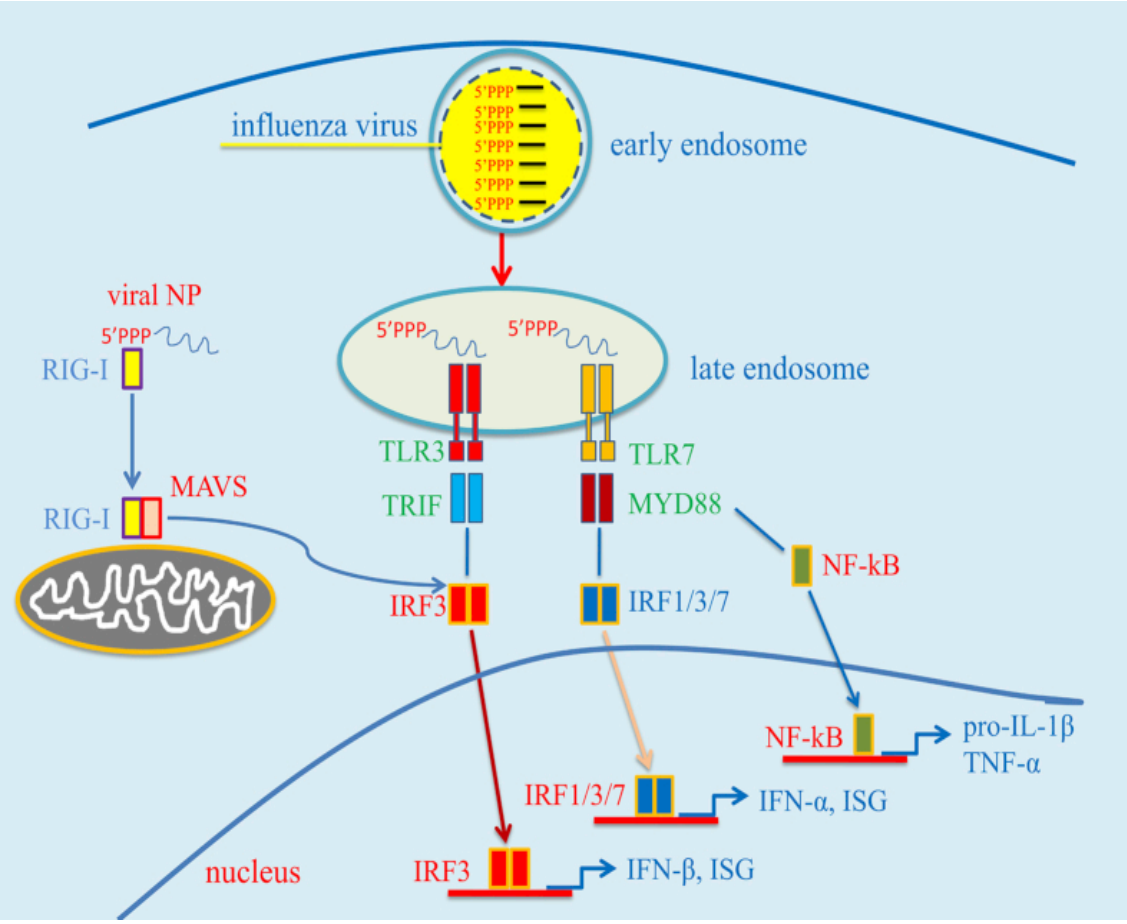

Figure 1.12 Representation of signal transduction pathways activated by influenza virus infection. After cell entry, the genome of influenza virus, consisting of 5′ tri-phosphorylated ssRNA segments, recognized by Toll-like receptors 3 and 7 (TLR3/7) in the endosome. TLR7 signaling induces via the MyD88 adaptor protein and activates NF-κB and IRF1/3/7. NF-κB activates the transcription of pro-inflammatory cytokine genes including IL-1β and TNF-α, while the IRFs induce type I interferons and some ISG. TLR3 activates IRF3 via the adaptor

TRIF. Viral RNA is recognized in the cytosol by RIG-I, leading to the induction of IFN-β and ISG via mitochondrial protein MAVS and IRF3.

Various mechanisms to counter these host anti-viral defense strategies have been evolved by influenza virus primarily through the actions of the NS1 and PB1-F2 proteins. NS1 protein is an RNA-binding protein that binds to the host factors E3 ubiquitin-protein ligase TRIM21 and E3 ubiquitin-protein ligase RNF135, which are required for RIG-I activation after viral RNA recognition. NS1 can also target different signaling proteins involved in JAK-STAT pathway, PKR [230], OAS, RNaseL [231] and ISG15 [232]. In addition to NS1, PB1–F2, which is a short viral nonstructural protein of 87–90 amino acids, generated from an alternative open reading frame present in the PB1 RNA, can suppresses the activation of mitochondrial antiviral-signaling protein (MAVS) [233, 234]. Beside PB1-F2, PB2 (a component of the viral polymerase) can also target MAVS activation [235].

2. Purpose of the study

The hydrolytic monomer of Ge-132, 3-(trihydroxygermyl) propanoic acid (THGP) exhibits diverse biological activities including analgesic, anti-inflammatory, anti-oxidative, anti-melanogenic, immunostimulatory, and antitumorigenic activity. THGP was developed for medical use and has undergone various animal experiments, and multiple clinical evaluations reported that it is safe. Thus, currently it is being used as a supplement in health foods and cosmetics in Japan, China, South Korea, and the United States. However, the detailed mechanisms of the immunomodulatory activities of THGP as well as its effect on innate immune sensor-mediated responses and viral infections remains to be clarified.

Thus, the purpose of this study is

- To elucidate the effect of THGP compound on innate immune signaling pathways and viral replication.

- To explore the mechanisms by which THGP modulate innate immune sensors.

3. Materials and Methods

3.1 Biotic and abiotic materials

All solutions were prepared with deionized water from the Milli-Q Advantage A10 Water Purification System (Millipore, USA). At a resistance of 18.2 MΩ.cm at 25°C and a TOC (Total organic carbon) value below 5 ppb obtained water is valid as desalted and is comparable to double-distilled water (ddH2O).

3.1.1 Instruments

Table 3.1 Instruments used in this study

Device	Producer	Country
CO_2 incubator	Panasonic	Japan
CO_2 incubator (for virus infection)	WAKENBTECH	Japan
Fluorescence microscope IX81	Olympus	Japan
Culture Microscope CK40	Olympus	Japan
ABI StepOnePlusTM Real-Time PCR Systems	Applied Biosystems	USA
ABI Veriti 96 well Thermal Cycler	Applied Biosystems	USA
ABI 3130 Genetic Analyzer	Applied Biosystems	USA
Autoclave HG-50	HIRAYAMA	Japan
Digital electronic balance AT201	METTLER TOLEDO	Switzerland
High speed refrigerated micro centrifuge	KUBOTA	Japan
High speed refrigerated CR21E centrifuge	HITACHI	Japan
Centrifuge without cooling	KOKUSAN	Japan
Vortex mixer	Scientific industries	USA
Synergy 4 Hybrid Multi-Mode Microplate Reader	BioTek	USA
Centro LB 960 Microplate Luminometer	Berthold Technologies	USA
Sunrise Microplate reader	Tecan	Switzerland
Labo-shaker	Ever Seiko	Japan
Incubator shaker	TAITEC	Japan
Rotator	NIPPON THERMONICS	Japan
Agarose Gel chambers	ATTO	Japan
UV Transilluminators	TOYOBO	Japan
NanoVue Plus spectrophotometer	GE Healthcare	UK
Mini-PROTEAN Electrophoresis System	Bio-Rad	USA
Trans-Blot Semi-Dry Transfer Cell	NIHON EIDO	Japan
pH-Meter	Denver Instrument	USA
Freezer (4/-20/-80 oC)	Panasonic	Japan

Clean bench	HITACHI	Japan
Water bath	TAITEC	Japan
Amersham biomolecular imager 680	Cytiva	USA
Pipettes (PIPETMAN P2, P20, P200, P1000)	Gilson	USA
Falcon Express Pipet-Aid	Biosciences	USA

3.1.2 Consumable items

Table 3.2 Consumable items used in this study

Consumable items	Producer	Country
1-200 µl, pipet tips	Wako	Japan
100-1000 µl pipet tips	Corning	USA
Serological pipet (2 ml, 5 ml, 10 ml, 25 ml)	SARSTEDT	France
Violamo tissue culture dishes (100 mm)	AS ONE	Japan
Violamo tissue culture plates (6-, 12-, 24-, 96-well)	AS ONE	Japan
1.5 ml and 2.0 ml microcentrifuge tubes	Corning	USA
15 ml centrifuge tubes	Greiner bio-one	UK
50 ml centrifuge tubes	Thermo Scientific	USA
0.2 mL 8 strip PCR tubes	NIPPON Genetics	Japan
96-well ultraAmp PCR plates	Sorenson BioScience	USA
qPCR adhesive seal	4titude	UK
96-well flat bottom white plates	Corning	USA
Falcon 96 well plates	Corning	USA
0.1-10 µl pipet tips	Wako	Japan
0.2 µm Syringe Filter	Advantec.	Japan
Hydrophobic immobilon-P polyvinylidene fluoride (PVDF) transfer membrane	Merck Millipore	UK

3.1.3 Chemicals and reagents

Table 3.3 Chemicals and reagents used in this study

Chemicals and reagents	Catalog Number	Producer	Country
Acrylamide	Cat# 304-93521	Wako	Japan
N,N'-Methylene-bis-acrylamide	Cat# 110-26-9	Wako	Japan
Agarose	Cat# 312-01193	Wako	Japan
Ammonium persulfate (APS)	Cat# 012-03285	Wako	Japan
Bromophenol blue (BPB)	Cat# 021-02911	Wako	Japan
Sodium Fluoride (NaF)	Cat# 7681-49-4	Wako	Japan
Sodium orthovanadate (Na3VO4)	Cat# 198-09752	Wako	Japan
Magnesium acetate (MgOAc)	Cat# 130-00095	Wako	Japan

Ethylenediaminetetraacetic acid (EDTA)	Cat# 345-01865	Dojindo	Japan
Sodium dodecyl sulfate (SDS)	Cat# 191-07145	Wako	Japan
Sodium acetate (NaOAc)	Cat# 198-01055	Wako	Japan
Polyoxyethylene(10) octylphenyl ether (Triton X-100)	Cat# T8787	Sigma-Aldrich	USA
10 w/v% Polyoxyethylene(20) (Tween-20)	Cat# 167-11515	Wako	Japan
Dithiothreitol (DTT)	Cat# 045-08974	Wako	Japan
Phenylmethanesulfonyl fluoride (PMSF)	Cat# 164-12181	Wako	Japan
Leupeptin	Cat# 4041	PEPTIDE INSTITUTE, INC.	Japan
Tetramethylethylenediamine (TEMED)	Cat# 202-04003	Wako	Japan
4% Paraformaldehyde (PFA)	Cat# 163-20145	Wako	Japan
Tris (hydroxymethyl) aminomethane (Tris)	Cat# 35406-91	Nacalai tesque	Japan
Sodium chloride (NaCl)	Cat# S9888	Sigma-Aldrich	USA
Isopropanol	Cat# 29113-95	Nacalai tesque	Japan
Ethanol (99.5%)	Cat# 14713-53	Nacalai tesque	Japan
Methanol (99.5%)	Cat# 21915-93	Nacalai tesque	Japan
Nonidet P-40 (NP-40)	Cat# 25223-75	Nacalai tesque	Japan
Geneticin (G418)	Cat# 108321-42-2	Nacalai tesque	Japan
Phenol:chloroform:isoamyl alcohol (25:24:1)	Cat# 25967-16	Sigma-Aldrich	USA
Ethidium bromide (EtBr)	Cat# 1239-45-8	Sigma-Aldrich	USA
Polyethyleneglycol 8000 (PEG 8000)	Cat# 81268-250G	Sigma-Aldrich	USA
Coomassie brilliant blue (CBB)	Cat# 031-17922	Sigma-Aldrich	USA
Chloroform	Cat# 07278-00	KANTO CHEMICAL	Japan
$NaHCO_3$	Cat# 37116-00	KANTO CHEMICAL	Japan
Bacto Agar	Cat# 01099-08	BD Biosciences	USA
Bacto Yeast Extract	Cat# 212750	BD Biosciences	USA
Bacto Tryptone	Cat# 211705	BD Biosciences	USA
L-Glutamine	Cat# 56-85-9	Gibco	USA
Dulbecco's Modified Eagle's Medium (DMEM)	Cat# 05919	Nissui Pharmaceutical	Japan
4-(2-hydroxyethyl)-1-piperazineethanesulfonic acid (HEPES)	Cat# 342-01375	Dojindo	Japan
Fetal bovine serum (FBS)	Cat# 10270-106	Life Technologies	USA
Sf-900 II SFM	Cat# 10902-088	Life Technologies	USA
Opti-MEM I reduced-serum medium	Cat# 31985-070	Life Technologies	USA
FuGENE HD transfection reagent	Cat# E231A	Promega	USA
FuGENE 6 transfection reagent	Cat# E269A	Promega	USA
Lipofectamine RNAiMAX Reagent	Cat# 13778-150	Invitrogen	USA

Lipofectamine 2000 Reagent	Cat# 11668-019	Invitrogen	USA
RNaseOUT	Cat# 10777019	Invitrogen	USA
Dynabeads M-280 Streptavidin	Cat# 11205D	Invitrogen	USA
Protein G Sepharose 4 Fast Flow	Cat# 10003D	Invitrogen	USA
Glutathione Sepharose 4B	Cat# 71024800-EG	GE Healthcare	UK
Can Get Signal^{TM}Immunoreaction Enhancer Solution 1	Cat# NKB-201	TOYOBO	Japan
ISOGEN	Cat# 319-90211	Nippon Gene	Japan
Bambanker Cell Freezing Media	Cat# CS-02-001	LYMPHOTEC	Japan
LPS	Cat# tlrl-3pelps	Invivogen	USA
Poly I:C	Cat# 27473201	GE Healthcare	UK
Herring testis DNA (HT-DNA)	Cat# D6898	Sigma-Aldrich	USA
Adenosine 5'-triphosphate disodium salt hydrate (ATP)	Cat# A2383	Sigma-Aldrich	USA
2-Deoxyadenosine 5'-triphosphate disodium salt (deoxy ATP)	Cat# D6500	Sigma-Aldrich	USA
Actinomycin D	Cat# A1410	Sigma-Aldrich	USA
Adenosine	Cat# 58-61-7	Wako	Japan
THGP	Shimada et al., 2018 [96]	Asai Germanium Research Institute, Japan	Japan
Alkaline phosphatase	Cat# 10556602103	Roche	UK
1xMEM Amino Acids Solution	Cat# 11130-051	Gibco	USA
Penicillin Streptomycin Solution	Cat# 168-23191	Wako	Japan
Albumin, from Bovine Serum (BSA)	Cat# 017-15124	Wako	Japan
Slowfade Gold antifade reagent	Cat# S36936	Invitrogen	USA
Hoechst 33342	Cat# H1399	Invitrogen	USA
Glycine	Cat# G8898	Sigma-Aldrich	USA
TOYOPEARL AF-Epoxy-650	Cat# 50-851-257	Tosoh Bioscience	USA
Mayer's hematoxylin	Cat# 131-09665	Wako	Japan
1% Eosin Y Solution	Cat# 051-06515	Wako	Japan
Protein-G Dynabeads	Cat# 10003D	Invitrogen	USA
0.25% w/v Trypsin	Cat# 201-16945	Wako	Japan

3.1.4 Kits

Table 3.4 Kits used in this study

Kits	Producer	Country
GenElute HP Plasmid Miniprep Kit	Sigma	USA
PureLink HiPure Plasmid Maxiprep Kit	Invitrogen	USA
Wizard SV Gel and PCR Clean-Up System	Promega	USA

ReverTra Ace qPCR RT kit	TOYOBO	Japan
DNase I (Amplification Grade)	Invitrogen	USA
SyBr premix Ex Taq (Tli RNaseH Plus)	TaKaRa	Japan
MEGAscript Kit T7	Ambion	USA
SYBR Gold Nucleic Acid Gel Stain Kit	Invitrogen	USA
Bac-to-Bac baculovirus expression system	Invitrogen	USA
BCA Protein Assay Kit	Pierce	USA
Pierce Western Blotting Substrate Plus	Thermo Scientific	USA
BigDye Terminator v3.1 Cycle Sequencing Kit	Applied Biosystems	USA
BigDye Xterminator Purification Kit	Applied Biosystems	USA
Cell Counting Kit-8	Dojin	Japan
VeriKine-HSTM Mouse IFN-β Serum ELISA kit	PBL	USA
Dual-Luciferase Reporter Assay system	Promega	USA
Label IT® Nucleic Acid Labeling Kit, Biotin for the preparation of biotin-3pRNA	Mirus Bio	USA
Label IT® Nucleic Acid Labeling Kit, Cy5 for the preparation of Cy5-3pRNA	Mirus Bio	USA

3.1.5 Enzymes and antibodies

Table 3.5 Enzymes and antibodies used in this study

Enzymes and antibodies	Producer	Country
Proteases K	Life Technologies	USA
Deoxyribonuclease I (DNase I)	Promega	USA
Ribonuclease A (RNase A)	Life Technologies	USA
Precision protease	GE Healthcare	UK
Restriction enzymes	TaKaRa	Japan
Anti-Flag (M2) antibody (mouse monoclonal)	Sigma-Aldrich	USA
Anti-beta-actin (AC-15) antibody (mouse monoclonal)	Sigma-Aldrich	USA
Anti-IRF-3 antibody (rabbit polyclonal)	Active Motif	USA
Anti-RIG-I (D14G6) antibody (rabbit monoclonal)	Cell Signaling	USA
Anti-MDA5 (D74E4) antibody (rabbit monoclonal)	Cell Signaling	USA
Anti-phospho-Ser396 IRF-3 (4D4G) antibody (rabbit monoclonal)	Cell Signaling	USA
Anti-TBK1 (EP611Y) antibody (rabbit monoclonal)	Abcam	UK
Anti-phospho-Ser172 TBK1 (D52C2) antibody (rabbit monoclonal)	Cell Signaling	USA
Anti-MAVS antibody (rabbit polyclonal)	Cell Signaling	USA
Anti-GST (B-14) antibody(mouse monoclonal)	Santa Cruz	USA
Rabbit/Mouse/Goat control IgG antibody	Santa Cruz	USA
Anti-goat IgG HRP-conjugated secondary antibody	Santa Cruz	USA

Anti-rat/mouse/rabbit IgG HRP-conjugated secondary antibodies	GE Healthcare	UK
Alexa Fluor 488 chicken polyclonal anti-rabbit IgG	Invitrogen	USA

3.1.6 Solutions

Table 3.6 Solutions used in this study

Solution	Component
Running buffer	25 mM Tris, 192 mM Glycine, 0.1% SDS.
Transfer buffer	25 mM Tris, 192 mM Glicine, 0.037% SDS, 20% methnol.
TBST buffer	20 mM Tris, 150 mM NaCl, 0.1% Tween-20, pH 7.4.
4x SDS sample buffer	40% Glycerol, 200 mM Tris pH 6.8, 8% SDS, 4% beta-mercaptoethanol, 0.08% bromophenol blue, 60 mM EDTA.
4x native PAGE sample buffer	25 mM Tris pH 6.8, 0.02% bromophenol blue, 60% glycerol.
1x Phosphate-buffered saline (PBS)	137 mM NaCl, 2.7 mM KCl, 10 mM Na_2HPO_4, 2 mM KH_2PO_4.
DMEM medium	DMEM with 10% FBS, 3.4 mM L-glutamine, 10% $NaHCO_3$.
Sf9 culture medium	Sf-900 II SFM with 5% FBS, 25 μg/ml gentamycin.
Lysogeny broth (LB) medium	1.0% Tryptone, 0.5% Yeast Extract, 1.0% NaCl, pH 7.0.

3.1.7 Oligonucleotides

Table 3.7 Sequences of primers for qPCR in this study

Gene	Forward (5'→3')	Reverse (5'→3')
IFNB1 (human)	ATGACCAACAAGTGTCTCCTCC	GCTCATGGAAAGAGCTGTAGTG
Ifnb1 (mouse)	GAGCTCCAAGAAAGGACGAAC	GGCAGTGTAACTCTTCTGTAT
Il-6 (mouse)	TAGTCCTTCCTACCCCAATTTCC	TTGGTCCTTAGCCACTCCTTC
Tnfa (mouse)	CCCTCACACTCAGATCATCTTCT	GCTACGACGTGGGCTACAG
GAPDH (human)	CATGAGAAGTATGACAACAGCCT	AGTCCTTCCACGATACCAAAGT
Gapdh (mouse)	AGGTCGGTGTGAACGGATTTG	TGTAGACCATGTAGTTGAGGTCA
Firefly luciferase	GTGGTGTGCAGCGAGAATAG	CGCTCGTTGTAGATGTCGTTAG
FluV PR8 NP RNA	GATTGGTGGAATTGGACGAT	AGAGCACCATTCTCTCTATT

Table 3.8 DNA oligonucleotides for 3pRNA

Name	Sequence (5'→3')	Description
3pRNA	**Sense:** TAATACGACTCACTATAGGGAAACTAAAAGGGAGAAGTGAAAGTG **Antisense:** CACTTTCACTTCTCCCTTTT AGTTTCCCTATAGTGAGTCGTATTA	For *in vitro* transcription

Table 3.9 gRNA Sequence of MAVS gene

Gene	gRNA sequence
MAVS (human)	5'-ATTGCGGCAGATATACTTAT-3'

3.1.8 Plasmids

(1) pIRM-3HA-RIG-I, pIRM-3HA-MAVS, pIRM-3HA-MDA5, pIRM-3HA-TRIF, pCXN2-Flag-TBK-1and pCAGGS-Flag-STING plasmids were constructed by inserting the full length of human RIG-I, MDA5, TRIF, TBK1 and STING open reading frames (ORFs) into the *Xho*I and *Not*I sites of pIRM-3HA, pCXN2-Flag and pCAGGS-YFP vectors (kindly provided by Dr. A. Miyawaki, Laboratory for Cell Function Dynamics, Brain Science Institute, RIKEN, Saitama, Japan), as previously reported [236-239]. The generated plasmids were used for overexpression experiments.

(2) pcDNA3.1(-)IRF-3/5D-FLAG for the constitutive active form of IRF-3, was provided by T. Kubota as previously reported [240].

(3) pISRE-Luc was purchased from Clontech and p-125Luc provided by T. Fujita together with expression vector or control vector as previously reported [238]. For the FluV luciferase activity based mini genome assay the expression plasmids for WSN-PB2, -PB1, -PA, and -NP, pPolI-NP(0)luc2(0) which expresses the firefly luciferase gene between the noncoding regions of the WSN-NP gene were provided by Y. Kawaoka as described previously [241].

(4) pX330 was which was a gift from F. Zhang (Addgene plasmid #42230, Watertown, MA) [242].

(5) pFAST-Bac-GST-RIG-I WT plasmid was generated by cloning the cDNA of RIG-I WT into pFAST-Bac-GST vector, which was derived from inserting a Glutathione S-transferase (GST) tag into pFAST-Bac vector (Invitrogen). The generated plasmid was used for expression of GST-tagged RIG-I WT.

3.1.9 Mice and virus

MAVS KO mice were obtained from Jackson Laboratory. Mice were infected with FluV (A/Puerto Rico/8/1934 H1N1 strain, 1 x 10^5 pfu/mice; i.n.). THGP was dissolved in PBS. Mice were pretreated with THGP (50 mg/kg or 100 mg/kg) by i.n. injection. At 3 h after treatment, mice were infected with FluV (i.n.). At indicated time after infection, the lung tissues were used for further experiments. These animal experiments were approved by the committee reviews of Hokkaido University.

3.1.10 Cells

RAW 264.7, HEK293T, A549 and MDCK cells were purchased from ATCC. All cells were maintained in culture medium as recommended by ATCC at 37 °C in a 5% CO2-incubator.

To generate MAVS KO A549 cells, we used pX330 vector which was a gift from F. Zhang (Addgene plasmid #42230). The plasmid containing guide RNA against MAVS gene (5'-ATTGCGGCAGATATACTTAT-3') was transfected and puromycin-resistant A549 cells were cloned by limiting dilution. The genomic sequences of clones were verified by DNA sequencing, in addition, the absence of MAVS protein was also confirmed by using western blotting. Cells were assayed by using 0.4% trypan blue uptake (Invitrogen) for measuring cell growth. Sf9 for recombinant protein expression was purchased from Invitrogen (USA) and cultured at 28°C in Sf9 culture medium shown in Table 3.6. E. coli DH5α competent cells were purchased from TaKaRa (Japan) and growth in LB medium as shown in Table 3.6.

3.1.11 Viruses

FluV(A/Puerto Rico/8/1934 H1N1 strain), VSV (New Jersey strain) and EMCV were used as previously reported [237]. All viruses were stocked at -80 °C until use for infection.

3.2 Methods

3.2.1 Preparation of THGP

1 g of Ge-132 (Asai Germanium Research Institute, Japan) was neutralized with sodium hydroxide, dissolved in sterilized water, and adjusted to pH 7.0 with hydrochloric acid. After measuring up to 10 mL, sterilization was performed with a 0.22 μm membrane filter, and THGP concentrations of 100 mg / ml, 10 mg / ml, 1 mg / ml, and 0.1 mg / ml were prepared.

3.2.2 Preparation of 3pRNA, MAMPs stimulation and transfection

5'-triphosphorylated RNA (3pRNA) oligo nucleotides shown in Table 3.9 which containing T7 promoter sequence were annealed and used as templates (300 ng template in 20 μl reaction mixture) for *in vitro* transcription under the control of the T7 promoter with MEGAscript kit following the manufacturer's protocol, the transcribed RNAs were purified by Isogen reagent. Stimulation with 3pRNA, polyI:C, and HT-DNA were conducted using OPTI-MEM (Invitrogen) and Lipofectamine 2000 Reagent (Invitrogen) according to the product protocol. The final concentration of 3pRNA, polyI:C, and HT-DNA were 1 μg/ml, 1 μg/ml, and 4 μg/ml, respectively. LPS (invivogen) derived from E. coli O111: B4 was mixed with the culture solution to a final concentration of 100 ng / ml, and stimulation was performed.

3.2.3 Viral infection

In the case of FluV infection, the culture medium was replaced with DMEM without FBS containing 0.0005% trypsin and PR8 was infected at 1.0 multiplicity of infection (MOI). VSV was infected at 0.1 MOI. In the case of EMCV, the culture media was changed to DMEM

containing no FBS, and the EMCV was infected at 1.0 MOI. After 1 h, FBS was added to the culture medium to a final concentration of 10%. SARS-CoV-2 RNA was prepared from culture medium of Vero cells infected with SARS-CoV-2.

3.2.4 ELISA

The levels of mouse IFN-β protein in culture supernatants were measured by using the VeriKine-HS Mouse IFN-β Serum ELISA kit (PBL; 42410) and following the manufacturer's protocol. This ELISA is for the detection of mouse IFN-β protein with a minimum detection limit of 0.94 pg/ml. There is no cross reactivity or interference detected according to the product specification of the vendor.

3.2.5 Plaque-forming assay

RAW264.7 cells were infected with FluV for 24 h, culture media were collected and serially diluted from 10^{-1} to 10^{-6}. MDCK cells were infected. After 1 h infection, cells were overlayed with MEM/Bacto Agar/trypsin mixture (1×MEM (Gibco), 0.3% BSA, 0.28% $NaHCO_3$, 1×MEM Amino Acids Solution (Gibco), 1×MEM Vitamine Liquid (Gibco), 2 mM L-Glutamine, 1×Penicillin Streptomycin Solution (Sigma), 0.0005% trypsin, 0.8% BactoAgar). After 2 days, the plaque number was counted.

3.2.6 qRT-PCR

RNA was collected by using guanidine thiocyanate phenol chloroform method using ISOGEN (Nippon gene) and dissolved in DNase and RNase free water. DNase I (Invitrogen) was added to the extracted RNA (1μg) and reacted at 25°C for 15 min to perform DNase treatment to degrade the genomic DNA. After the reaction, DNase I was inactivated by adding 1 μl of 25 mM EDTA and reacting at 65°C for 10 min. Subsequently, RNA was reverse transcribed using ReverTra Ace qPCR RT Kit (Toyobo), 7 μl of RNA was mixed with 2 μl RT Buffer, 0.5 μl Enzyme mix and 0.5 μl primer mix to synthesize cDNA. The reverse transcribed cDNA sample was added 40 μl ddH_2O and stocked at -20℃ or performed real-time qPCR analysis immediately. Quantitative PCR was performed by the intercalator method using SYBR Premix Ex Taq ™ (Takara), quantified by the StepOnePlus™ Real-Time PCR System (Applied Biosystems), and analyzed by the ΔΔCt method. The reaction conditions were 40 cycles of initial denaturation at 95 ° C. for 10 seconds, followed by two steps of denaturation reaction at 95 ° C. for 5 seconds, annealing at 60 ° C. for 30 seconds, and extension reaction. Gapdh was used as an internal standard. Detailed information about the primers used here is shown in Table 3.7.

3.2.7 Creation of tagged 3pRNA

Biotinylated 3pRNA and Cy5-3pRNA were prepared according to the product protocol of Label IT® Biotin Labeling Kit, Biotin (Mirus) or Label IT® Nucleic Acid Labeling Kit, Cy5 (Mirus).

3.2.8 Immunofluorescence

RAW264.7 cells seeded on a coverslip (Matsunami Glass) were treated with THGP for 24 h, stimulated with Cy5-3pRNA, and incubate at 37°C for 2 h. Cells were fixed with 4% paraformaldehyde/phosphate buffer (Wako) for 20 min, permeabilized with 0.2% Triton-X for 10 min at room temperature, permeabilized with 0.2% Triton-X for 15 minutes at room temperature, permeabilized with 0.2% Triton-X for 15 minutes at room temperature and blocked with 1% BSA in PBS. The coverslips were incubated for 1 h in primary antibody diluted in 1% BSA in PBS. Following washing with PBS, the coverslips were incubated for 1 h in appropriate secondary antibodies conjugated with Alexa Fluor 488/594 (Invitrogen) diluted in 1% BSA in PBS. Subsequently, the coverslips were mounted in Slowfade Gold antifade reagent (Invitrogen) with Hoechst 33342 (Invitrogen). Confocal microscopy was performed with an IX-81S confocal microscope (Olympus, Tokyo, Japan). More than 30 cells in each condition were randomly chosen and representative images are shown in Figures.

3.2.9 FACS analysis

The cells treated with Cy5-3pRNA in the presence of THGP were suspended in 2% FBS-PBS and transferred to a tube with a cell strainer cap (Falcon). The fluorescence in the cells was measured with FACS CantoII (BD), and a total of 20,000 cells were counted, and the proportion of cells containing the fluorescent dye was calculated.

3.2.10 Recombinant RIG-I protein

GST-tagged RIG-I WT was expressed in Sf9 cells according to the manufacturer's instructions for Bac-to-Bac baculovirus expression system. Briefly, pFAST-Bac-GST-RIG-I WT vector was transformed into DH10Bac *E. coli* cells, and the recombinant bacmid DNA was isolated and transfected into Sf9 cells, after 3 days transfection, the produced recombinant baculovirus particles were collected for second time infection of Sf9 cells. After 3 days infection, the Sf9 cells were harvested by centrifugation (3,000 rpm for 10 min at 4°C), resuspended in lysis buffer (1% Triton X-100, 50 mM Tris, 150 mM NaCl, 1 mM EDTA, and 1 mM PMSF [pH 8.0]), and lysed by sonication. The lysate was incubated on ice for 30 min and then centrifuged at 12,000 rpm for 10 min at 4 °C, the supernatant was incubated with Glutathione Sepharose 4B beads for 2 hours at 4 °C, then the beads were washed 3 times with

wash buffer (0.1% Triton X-100, 50 mM Tris, 300 mM NaCl, 1 mM EDTA [pH 8.0]) and wash one time with cleavage buffer (50 mM Tris, 150 mM NaCl, 1 mM EDTA, 1 mM DTT [pH 7.5]), the GST tags were cleaved from recombinant GST protein by using Precision protease in cleavage buffer overnight at 4 °C. The concentration of cleaved recombinant RIG-I WT was measured by using BCA Protein Assay Kit, and the purity of recombinant protein was higher than 95% as judged by CBB staining.

3.2.11 *In vitro* RNA pull down assay

After incubation of indicated concentrations of THGP and biotinylated 3pRNA (100 ng) in lysis buffer (20 mM HEPES, 150 mM NaCl, 1 mM EDTA, 0.1% NP-40, 1 mM PMSF) for 30 min at room temperature, 2 μg of GST-RIG-I was added, and further mixed by inverting at room temperature for 1 h. Next, Dynabeads M-280 Streptavidin (Invitrogen) were added and mixed by inverting for 1 h at room temperature and washed 3 times with wash buffer (20 mM HEPES, 150 mM NaCl, 1 mM EDTA, 0.1% NP-40). Then, 20 μl of 2 × sample buffer was added and then boiled at 100 °C. for 5 min, then the sample was subjected to western blotting.

3.2.12 Preparation of protein

Whole cell lysate used for SDS-PAGE (polyacrylamide gel electrophoresis) analysis was prepared by lysing cells in lysis buffer (0.5%SDS/1×PBS), for detection of phosphorylation state of target protein, 10 mM NaF and 1 mM Na_3VO_4 were added in the lysis buffer. The cell lysate was further disrupted by sonic disintegration and then heat at 100 °C for 10 min. The protein concentration was measured by using BCA Protein Assay Kit.

3.2.13 SDS-PAGE and Western-blotting

Protein samples were mixed with 4x SDS sample buffer (As shown in Table 3.6) and boiled for 10 min at 100°C. The indicated amount of protein was applied to SDS-PAGE gel. As a standard for protein size, a pre-stained protein marker was added. After proteins were separated by electrophoresis, then transferred with transfer buffer (As shown in Table 3.6) from the SDS-PAGE gel onto a methanol-activated PVDF membrane using a semi-dry transfer cell. The amperage was calculated with the following formula: 2.4 mA/cm^2 of the gel for 70 min transfer. After protein transfer the membrane was blocked in blocking solution (5% w/v skim milk in TBST buffer. As for the detection of phosphorylation state of target protein, 2% BSA in TBST buffer with 1 mM Na_3VO_4 was used for blocking) for 1 hour at RT (room temperature) and probed over night at 4°C with the indicated antibody (As shown in Table 3.5) in Immunoreaction Enhancer Solution 1. After 3 times wash with TBST 5 min each, the respective

secondary HRP-conjugated antibody (1:5000) was added in Immunoreaction Enhancer Solution 2 and incubated for 1 hour at RT. Membranes were again washed 3 times, 15 min each with TBST buffer. The detection was performed with the Pierce Western Blotting Substrate Plus detection kit by using Amersham biomolecular imager 680 system.

3.2.14 Binding assay using THGP immobilized column

For preparation of THGP-conjugated beads, THGP was immobilized with TOYOPEARL AF-Epoxy-650 (Tosoh Bioscience, Japan) via ring-cleavage reaction between epoxy group and amino acid derivative of THGP. Unreacted epoxy group was inactivated with mono ethanolamine. As for binding assay, the beads were pretreated with 0.5 M NaOH, and washed with RNase-free water until the pH reached 7.0. 3pRNA, polyI:C, or HT-DNA (2μg each) were added to a THGP-immobilized column or control beads, the mixture was incubated with gentle rotation at room temperature for 60 min, and centrifuged for 5 min. The beads were washed 3 times with 100% methanol and eluted with 0.5 M HCl. The concentration of the nucleic acids was measured using a micro ultraviolet visible spectrophotometer Q5000 (Tomy).

3.2.15 Luciferase assay

As for the measurement of promoter activity of IFN-β and IFN-stimulated response element (ISRE), cells seeded on 24-well plates were transiently co-transfected with luciferase reporter plasmids (100 ng each of pISRE-Luc (Clontech), and p-125Luc (provided by T. Fujita)), together with expression vector or control vector. As for the FluV luciferase activity based mini genome assay for the measurement of FluV polymerase activity, cells seeded on 24-well plates were co-transfected with expression plasmids for WSN-PB2, -PB1, -PA, and -NP (50 ng each); pPolI-NP(0)luc2(0) (2.5 ng), which expresses the firefly luciferase gene between the noncoding regions of the WSN-NP gene (provided by Y. Kawaoka), as described previously. As an internal control, 5 ng renilla luciferase reporter plasmid (pTK-RL; TOYO INK) was transfected simultaneously. At 24 h after transfection, cells were stimulated with indicated concentrations of THGP for 24 h and luciferase activity was measured with the Dual-Luciferase Reporter Assay system (Promega), and a photon counter (Centro LB 960; BERTHOLD).

3.2.16 RNA immunoprecipitation assay

A549 MAVS KO cells were lysed with buffer A (20 mM HEPES, 150 mM NaCl, 1 mM EDTA, 1% NP-40, 1 mM PMSF, 1 mM DTT, 1 μg/ml leupeptin, 100 U/ml RNase OUT (Invitrogen) [pH 7.3]) and 20 μl of the supernatant was saved as input for qRT-PCR analysis. Anti-Flag or control IgG were added to cell lysates. After 2 h incubation with the antibody, as indicated for immunoprecipitation at 4 °C with gentle rotation, Protein-G Dynabeads

(Invitrogen) were added, and further incubated for 1 h with gentle shaking. Beads were washed three times with wash buffer (20 mM HEPES, 150 mM NaCl, 1 mM EDTA, 0.5% NP-40 [pH 7.3]). The precipitated RNAs were eluted with Isogen and analyzed by qRT-PCR. The amount of immunoprecipitated RNAs is represented as the percentile of the amount of input RNA (%input).

3.2.17 Plasmid extraction

All the plasmids used in this study were firstly purified by GenElute HP Plasmid Miniprep Kit for small-scale extraction following the manufacturer's protocol, and after the sequences were confirmed by sequencing using the BigDye Terminator v3.1 sequencing kit, large-scale extraction was performed by using PureLink HiPure Plasmid Maxiprep Kit according to the manufacturer's protocol. All of plasmids were dissolved in TE (tris-EDTA) buffer and stored at -20 °C until use.

3.2.18 Mice experiment.

MAVS KO mice (#008634) mice were obtained from Jackson Laboratory and and C57BL/6J were obtained from Crea Japan. Mice were pretreated with THGP (50 or 100 mg/kg) by i.n. injection at 3 h before infection. Mice were infected with FluV (A/Puerto Rico/8/1934 H1N1 strain, 1 x 10^5 pfu/mice; i.n.). At indicated time after infection, the lung tissues were used for further experiments. These animal experiments were approved by the committee reviews of Hokkaido University. For Hematoxylin-Eosin Stain, formalin fixed paraffin embedded lung tissues were stained with Mayer's hematoxylin (Wako) and 1% Eosin Y (Wako). For determining survival rate, C57BL/6J mice were treated with THGP (50 mg/kg) once per two days.

3.2.19 ^{1}H-NMR.

The ^{1}H-NMR spectrum of each sample was measured using a Mercury Plus 300 MHz instrument (Agilent Technologies Inc.) as described previously [98].

4. Results

4.1 THGP does not affect cell growth and activate IFN-β itself

Previously it has already been reported that THGP does not have any toxic effect, thus I first examined whether THGP can affect cell viability. Two cell lines, Raw 264.7 (a murine macrophage cell line) and HEK 293T (human embryonic kidney cell line) were used to determine the proliferation of cells by the trypan blue method. Raw 264.7 (Figure 4.1A) and HEK293T (Figure 4.1B) cells were counted at 0 hour, 24 hours, 48 hours, and 72 hours after the treatment of THGP with the indicated concentrations of 0, 2, 20, 200, 2000 µg/ml. The graphical representation was indicating that none of the mentioned concentrations affected cell growth and viability and suggesting that there was no cytotoxicity of THGP up to the highest concentration of 2000 µg/ml. This result was consistent with the previous reports [99-102], which also have shown that THGP is safe. THGP has shown immunomodulatory effects and the induction of interferons (IFNs) is known to the hallmark of innate immune responses, so I tested the effect of THGP on the expression of Ifn-β mRNA in Raw264.7 cells. After stimulation of Raw264.7 cells by THGP for 24 hours with the indicated concentrations of 0, 2, 20, 200, 2000 µg/ml, RNA was isolated to check the Ifn-β mRNA by quantitative qRT-PCR (Figure 4.1C), which revealed that THGP did not influence Ifn-β mRNA induction by itself where as 3pRNA (prepared as positive control) elevated Ifn-β mRNA level about 10 times compared to mock sample.

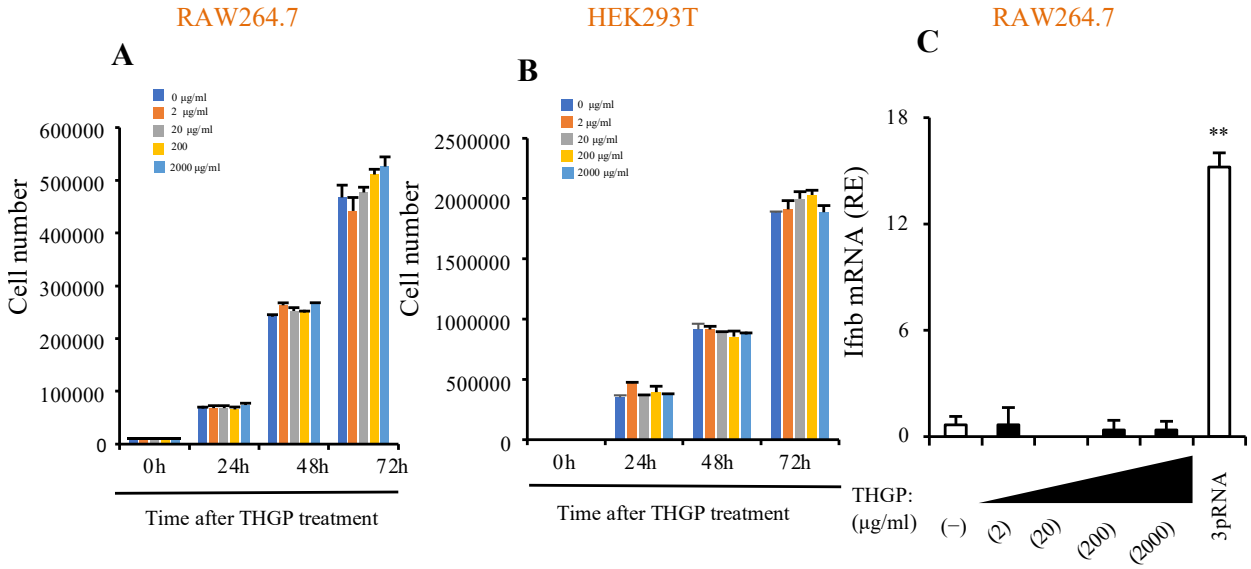

Figure 4.1 Effect of THGP on cell growth and IFN-β mRNA induction. (A, B) The cell number of RAW264.7 (A) and HEK293T (B) at indicated time after THGP treatment. Data are presented as mean and s.d. (n = 3) and are representative of at least three independent experiments. (C) qRT-PCR analysis of Ifnb mRNA levels at 24 h after stimulation with indicated concentrations (0, 2, 20, 200, 2000 μg/ml) of THGP and 3pRNA as positive control in RAW 264.7 cells. **P < 0.01 vs control. NS, not significant.

4.2 THGP represses IFN induction in response to 3pRNA but not Poly I:C, HT-DNA, and LPS both at RNA and protein levels

Although it is reported that THGP may regulate the innate immune system, the detailed mechanism of the immunoregulatory activities of THGP as well as its effect on innate immune responses remains to be clarified. As the activation of pattern-recognition receptors (PRRs) mediated immune signaling pathways is the first critical step that initiates the innate immune responses against invasion by a variety of microbes, I examined the effect of THGP on PRR-mediated innate immune signaling pathways. RAW264.7 cells were pretreated with THGP with the indicated concentrations of 0, 2, 20, 200 μg/ml for 24hrs and quantitative qRT-PCR was done to analyze Ifn-β mRNA induction at 8 hours upon stimulation with 5'-triphosphate RNA (3pRNA) (Figure 4.2A), Polyinosinic:polycytidylic acid (polyI:C) (Figure 4.2B), herring testis-DNA (HT-DNA) (Figure 4.2C), and lipopolysaccharide (LPS) (Figure 4.2D), which are known as ligands for RIG-I, MDA5, cGAS, and TLR4, respectively. In addition, the IFN-β protein levels in Raw264.7 cells pretreated with THGP with the indicated concentrations of 0, 2, 20, 200 μg/ml at 24hrs after stimulation with 3pRNA (Figure 4.2E), polyI:C (Figure 4.2F), HT-DNA (Figure 4.2G), and LPS (Figure 4.2H) were also measured by enzyme-linked immunosorbent assay (ELISA). These results suggested that treatment with THGP inhibited Ifn-β response induced by 3pRNA but not the other ligands in a dose-dependent manner.

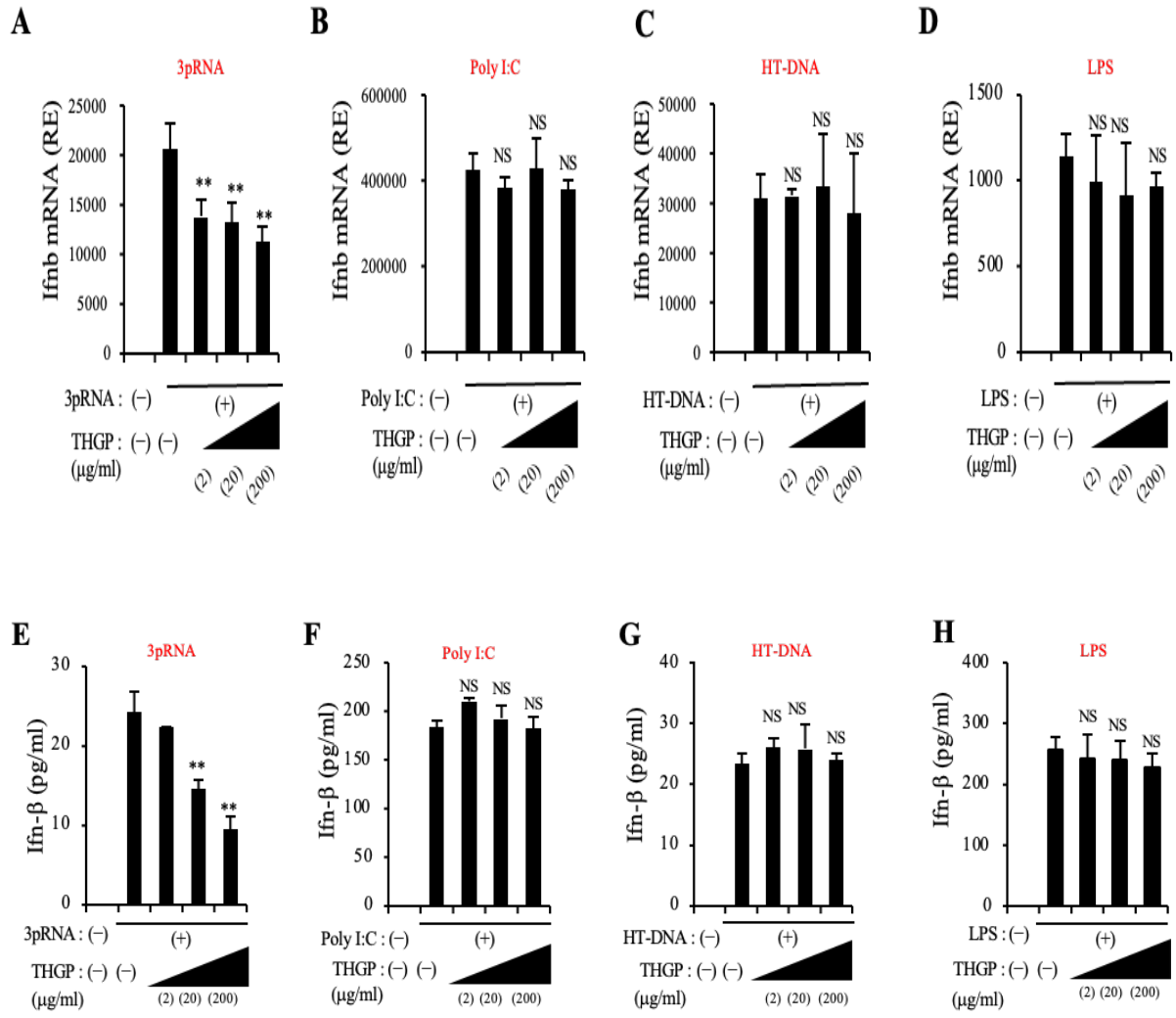

Figure 4.2 Suppression of IFN induction in response to 3pRNA but not Poly I:C, HT-DNA, and LPS. (A-D) Quantitative RT-PCR (qRT-PCR) analysis of Ifnb1 mRNA levels at 8 h after stimulation with control or 3pRNA (A), poly I:C (B), HT-DNA (C), and 2 h after stimulation with LPS (D) in RAW264.7 cells pretreated with indicated concentrations (0, 2, 20, 200 μg/ml) of THGP. (E-H) ELISA of Ifn-β levels at 24 h after stimulation with 3pRNA (E), polyI:C (F), HT-DNA (G), and LPS (H) in RAW264.7 cells pretreated with indicated concentrations of THGP for 24 h. Data are presented as mean and s.d. (n = 3). **P < 0.01 vs control. NS, not significant.

4.3 The activation of TBK-1 and IRF-3 has been suppressed by THGP in response to 3pRNA, but not poly I:C, HT-DNA, and LPS

To determine whether THGP can activate the downstream signaling proteins such as TANK-binding kinase 1 (TBK1) and Interferon Regulatory Factor 3 (IRF-3) of PRR-mediated

immune response after binding of ligands with their respective PRRs, whole lysates of Raw264.7 cells pretreated with THGP (200 μg/ml) were collected at 0 hour, 2hours, 3 hours and 4 hours after stimulation with 3pRNA (Figure 4.3A), polyI;C (Figure 4.3B), HT-DNA (Figure 4.3C) and LPS (Figure 4.3D) and immunoblotting was performed with anti-pTBK1, anti-TBK1, anti-pIRF-3, anti-IRF-3, and anti β-actin antibodies. This WB data represented that treatment with THGP also suppressed the phosphorylation of both TBK1 and IRF-3 induced by 3pRNA, but not the other ligands suggesting that THGP have a suppressive effect on 3pRNA-induced activation of RIG-I pathway.

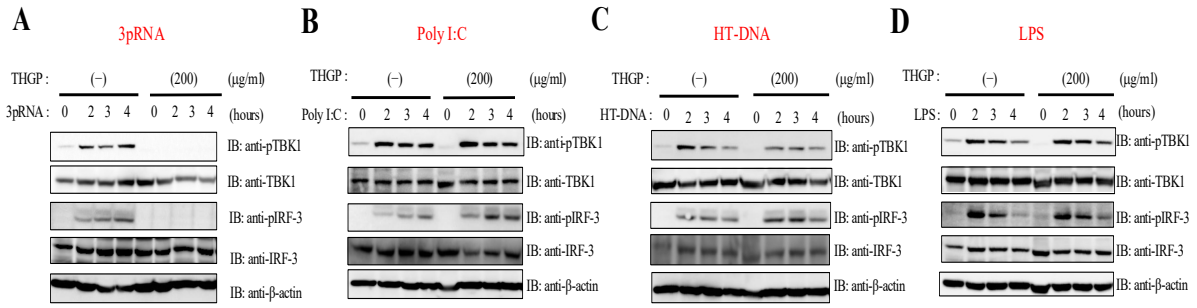

Figure 4.3 Repression of TBK-1 and IRF-3 activation in response to 3pRNA but not poly I:C, HT-DNA, and LPS by THGP. (A-D) Whole cell lysates at indicated time after stimulation with 3pRNA (A), polyI:C (B), HT-DNA(C) and LPS (D) in RAW264.7 cells pretreated with THGP were prepared, and subjected to immunoblotting with anti-pTBK1, TBK1, pIRF-3, IRF-3, and β-actin antibodies. **P < 0.01 vs control. NS, not significant. Data are representative of at least three independent experiments.

4.4 Treatment with THGP results in dose dependent inhibition of IFN, IL-6 and TNF-a induction in response to FluV, VSV but not EMCV infection

Next, I investigated whether THGP affect the activation of RIG-I pathway during viral infections. To address this, I tested the effect of THGP on cytokine responses to infections with influenza virus (FluV) [243] or vesicular stomatitis (VSV) [244], which are known to be detected by RIG-I and EMCV, which is reported to be recognized mainly by MDA5 rather than RIG-I [223]. Raw264.7 cells were pretreated with THGP with the indicated concentrations of 0, 2, 20, 200, 2000 μg/ml for 24 hours and RNA was collected at 8 hours after infections with FluV, VSV, and EMCV to check the level of Ifnb, Il6, and Tnfa mRNA. Consistent with the result shown in Figure 5.2, Ifn-β mRNA induction in response to FluV (Figure 4.4A) or VSV

(Figure 4.4B) infection was suppressed by treatment with THGP in a dose-dependent manner, while THGP did not affect Ifnb induction in response to EMCV infection (Figure 4.4C). Similar findings were also obtained for other cytokines induced by innate immune sensors, such as IL-6 (Figures 4.4D-F), and TNF-α (Figures 4.4G-I). These results all together suggested that THGP can suppress cytokine responses downstream of RIG-I but not MDA5 pathway upon viral infections.

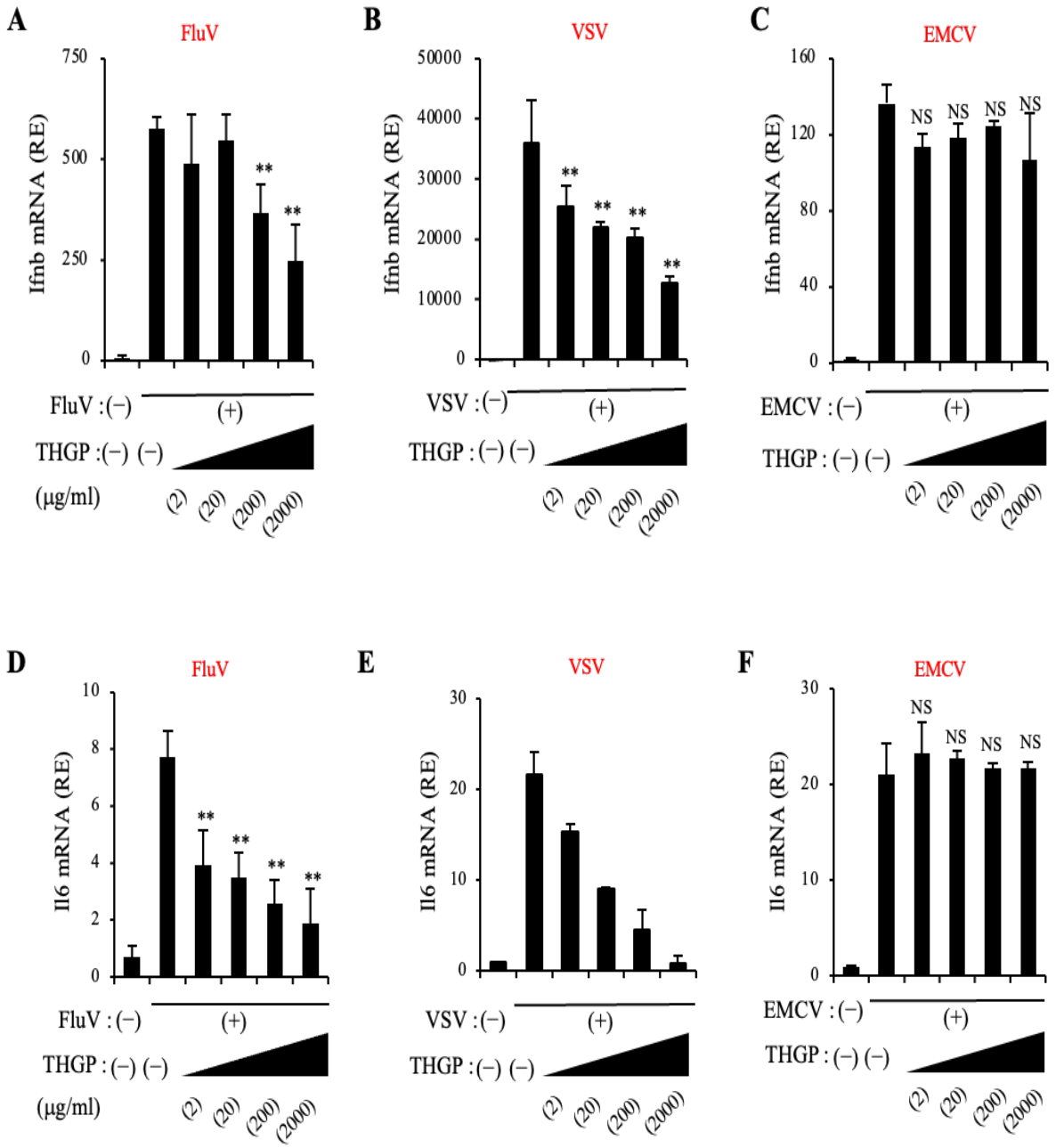

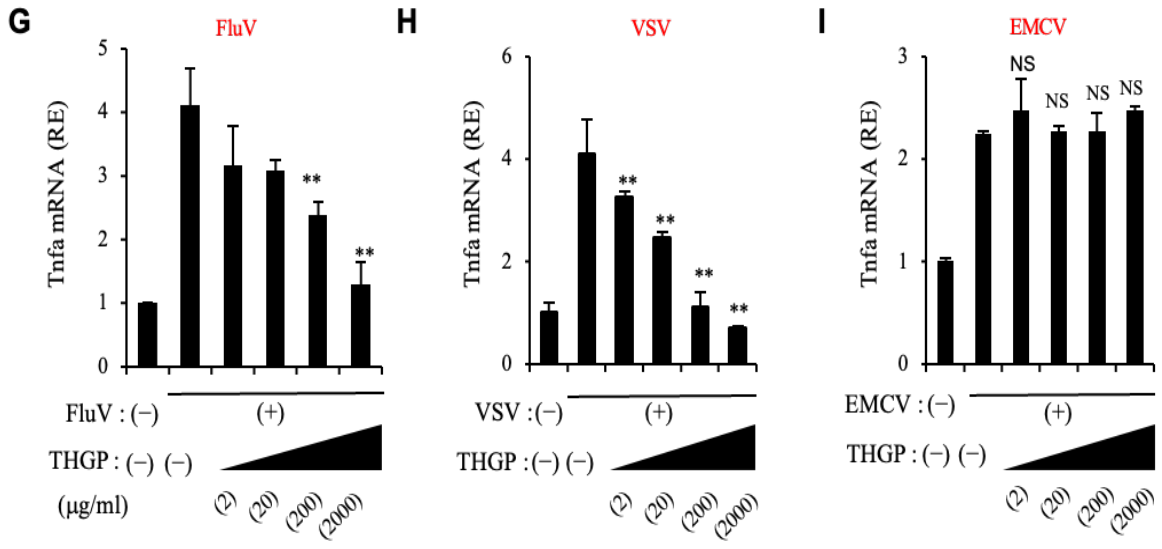

Figure 4.4 THGP reduces IFN, IL-6 and TNF-a induction in response to IAV, VSV but not EMCV infection. (A-I) qRT-PCR analysis of Ifnb (A-C), Il6 (D-F), and Tnfa (G-I) mRNA levels at 8 h after infection with control or FluV (A, D, G), VSV (B, E, H), and EMCV (C, F, I) in RAW264.7 cells pretreated with indicated concentrations of THGP. **P < 0.01 vs control. NS, not significant. Data are presented as mean and s.d. (n = 3) and are representative of at least three independent experiments.

4.5 THGP constrains 3pRNA-induced IFNB1 gene activation but fails to show such a concealing activity upon RIG-I, MAVS, MDA5, TBK1, STING, IRF-3CA, and TRIF overexpression

To clarify the mechanism for how THGP suppresses the RIG-I pathway, I tried to determine THGP acts on which level of RIG-I signaling pathway. I first checked whether THGP affected the activation of IFNB1 gene promoter upon overexpression of RIG-I or its adaptor MAVS and other signaling proteins. HEK293T cells were pretreated with THGP with the indicated concentrations of 0, 2, 20, 200, 2000 μg/ml for 24 hours and luciferase activity of IFNB1 promoter had been checked at 24 hours following transfection of 3pRNA, RIG-I, MAVS, MDA5, TBK1, STING, IRF3 CA and TRIF plasmids by using lipofectamine 2000. Interestingly, while 3pRNA-induced IFNB1 gene activation (Figure 4.5A) was suppressed by THGP treatment in a dose-dependent manner, it failed to show such a suppressing activity upon RIG-I overexpression even at a high concentration of THGP (Figures 4.5B). In addition, similar results showed that THGP did not affect IFNB1 gene activation induced by the overexpression of MAVS (Figure 4.5C), MDA-5 (Figure 4.5D), TBK1(Figure 4.5E), STING (Figure 4.5F), a constitutively active form of IRF-3 (K152R) (Figure 4.5G) and TRIF (Figure 4.5H). These

results recommended that THGP may act on some process(es) upstream of RIG-I, including the transfection of 3pRNA into the cytoplasm and/or its interaction with RIG-I.

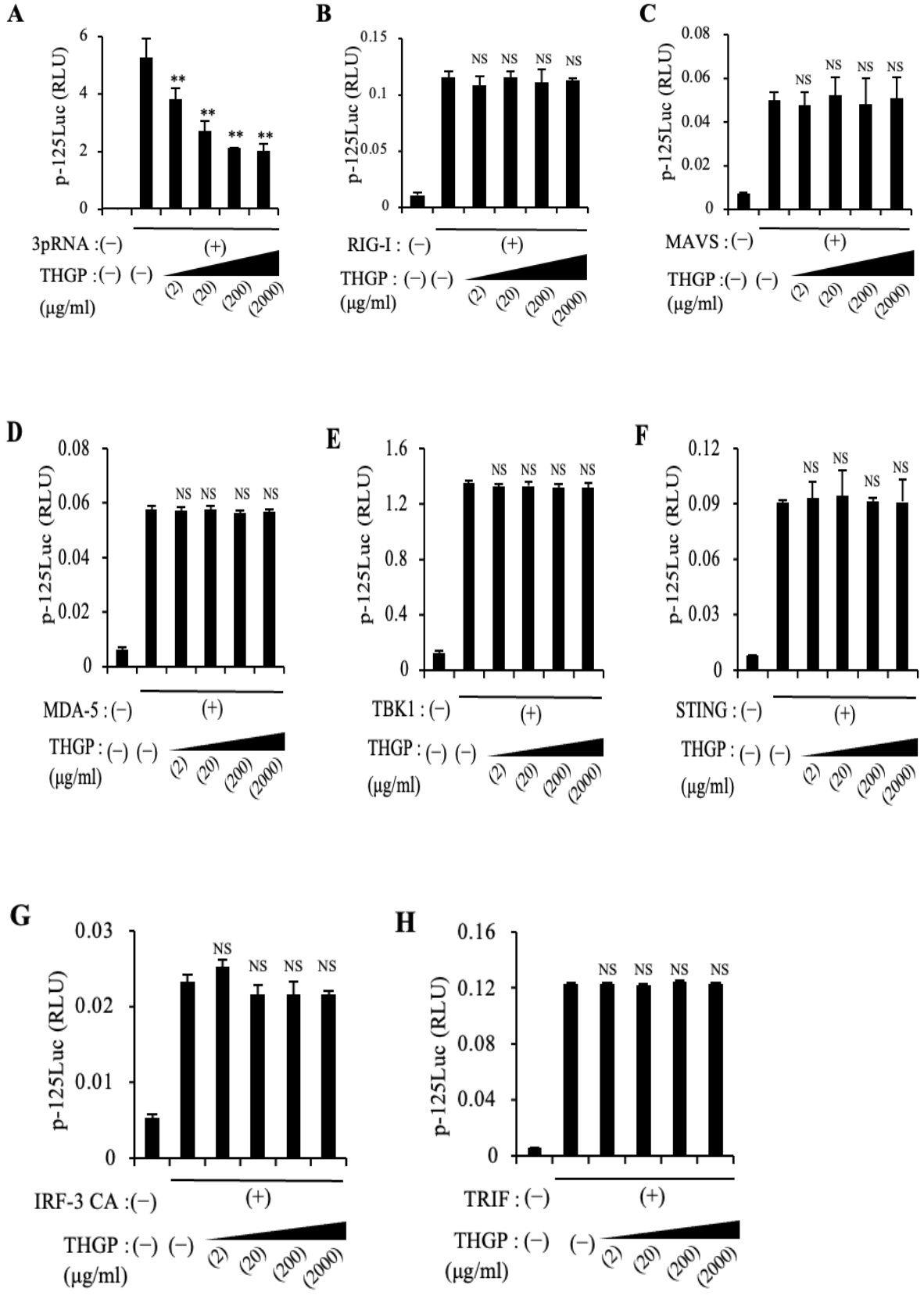

Figure 4.5 Inhibition of 3pRNA-induced Ifn-b gene activation by THGP excluding RIG-I, MAVS, MDA5, TBK1, STING, IRF-3CA, and TRIF overexpression. Luciferase assay of IFNB1 promoter after treatment of indicated concentrations of THGP 0, 2, 20, 200, 2000 μg/ml following transfection of 3pRNA (A), RIG-I (B), MAVS (C), MDA-5 (D), TBK1 (E), STING (F), constitutively active IRF-3 (IRF-3 CA) (G), and TRIF (H) in HEK293T cells. NS, not significant. Data are presented as mean and s.d. (n = 3) and are representative of at least three independent experiments.

4.6 THGP does not act on the uptake of 3pRNA into the cell

Next, I prepared Cy5-labelled 3pRNA Label IT® Nucleic Acid Labeling Kit, Cy5 (Mirus) to examine the effect of THGP on uptake of 3pRNA into the cell. Raw264.7 cells were pretreated with THGP for 24 hours and Cy5-conjugated 3pRNA were transfected by lipofectamine 2000, at 2 hours following transfection cells were then subjected to FACS (Figure 4.6A) and immunofluorescence (Figure 4.6B) analyses. However, any effect of THGP treatment on the uptake of Cy5-labeled 3pRNA was not observed (Figure 4.6C).

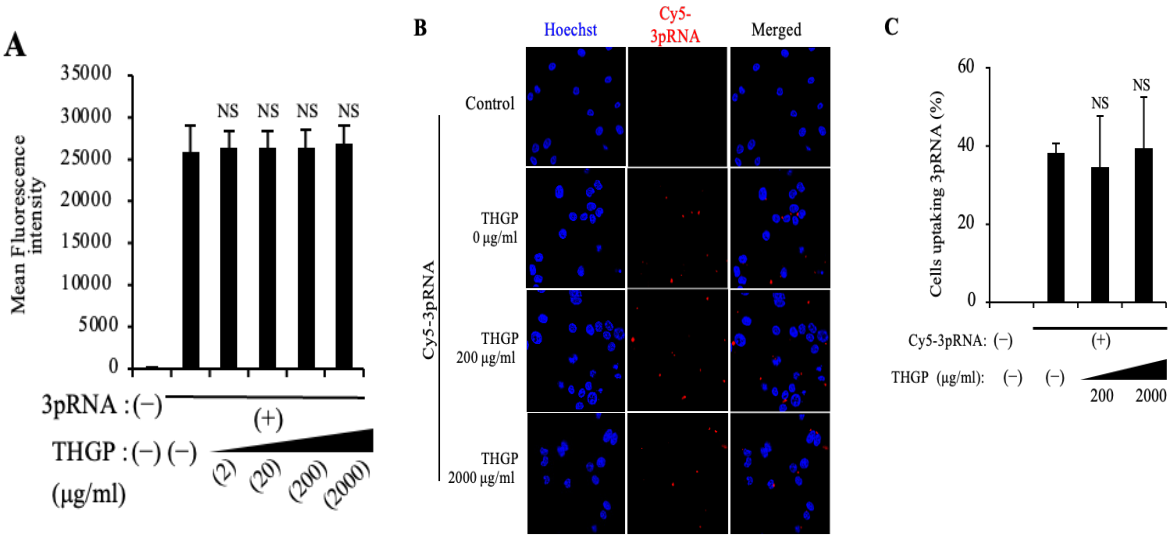

Figure 4.6 Effect of THGP on the uptake of 3pRNA. (A) FACS analysis at 2 h after transfection with Cy5-3pRNA in RAW264.7 cells. (B) RAW264.7 cells were transfected with Cy5-conjugated 3pRNA in the presence of indicated concentrations of THGP. After 2 h, cells were fixed and subjected to confocal microscopic analysis. (C) The quantification of (B) is shown.

4.7 The interaction of THGP with 3pRNA has been mediated specifically by the 5′-triphosphate moieties of 3pRNA

As THGP did not affect the uptake of 3pRNA into the cells, I further tested whether THGP interfered with the interaction between RIG-I and its ligand. I incubated THGP-conjugated beads prepared by Asai Germanium Institute with 3pRNA, poly I:C, HT-DNA and dephosphorylated 3pRNA and performed THGP beads pull down assay and measured the amount of precipitated RNA/DNA with THGP and control beads to examine the binding of THGP to RIG-I ligands, 3pRNA and short-form ds-RNA. The experimentation revealed that THGP preferentially associated with 3pRNA, but not short-form polyI:C (approximately 4 kb) or HT-DNA (Figure 4.7A). Such an interaction was not observed when dephosphorylated 3pRNA was used, suggesting that its 5′-triphosphate moiety was a key target for the interaction of THGP with 3pRNA (Figure 4.7B).

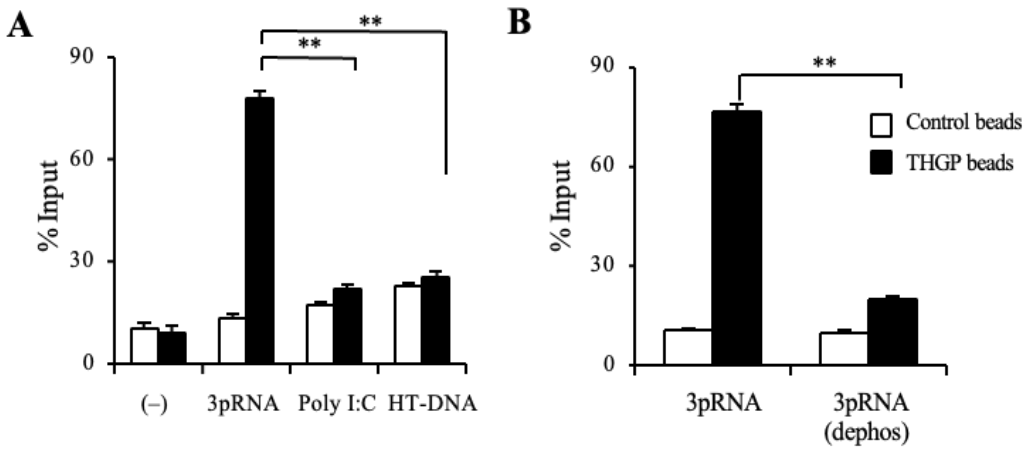

Figure 4.7 Interaction of THGP and 3pRNA. (A)THGP beads pull down assay of 3pRNA, Poly I:C, and HT-DNA. The amount of precipitated RNA/DNA with THGP beads (filled bar) or control beads (opened bar) is shown. (B) THGP beads pull down assay of 3pRNA and 3pRNA treated with alkaline phosphatase. The amount of precipitated RNA/DNA with THGP beads (filled bar) or control beads (opened bar) is shown.

4.8 ATP and deoxy ATP but not adenosine compete with 3pRNA to bind with THGP suggesting THGP may interact mostly with phosphate region of 3pRNA

Previously several reports have shown that THGP can interact with compounds containing cis-diol bonds, such as adrenaline, ATP, and L-DOPA [97, 98]. Further ^{1}H-NMR analysis comparing ATP and deoxy-ATP (Figure 4.8A) here indicated that cis-diol group of ATP plays

important role for binding with THGP (Figures 4.8B, C). In this respect, I incubated THGP-conjugated beads with ATP, deoxy-ATP, and adenosine in the presence of 3pRNA to perform THGP beads pull down competitive inhibition assay and measured the amount of precipitated compound with THGP and control beads. THGP beads pull-down assay in the presence of competitors including ATP, deoxy-ATP, or adenosine suggested that the triphosphate region is more important rather than the cis-diol for the interaction between 3pRNA and THGP (Figures 4.8D-F).

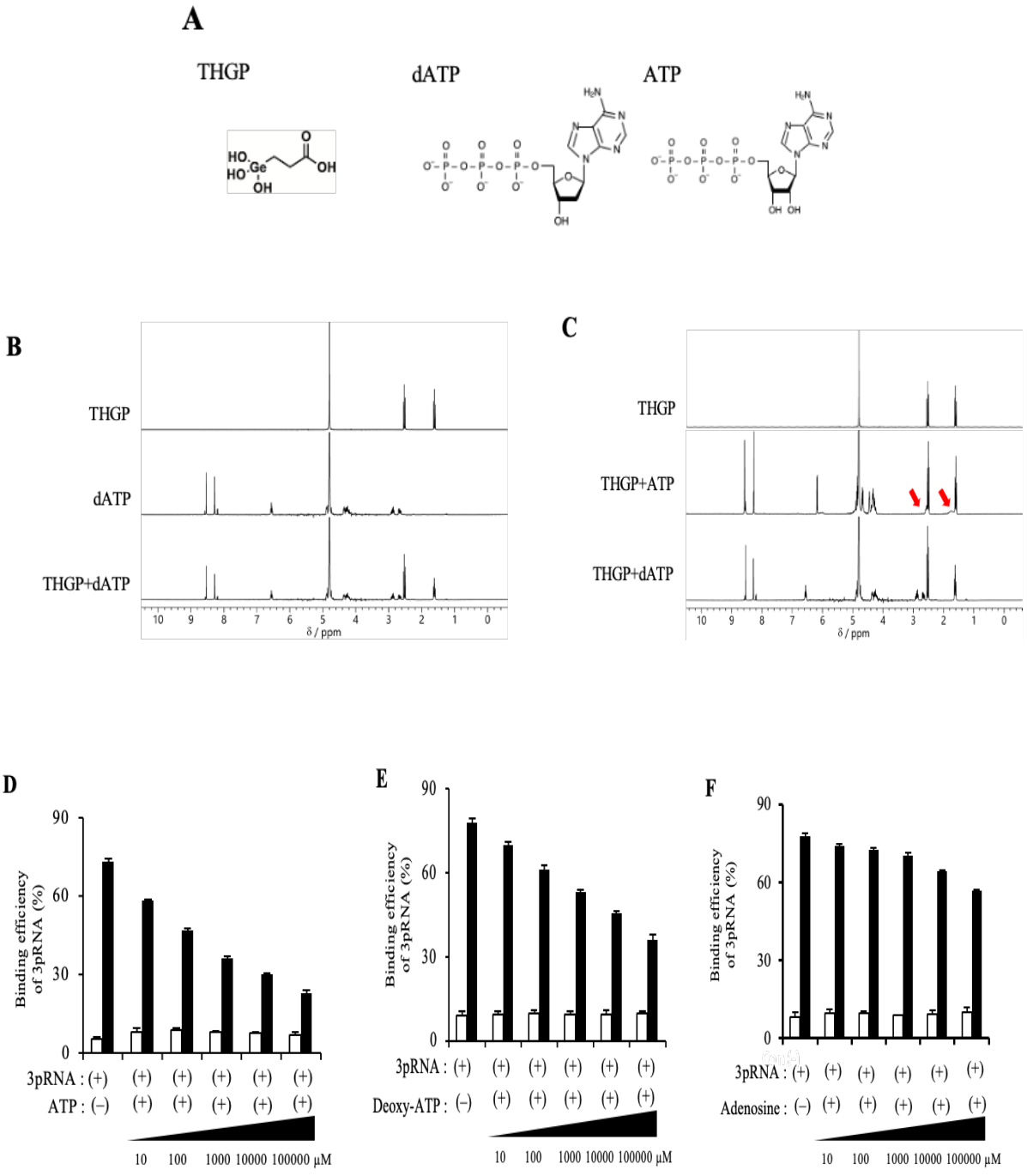

Figure 4.8 Competitive inhibition of the interaction between THGP and 3pRNA. (A) Structure of THGP, deoxy-ATP, and ATP. (B, C) The formation of a complex between deoxy-ATP, ATP, and THGP was analyzed by 1H-NMR (300 MHz). Red arrows indicated complex between ATP, and THGP. (D-F) THGP pull down assay of 3pRNA in the presence of ATP (D), deoxy-ATP (E), adenosine (F). The % input of precipitated RNA with THGP beads is shown. The IC50 values of ATP, deoxy-ATP, and adenosine are 912.01 μM, 2.37 mM, 27 M, respectively. **P < 0.01 vs control. Data are presented as mean and s.d. (n = 3 in (D-F).

4.9 THGP prohibits the binding of RIG-I with 3pRNA but does not interact with RIG-I protein itself

To examine whether THGP can bind with RIG-I protein, I labeled 3pRNA with biotin by using Label IT® Biotin Labeling Kit, Biotin (Mirus) and performed pull down assay following western blotting with anti-RIG-I antibody, which indicated that THGP cannot interact with RIG-I protein itself (Figure 4.9A). In addition, RNA pull-down assay with biotin-conjugated 3pRNA showed that THGP treatment inhibited the co-precipitation of 3pRNA and endogenous RIG-I in a dose dependent manner (Figure 4.9B). Similar observation also found in case of pull-down assay of biotin-conjugated 3pRNA and GST-RIG-I recombinant protein (Figure 4.9E). On the other hand, THGP did not affect the interaction between MDA5 and poly I:C (Figure 4.9C). Immunofluorescence analysis represented that RIG-I can colocalize with Cy5-3pRNA in RAW264.7 cells and this intracellular colocalization was suppressed by THGP treatment with indicated concentrations of THGP 200, 2000 μg/ml (Figure 4.9D). These results suggesting that THGP binds to 3pRNA to suppress the interaction between RIG-I and 3pRNA, which leads to the suppressed activation of RIG-I pathway.

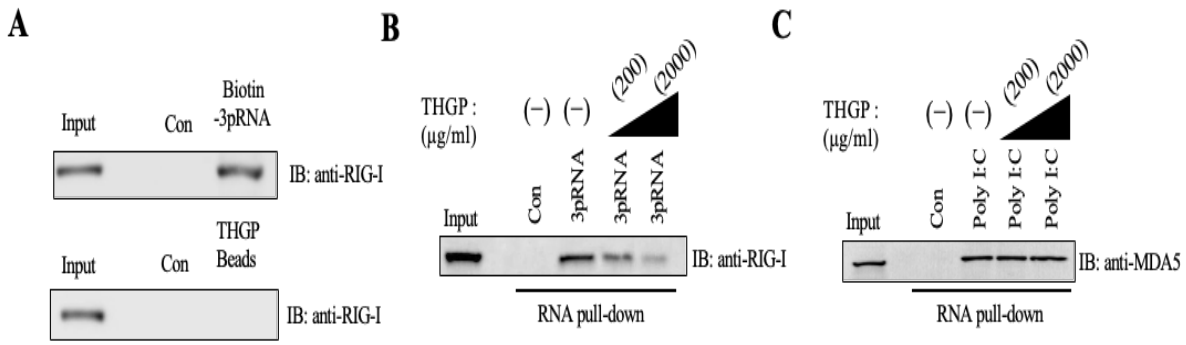

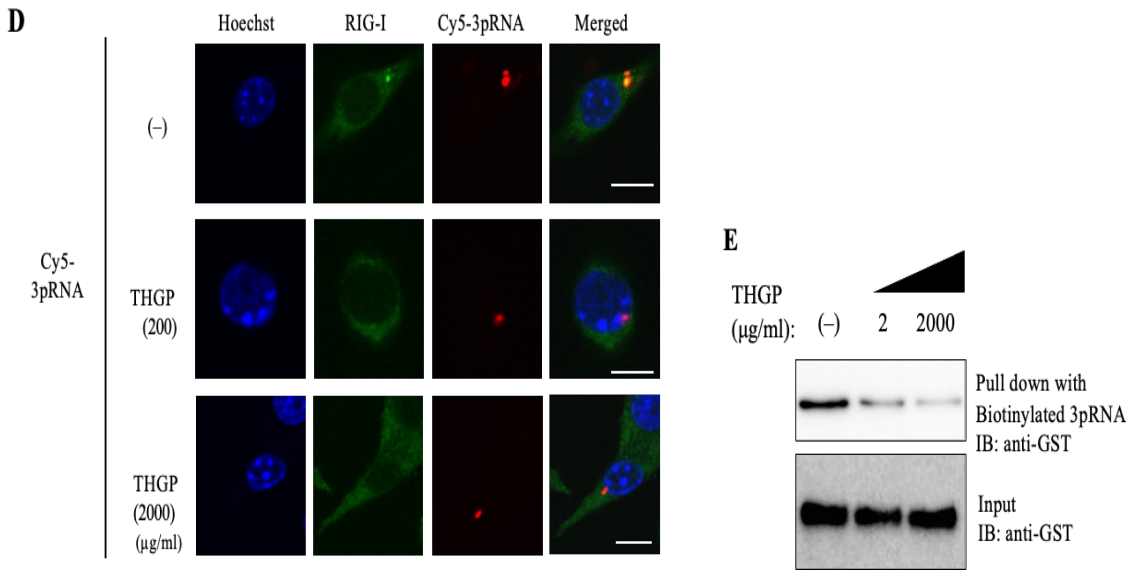

Figure 4.9 THGP inhibits binding of 3pRNA with RIG-I. (A) Pull-down assay showing the binding of biotinylated 3pRNA to RIG-I (top) and THGP to RIG-I (bottom). (B, C) 3pRNA (B) and poly I:C (C) pull down assay, that test the interaction of biotinylated 3pRNA and RIG-I and biotinylated poly I:C and MDA-5 in RAW264.7 cells. Co-precipitated proteins with biotinylated RNA in the presence of indicated concentrations of THGP 200, 2000 μg/ml were subjected to western blotting using anti-RIG-I and anti-MDA-5 antibodies. (D) Immunofluorescence analysis for the co-localization of RIG-I and Cy5-3pRNA in the presence of the indicated concentrations of THGP. A representative of more than 30 captured cells is presented. Bar: 10 μm. (E) 3pRNA pull down assay, that test the interaction of biotinylated 3pRNA and GST-RIG-I recombinant proteins. Co-precipitated GST-RIG-I proteins with biotinylated 3pRNA in the presence of indicated concentrations of THGP were subjected to western blotting using anti-GST antibody.

4.10 Organization of A549 MAVS KO cells and IFN response to respective ligands and effect of THGP on ISRE response

To investigate whether THGP has any influence on RIG-I signaling defective cells, CRISPR/Cas9 system was utilized to generate MAVS-deficient A549 cells (adenocarcinomic human alveolar basal epithelial cells). gRNA corresponding to the exon 2 of MAVS (Figure 4.10A) was inserted in pX330 vector, following lipofectamine transfection to the A549 WT cells and performed limited dilution of transfected cells. A549 MAVS KO clones (Figures 4.10B, C) were selected by western blotting and sequencing of genomic DNA. Quantitative RT-PCR analysis of IFNB1 mRNA of A549

MAVS KO cells pretreated with 3pRNA, poly I:C had shown that KO cells failed to induce both RIG-I- and MDA5-mediated type I IFN induction (Figure 4.10D). A549 MAVS KO cells were pretreated with the indicated concentration of THGP 2, 20, 200, 2000 µg/ml for 24 hours and luciferase assay was performed to determine the activation of ISRE (Interferon-stimulated response element) with IFN-α as a positive control (Figure 4.10E). No activation of ISRE had been observed in A549 MAVS KO cells after THGP treatment.

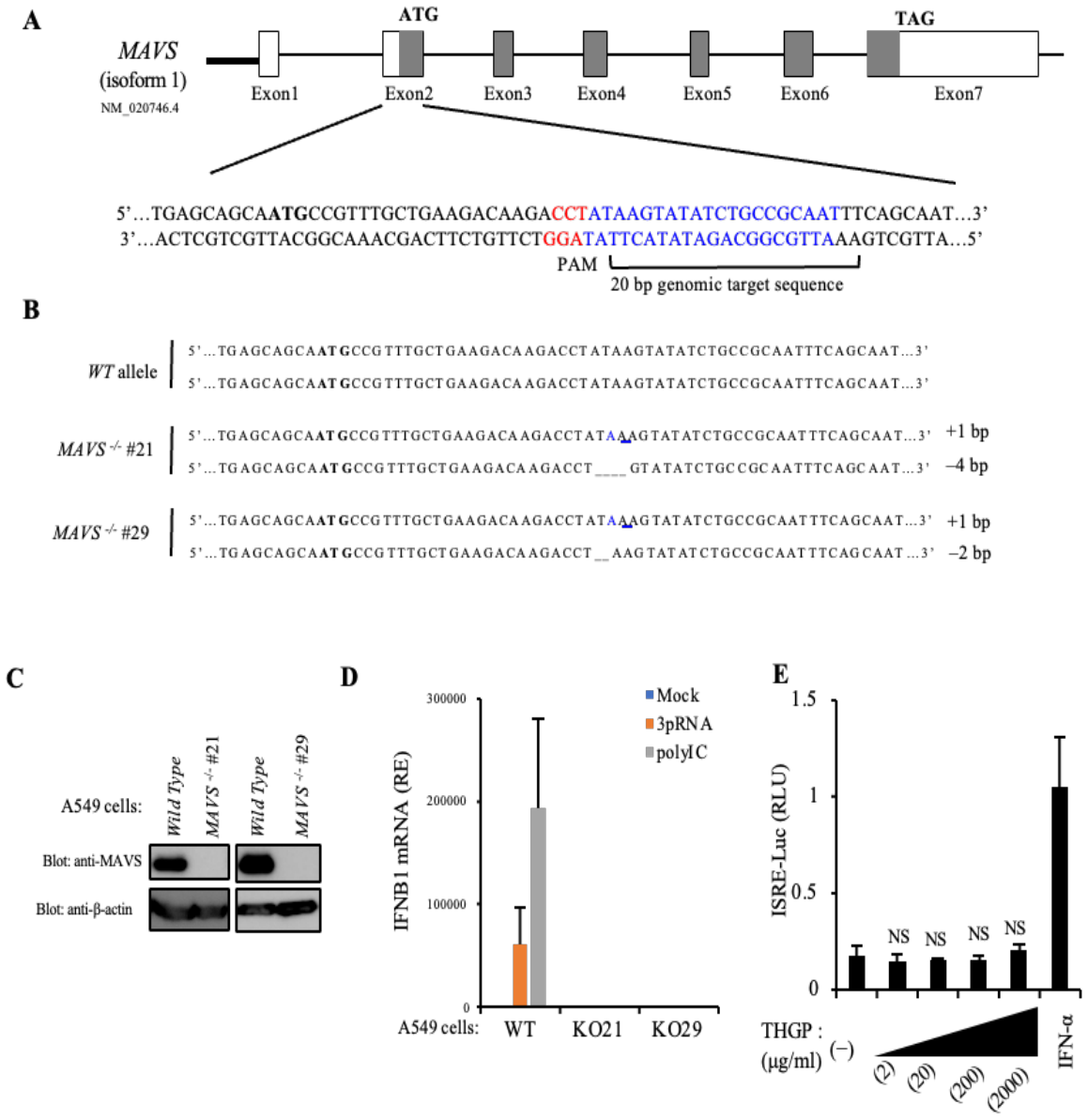

Figure 4.10 Establishment of A549 MAVS KO cells and effect of THGP on ISRE response. (A) Schematic representation of the MAVS locus. The gray boxes indicate the MAVS open reading frame (ORF). The start codon (ATG) and stop codon (TAG) of ORF

are shown in bold. The 20 bp genomic sequence targeted by the single guide RNA (sgRNA) is indicated by blue letters. The protospacer-adjacent motif (PAM) sequence is shown in red. (B) Genomic DNA sequences of MAVS locus in the indicated wild-type (WT) and knock-out A549 cells. The sizes of the insertion (+) or deletion (–) are indicated to the right of each mutated allele. The inserted nucleotides are indicated in blue and underlined, and deleted nucleotides are indicated as underlined. All mutations cause frameshift and ablate MAVS protein expression. (C) Immunoblot analysis of MAVS protein and β-actin in A549 WT and MAVS KO cells. (D) qRT-PCR analysis of IFNB1 mRNA levels at 8 h after stimulation with control, 3pRNA and poly I:C in A549 WT or MAVS KO cells. (E) Luciferase assay of ISRE promoter after treatment of indicated concentrations of THGP or 1,000 U of IFN-a in MAVS KO A549 cells. **P < 0.01 vs control. *P < 0.05 vs control. NS, not significant. Data are presented as mean and s.d. (n = 3).

4.11 THGP directly counteract the replication of FluV in a dose dependent manner

As FluV infection can produce RNA species carrying 5'-triphosphate moiety which is known to be recognized by RIG-I, next I evaluated the effect of THGP treatment on viral genome replication upon FluV infection. Treatment with the indicated concentrations of THGP significantly reduced the viral titers 24 hours after infection in Raw264.7 cells (Figure 4.11A). Therefore, it can be speculated that THGP binding to FluV RNAs might exert a direct antiviral activity to viral replication. To test this hypothesis, I used the luciferase activity-based mini genome assay previously described as Muramoto et al., 2013 [245] to quantitatively evaluate FluV replication in a human lung cell line A549. It had been observed that FluV replication, was reduced by THGP in a dose-dependent manner (Figure 4.11B). In addition, THGP comparatively showed a dose-dependent suppressing effect on FluV replication also in MAVS-deficient cells prepared by using CRISPR/Cas9 system (Figure 4.11C). A549 an A549 MAVS KO cells were pretreated with the indicated concentrations 2, 20, 200, 2000 µg/ml of THGP for 24 hours and to perform luciferase-activity based mini-genome assay FluV-related plasmids including pPolI/ NP(0)luc2(0), Flag-PB2, PB1, PA, NP were transfected and the reporter activity of viral polymerase had been measured after 24 hours of transfection. These results suggested that THGP has a direct antiviral activity.

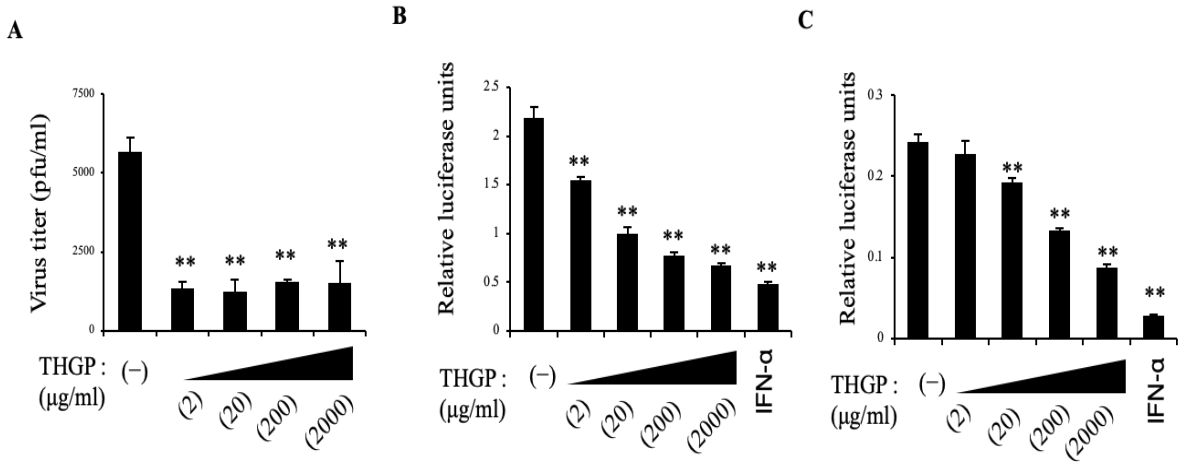

Figure 4.11 Suppression of FluV replication by THGP. (A) Viral titers measured in MDCK cells after 24 h of infection with FluV in RAW264.7 cells in the presence of the indicated concentrations of THGP. pfu, plaque-forming units. n = 3 samples per group. (B-C) Luciferase activity-based mini-genome assay of FluV replication in the presence of indicated concentrations of THGP or 1,000 U of IFN-a for 24 h in A549 WT (B) and A549 MAVS KO cells (C) after 24 h of transfection with FluV-related plasmids including pPolI/ NP(0)luc2(0), Flag-PB2, PB1, PA, NP. **P < 0.01 vs control. *P < 0.05 vs control. NS, not significant. Data are presented as mean and s.d. (n = 3 in A-C)

4.12 THGP impedes the access of FluV polymerase to viral RNA

To investigate whether THGP mediates antiviral activity through its interaction with the 5'-triphosphate of FluV genome I did THGP beads pull down assay which showed that FluV-derived RNA but not EMCV and SARS-CoV-2-derived RNA was remarkably co-precipitated with THGP conjugated with epoxy beads (Figure 4.12A). Since it has been reported that the 5'-region of viral genome contains the binding site of FluV-derived RNA polymerase complex [246], it can be speculated that THGP abolished the access of FluV polymerase to viral RNA. Next, to test the interaction of viral RNA and viral polymerase, I performed RIP assay with MAVS-deficient A549 cell lysates prepared after 48 hours of transfection with the FluV-related plasmids including pPolI/ NP(0)luc2(0), Flag-PB2, PB1, PA, NP by using anti-Flag, or control immunoglobulin G revealed that THGP competitively suppressed the interaction of Flag-tagged polymerase subunit basic protein 2 (PB2) with viral RNA (nucleoprotein; NP) as judged by qRT-PCR (Figure 4.12B). These results indicated that THGP inhibits the recognition of viral RNA by viral polymerase.

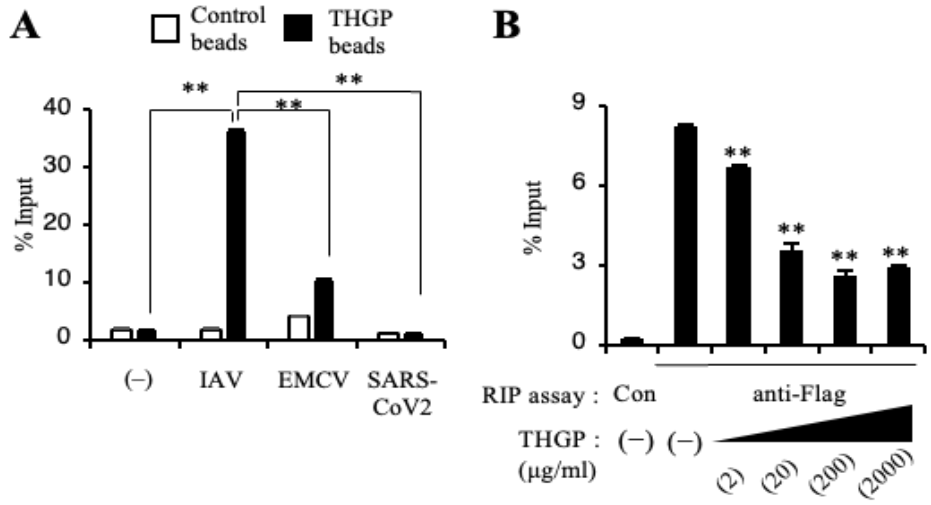

Figure 4.12 Inhibition of access of FluV polymerase to viral RNA by THGP. (A) THGP pull down assay of RNA prepared from RAW264.7 cells infected with FluV and EMCV, RNA of SARS-CoV-2. The % input of precipitated RNA with THGP beads is shown. (B) RIP assay with A549 MAVS KO cell lysates prepared after 48 h of transfection with the FluV-related plasmids including pPolI/ NP(0)luc2(0), Flag-PB2, PB1, PA, NP by using anti-Flag, or control immunoglobulin G (con). The immunoprecipitated FluV RNA was measured by qRT-PCR. **P < 0.01 vs control. *P < 0.05 vs control. NS, not significant. Data are presented as mean and s.d. (n = 3).

4.13 THGP suppresses FluV replication *in vivo*

Lastly, to examine whether the inhibitory effect of THGP can also be seen *in vivo* during FluV infection, I used MAVS-deficient mice (#008634), obtained from Jackson Laboratory. The viral titers on Day 2 after FluV infection were significantly decreased by THGP treatment (Figure 4.13A) analyzed by qRT-PCR. Next, C57BL/6J mice were used to determine the effect of THGP on survival of mice during FluV infection. THGP itself did not affect the survival (Figure 4.13B) and the body-weight curves (Figure 4.13D) of uninfected mice, whereas treatment with THGP during FluV infection showed improved survival rate (Figure 4.13C) and restored the body weight loss of mice (Figure 4.13E). Further, hematoxilin and eosin staining showed that administration of THGP reduced alveolar hemorrhage, inflammatory infiltration, and interstitial thickening in the alveolar lesion of lung tissue during FluV infection (Figure 4.13F). Thus, these data suggest that THGP is capable of negatively regulating FluV replication

possibly by blocking the interaction of FluV RNA and viral polymerase. Therefore, THGP can function as a direct antiviral agent that inhibits viral RNA recognition during FluV replication.

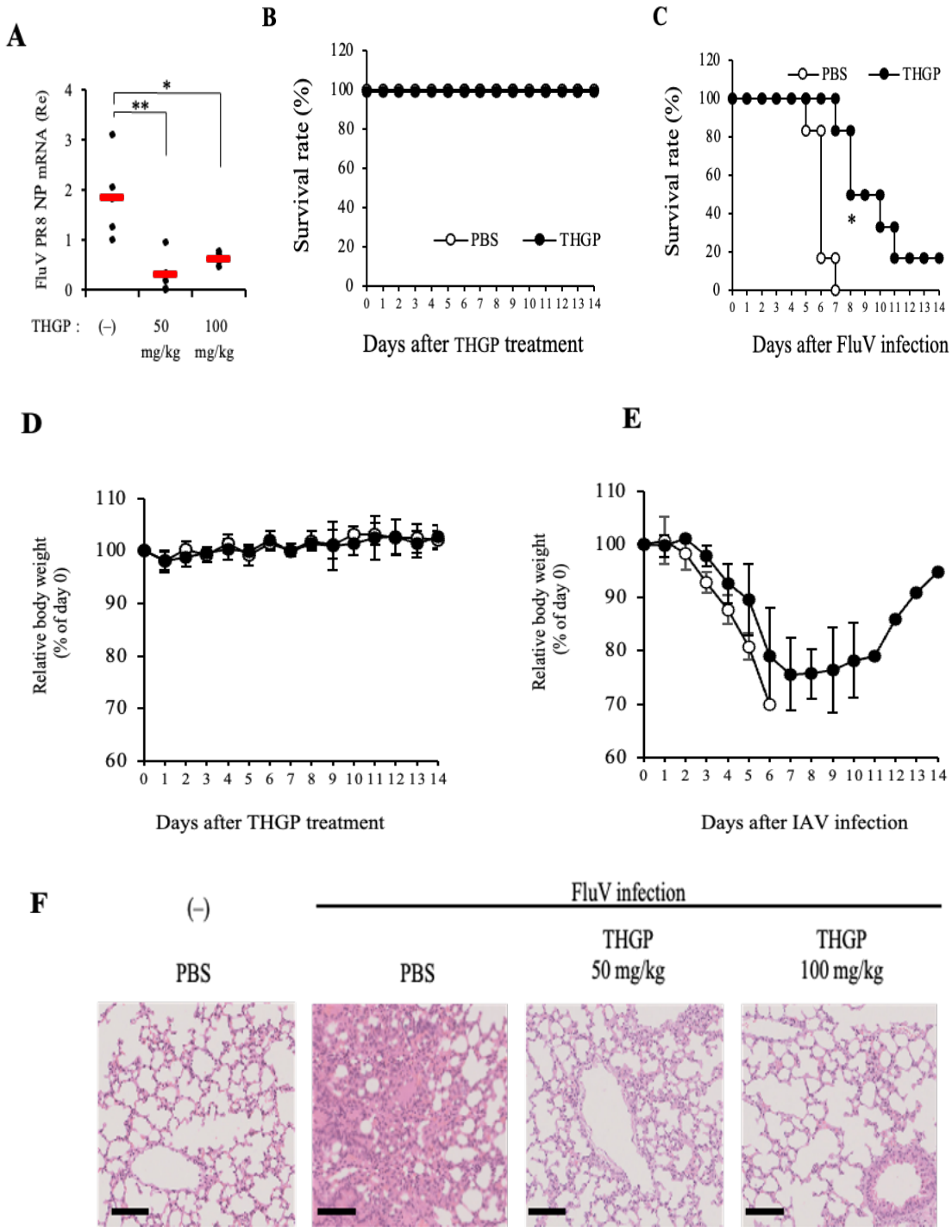

Figure 4.13 *in vivo* suppression of FluV replication by THGP. (A) qRT-PCR analysis of FluV NP RNA levels in the lung tissues of MAVS KO mice at 48 h post-infection of FluV following administration with PBS (–), THGP (50 mg/kg), or THGP (100 mg/kg). (B) Survival

rate of C57BL/6J mice, treated with THGP (50 mg/kg) once/ two days. (C) Survival rate of FluV (A/Puerto Rico/8/1934 H1N1 strain, 1 x 105 pfu/mice; i.n.) infected C57BL/6J mice, treated with THGP (50 mg/kg) once/ two days. C57BL/6J mice were intranasally administrated with THGP or PBS at a dose of 50 mg/kg of body weight every 2 days for 14 days. (D) Body weight changes of uninfected mice. (E) Body weight changes of FluV (A/Puerto Rico/8/1934 H1N1 strain, 1 x 105 pfu/mice; i.n.) infected C57BL/6J mice. (F) H&E staining of lung tissues at 72-h post-infection in MAVS KO mice following i.n. administration with PBS (–), THGP (50 mg/kg), or THGP (100 mg/kg). Bar: 100 μm. **P < 0.01 vs control. *P < 0.05 vs control. NS, not significant. Data are presented as mean and s.d. (n=6) and are representative of at least three independent experiments.

5. Discussion

The innate immune system provides first line of defense against diverse viral infections to our body. Germ-line encoded host sensors, PRRs (pattern recognition receptors) play a critical role in recognizing invading viruses and activate their downstream signaling to induce type I and III IFN genes, which confer antiviral states to the cell. Sensing of viral nucleic acids (RNA and DNA) during viral infections is central to the initiation of antiviral immune responses. Among different viral nucleic acid sensors, RIG-I and MDA5 are ubiquitously expressed and recognize viral RNAs in the cytoplasmic space. Particularly, RIG-I is a key cytoplasmic PRR for the detection of RNA viruses including influenza virus, hepatitis C virus, hepatitis B virus, measles virus, etc., which are causative mediators for human infectious diseases. RIG-I usually recognizes RNA carrying 5'-triphosphate modification (3pRNA) and/or short dsRNA. Upon ligand-binding, RIG-I activates the ATPase activity of its helicase domain to change its conformation and subsequently oligomerized RIG-I interacts with the adaptor protein MAVS/IPS-1 through its CARD domains, leading to the activation of the downstream gene induction programs such as IFNs and proinflammatory cytokines. There are many accumulating evidences that an organo-germanium compound, 3-(trihydroxygermyl) propanoic acid (THGP), which is a hydrolysate of Ge-132, employs diverse physiological effects such as anti-cancer, antimicrobial, analgesic, anti-inflammatory, anti-oxidative, immunomodulatory and also shows an antiviral effect on FluV infection. However, the detailed mechanisms of the antiviral activities of THGP as well as its effect on innate sensor-mediated immune responses remains unclear. Thus, elucidation of THGP effect on host immune response against FluV infection is crucial. In this study, I tried to represent a novel mechanism, by which THGP inhibited not only FluV replication but also RIG-I signaling. The observations of this study revealed the dual effect of an organogermanium compound THGP on innate signaling pathways activated by RIG-I and viral replication during FluV infection.

Here, I found treatment of THGP did not affect cell proliferation rate and did not induce interferon response itself (Figure 4.1) and it selectively suppressed 3pRNA but not ds-RNA-mediated cytokine response. In addition, THGP repressed only RIG-I but not MDA-5, cGAS and TLR4 mediated innate signaling pathways (Figures 4.2, 4.3). Consistent with these results, this study showed that THGP attenuated type I IFN responses and inflammatory cytokines such as Il-6 and Tnfα (Figure 4.4) upon infections with VSV and FluV, which are reported to be sensed by RIG-I [247], whereas such a strangling effect was not observed upon infection with

EMCV, which is recognized by MDA5 [248]. Interestingly, the suppressive effect was continued to the induction of 3pRNA induced IFNB1 gene promoter but was not observed by the overexpression of RIG-I and the related signaling proteins such as MDA-5, MAVS, STING, TBK-1, IRF-3, and TRIF (Figure 4.5). Further investigation through FACS and immunofluorescence analyses revealed that THGP did not influence the uptake of 3pRNA into cell (Figure 4.6). According to data of this study, THGP preferentially interacts with 3pRNA, which abrogated RIG-I-mediated recognition of 3pRNA but not polyI:C, and HT-DNA (Figure 4.7A). Several reports previously showed that THGP has a characteristic to interact with compounds containing cis-diol structures, such as adrenaline, adenosine, ATP, and L-DOPA and this interaction is responsible for the physiological effects of THGP [97, 98]. Here, ^{1}H-NMR (300 MHz) analysis comparing ATP and deoxy-ATP indicated that cis-diol of ATP plays important role for binding with THGP (Figures 4.8 A-C). Therefore, it was presumable that the cis-diol group of 3pRNA would be a possible binding site of THGP but obtained data in this study indicated that modified 3pRNA, which contain one cis-diol at 3′ end, can still bind to THGP. THGP targeted the 5′ triphosphate group of 3pRNA, which was supported by the result that the dephosphorylation of 3pRNA partially lost the binding activity of THGP with 3pRNA (Figure 4.7B). Moreover, THGP beads pull-down assay in the presence of 3pRNA and competitors including ATP, deoxy-ATP, or adenosine suggested that the triphosphate region is more important rather than the cis-diol for the interaction between 3pRNA and THGP (Figures 4.8 D-F). It has also been found that THGP did not interact with RIG-I itself but reduced the co-immunoprecipitation of RIG I and 3pRNA (Figure 4.9). Detailed X-ray crystallographic analysis is further required to structurally show the complex formation between 3pRNA and THGP. A model of possible interaction between THGP and 5′ppp RNA has been illustrated in Figure 5.1.

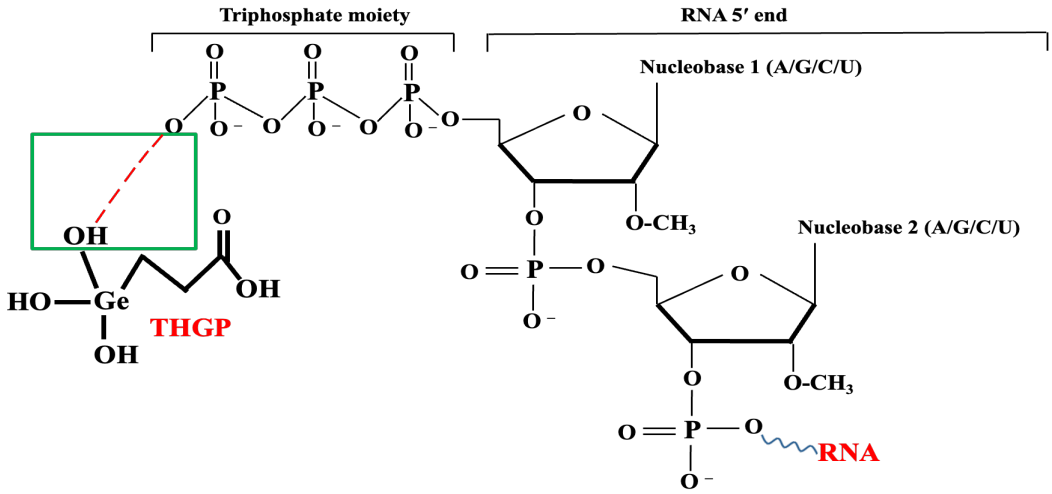

Figure 5.1 A model of possible interaction between THGP and 5′PPP RNA. The point of possible interaction between THGP and 5'PPP RNA has been depicted in red color enclosed within the green box. A: adenine, C: cytosine, G: guanine, or U: uracil, RNA: ribonucleic acid.

This study also showed that THGP interacted only with FluV-derived RNA, but not EMCV-derived RNA and SARS-CoV-2-derived RNA (Figure 4.12). As THGP inhibited RIG-I signaling, I tested whether THGP can promote viral replication. However, unexpectedly it had been observed that THGP treatment suppressed FluV replication both in vitro and in vivo (Figures 4.11, 4.13). Moreover, it had been observed that THGP treatment did not influence the survival rate and the body weight curves of mice by itself but in response to FluV infection treatment with THGP reinstated the body weight loss and increased mice survival rate (Figure 4.13). Mechanistically, I found that binding of THGP to FluV RNA restricted the accessibility of viral RNA polymerase to RNA genome (Figure 4.12), which is essential to initiate viral replication, suggesting a novel direct antiviral action of THGP on FluV RNA possibly or other virus-derived RNA containing a 5'-triphosphate moiety. In addition, viral RNAs of EMCV and SARS-CoV-2, which contains 7-methylguanosine (m7G) cap at the terminal phosphate group of 5' end [249] did not interact with THGP.

Due to the rapid mutation of surface glycoproteins of FluV, it is difficult to select annual FluV vaccine strain to match with circulating viruses. Since developing universal vaccines is extremely challenging due to the high plasticity of FluV, it is necessary to develop effective counter measures including broad spectrum antivirals. Currently, FDA-approved two classes of anti-FluV compounds: M2 ion channel inhibitors (amantadine, rimantadine), and neuraminidase (NA) inhibitors (oseltamivir, zanamivir, laninamivir and peramivir). M2 ion channel inhibitors block the influx of hydrogen ions from the acidic late endosome into the interior of the virion, which is crucial for the release of vRNPs into the cytoplasm. However, these inhibitors are no longer recommended for use as most circulating FluVs are resistant to these compounds [250]. Neuraminidase (NA) inhibitors block the enzymatic activity of NA that is required for efficient virus replication. Despite several antiviral drugs, drug resistance, toxicity and cost remain unresolved in the fight against FluV infections. Thus, the development of novel anti-viral agents which would be used alone or in combination with existing anti-viral drugs is of high weight. In this regard, THGP may provide a therapeutic potential as a novel type of antiviral agent that directly interferes with the interaction between viral RNA and FluV

polymerase targeting FluV genome. This could also be a unique approach that does not use any nucleic acids to target viral genomes, and it can be expected that unlike commonly used antivirals, THGP may have less emergence of resistance.

On the other hand, due to the suppressive effect of THGP on RIG-I mediated immune signaling, it might also be a new therapeutic option for the patients with inflammatory diseases caused by RIG-I hyperactivation. The superkiller viralicidic activity 2-like (SKIV2L) RNA helicase, one of causative genes for tricho-hepato-enteric syndrome (THES) also known as syndromic diarrhoea (SD) or phenotypic diarrhoea (PD), is known to be involved in the formation of an RNA exosome that inhibits ER stress such as thapsigargin-induced RIG-I signaling pathway. SKIV2L is a negative regulator of the RLR-mediated antiviral response and it has been reported that humans with deficiency in SKIV2L have a type I IFN signature in their peripheral blood, suggesting a possible therapeutic application of THGP for the treatment of such inflammatory diseases. In addition to this, there would be a potential of THGP in excessive inflammation during viral infections. It has been reported that hyperactivation of proinflammatory cytokine response which can be defined as "cytokine storm" are often associated with complications or ultimately death arising from viral infections such as severe influenza [251]. Dual activity of THGP, regarding suppression of RIG-I pathway and direct antiviral effect, might also be promising in such a clinical condition. Although, the outcomes of dual effect of THGP on RIG-I mediated viral sensing and FluV replication through the binding with 5'ppp RNA acts in opposite directions, THGP mediated improved survival rate of mice during FluV infection suggests that the inhibiting effect of THGP on FluV replication is dominant rather than the inhibition on RIG-I responses. Thus, present study provides a novel aspect of THGP as a potentially attractive clinical option for the therapy against infectious diseases caused by not only FluV but also possibly other viruses, which contain tri-phosphorylated 5′ (5′ppp) terminus in their genome such as Vesicular stomatitis virus (VSV), Rift Valley fever virus (RVFV), La Crosse virus (LACV), Newcastle disease viruses (NDV), Ebola virus (EBOV), and Sendai virus (SenV) and rabbis virus [252-257].

References

1. Nicholson, L. B. The immune system. *Essays in biochemistry* 60, 275–301, 2016.
2. Abbas, A.K., Lichtman, A.H., Pillai S. *Basic Immunology: Functions and Disorders of the Immune System.* Amsterdam: Elsevier, 2016.
3. Kindt, T. J., Goldsby, R. A., Osborne, B. A., & Kuby, J. *Kuby immunology*. New York: W.H. Freeman, 2007.
4. Netea, M.G., Balkwill, F., Chonchol, M., Cominelli, F., Donath, M.Y., Giamarellos-Bourboulis, E.J., Golenbock, D., Gresnigt, M.S., Heneka, M.T., Hoffman, H.M., *et al.* A guiding map for inflammation. *Nat. Immunol*. 18, 826-831, 2017.
5. Farber, D., Netea, M., Radbruch, A. *et al.* Immunological memory: lessons from the past and a look to the future. *Nat Rev Immunol.* 16, 124–128, 2016.
6. Netea, M. G., Schlitzer, A., Placek, K., Joosten, L. A. B., Schultze, J. L. Innate and Adaptive Immune Memory: An Evolutionary Continuum in the Host's Response to Pathogens, *Cell Host & Microbe* 25, 13-26, 2019.
7. Marshall, J.S., Warrington, R., Watson, W. *et al.* An introduction to immunology and immunopathology. *Allergy Asthma Clin Immunol.* 14, 49, 2018.
8. Turvey, S.E., Broide, D.H. Innate immunity. *J Allergy Clin Immunol.* 25, 24–32, 2010.
9. Bonilla, F.A., Oettgen, H.C. Adaptive immunity. *J Allergy Clin Immunol.*125, 33–40, 2010.
10. Takeuchi, O., Akira, S. Pattern recognition receptors and inflammation. *Cell* 140, 805-820, 2010.
11. Alberts, B., Johnson, A., Lewis, J., Raff, M., Roberts, K., Walter, P. *Innate Immunity*, 2002.
12. Schroder, K., Tschopp, J. The inflammasomes. *Cell* 140, 821–32, 2010.
13. Broz, P., Monack, D.M. Newly described pattern recognition receptors team up against intracellular pathogens. *Nat Rev Immunol.* 13, 551-565, 2013.
14. Kumar, H., Kawai, T., Akira, S. Pathogen recognition by the innate immune system. *International Reviews of Immunology* 30, 16–34, 2011.
15. Yoneyama, M., and Fujita, T. Structural mechanism of RNA recognition by the RIG-I-like receptors. *Immunity* 29, 178–181, 2008.

16. Loo, Y.M., Fornek, J., Crochet, N., Bajwa, G., Perwitasari, O., Martinez-Sobrido, L., Akira, S., Gill, M.A., Garcia-Sastre, A., Katze, M.G., Gale, M. J. Distinct RIG-I and MDA5 signaling by RNA viruses in innate immunity. *J. Virol*. 82, 335-345, 2008.
17. Satoh, S., Kato, H., Kumagai, Y., Yoneyama, M., Sato, S., Matsushita, K., Tsujimura, T., Fujita, T., Akira, S., Takeuchi, O. LGP2 is a positive regulator of RIG-I- and MDA5-mediated antiviral responses. *Proc. Natl. Acad. Sci.* 107, 1512-1517, 2010.
18. Hornung, V., Ellegast, J., Kim, S., Brzozka, K., Jung, A., Kato, H., Poeck, H., Akira, S., Conzelmann, K.K., Schlee, M. *et al.* 5′-Triphosphate RNA is the ligand for RIG-I. *Science* 314, 994-997, 2006.
19. Pichlmair, A., Schulz, O., Tan, C.P., Naslund, T.I., Liljestrom, P., Weber, F., Sousa C. R. RIG-I-mediated antiviral responses to single-stranded RNA bearing 5′-phosphates. *Science* 314, 997-1001, 2006.
20. Kawai, T., Akira. S. Innate immune recognition of viral infection. *Nat. Immunol.* 7, 131-137, 2006.
21. Luo, D., Ding, S.C., Vela, A., Kohlway, A., Lindenbach, B.D., Pyle, A.M. Structural insights into RNA recognition by RIG-I. *Cell* 47, 409–22, 2011.
22. Jiang, F., Ramanathan, A., Miller, M.T., Tang, GQ, Gale, M. Jr., Patel, S.S., et al. Structural basis of RNA recognition and activation by innate immune receptor RIG-I. *Nature* 479, 423–7, 2011.
23. Kowalinski, E., Lunardi, T., McCarthy, A.A., Louber, J., Brunel, J., Grigorov, B., et al. Structural basis for the activation of innate immune pattern-recognition receptor RIG-I by viral RNA. *Cell* 147, 423–35, 2011.
24. .Meylan, E., Curran, J., Hofmann, K., Moradpour, D., Binder, M., Bartenschlager, R, et al. Cardif is an adaptor protein in the RIG-I antiviral pathway and is targeted by hepatitis C virus. *Nature* 437,1167–72, 2005.
25. Tan, P., He, L., Cui, J., Qian, C., Cao, X., Lin, M., et al. Assembly of the WHIP-TRIM14-PPP6C mitochondrial complex promotes RIG-I-mediated antiviral signaling. *Mol Cell.* 68, 293–307, 2017.
26. Vallabhapurapu, S., Karin, M. Regulation and function of NF-kappaB transcription factors in the immune system. *Annu Rev Immunol* 27, 693–733, 2009.
27. Paz, S., Vilasco, M., Werden, S.J., Arguello, M., Joseph-Pillai, D., Zhao, T., et al. A functional C-terminal TRAF3-binding site in MAVS participates in positive and negative regulation of the IFN antiviral response. *Cell Res* 21, 895–910, 2011.

28. Newton, K., Dixit, V.M. Signaling in innate immunity and inflammation. *Cold Spring Harb Perspect Biol* 4, a006049, 2012.
29. Paludan, S. R. & Bowie, A. G. Immune sensing of DNA. *Immunity* 38, 870–880, 2013.
30. Sun, L., Wu, J., Du, F., Chen, X. & Chen, Z. J. Cyclic GMP-AMP synthase is a cytosolic DNA sensor that activates the type I interferon pathway. *Science* 339, 786–791, 2013.
31. Li, X. D. et al. Pivotal roles of cGAS-cGAMP signaling in antiviral defense and immune adjuvant effects. *Science* 341, 1390–1394, 2013.
32. Zhang, X., Bai, X.C., Chen, Z.J. Structures, and mechanisms in the cGAS-STING innate immunity pathway. *Immunity* 53, 43–53, 2020.
33. Ouyang, S., Song, X., Wang, Y., Ru, H., Shaw, N., Jiang, Y., Niu, F., Zhu, Y., Qiu, W., Parvatiyar, K., et al. Structural analysis of the STING adaptor protein reveals a hydrophobic dimer interface and mode of cyclic di-GMP binding. *Immunity* 36, 1073–86, 2012.
34. Donovan, J., Dufner, M., Korennykh, A. Structural basis for cytosolic double-stranded RNA surveillance by human oligoadenylate synthetase 1. *Proc Natl Acad Sci* 110, 1652–7, 2013.
35. Li, X., Shu, C., Yi, G., Chaton, C.T., Shelton, C.L., Diao, J., Zuo, X., Kao, C.C., Herr, A.B, Li, P. Cyclic GMP-AMP synthase is activated by double-stranded DNA-induced oligomerization. *Immunity* 39, 1019–31, 2013.
36. Kranzusch, P.J., Lee, A.S.Y., Wilson, S.C., Solovykh, M.S., Vance, R.E., Berger, J.M., Doudna, J.A. Structure-guided reprogramming of human cGAS dinucleotide linkage specificity. *Cell* 158, 1011–21, 2014.
37. Martin, M., Hiroyasu, A., Guzman, R.M., Roberts, S.A., Goodman, A.G. Analysis of drosophila STING reveals an evolutionarily conserved antimicrobial function. *Cell Rep.* 23, 3537–3550, 2018.
38. Saeed, A., Ruan, X., Guan, H., Su, J., Ouyang, S. Regulation of cGAS-mediated immune responses and immunotherapy. *Adv Sci (Weinh)* 7, 1902599, 2020.
39. Andreeva, L. et al. cGAS senses long and HMGB/TFAM-bound U-turn DNA by forming protein-DNA ladders. *Nature* 549, 394–398, 2017.
40. Du, M. & Chen, Z. J. DNA-induced liquid phase condensation of cGAS activates innate immune signaling. *Science* 361, 704–709, 2018.
41. Gao, D., Li, T., Li, X.D., Chen, X., Li, Q.Z., Wight-Carter, M., Chen, Z.J. Activation of cyclic GMP-AMP synthase by self-DNA causes autoimmune diseases. *Proc Natl Acad Sci.* 112, 5699–705, 2015.

42. Luecke, S. et al. cGAS is activated by DNA in a length-dependent manner. *EMBO Rep.* 18, 1707–1715, 2017.
43. Ishikawa, H., Ma, Z. & Barber, G. N. STING regulates intracellular DNA-mediated, type I interferon-dependent innate immunity. *Nature* 461, 788–792, 2009.
44. Zhou, W., Whiteley, A.T., de Oliveira Mann, C.C., Morehouse, B.R., Nowak, R.P., Fischer, E.S., Gray, N.S., Mekalanos, J.J., Kranzusch, P.J. Structure of the human cGAS-DNA complex reveals enhanced control of immune surveillance. *Cell* 174, 300–311, 2018.
45. Wu, J., Sun, L., Chen, X., Du, F., Shi, H., Chen, C., Chen, Z.J. Cyclic GMP-AMP is an endogenous second messenger in innate immune signaling by cytosolic DNA. *Science* 339, 826–30, 2013.
46. Motwani, M., Pesiridis, S., Fitzgerald, K.A. DNA sensing by the cGAS-STING pathway in health and disease. *Nat Rev Genet*. 20, 657–74, 2019.
47. Srikanth, S., Woo, J.S., Wu, B., El-Sherbiny, Y.M., Leung, J., Chupradit, K., Rice, L., Seo, G.J., Calmettes, G., Ramakrishna, C., et al. The Ca (2+) sensor STIM1 regulates the type I interferon response by retaining the signaling adaptor STING at the endoplasmic reticulum. *Nat Immunol*. 20, 152–62, 2019.
48. Ramanjulu, J.M., Pesiridis, G.S., Yang, J., Concha, N., Singhaus, R., Zhang, S.Y., Tran, J.L., Moore, P., Lehmann, S., Eberl, H.C., et al. Design of amidobenzimidazole STING receptor agonists with systemic activity. *Nature* 564, 439–43, 2018.
49. Dobbs, N., Burnaevskiy, N., Chen, D., Gonugunta, V.K., Alto, N.M., Yan, N. STING activation by translocation from the ER is associated with infection and autoinflammatory disease. *Cell Host Microbe* 18, 157–68, 2015.
50. Shang, G., Zhang, C., Chen, Z.J., Bai, X.C., Zhang, X. Cryo-EM structures of STING reveal its mechanism of activation by cyclic GMP-AMP. *Nature* 567, 389–93, 2019.
51. Ergun, S. L., Fernandez, D., Weiss, T. M. & Li, L. STING polymer structure reveals mechanisms for activation, hyperactivation, and inhibition. *Cell* 178, 290–301, 2019.
52. Mukai, K., Konno, H., Akiba, T., Uemura, T., Waguri, S., Kobayashi, T., Barber, G.N., Arai, H., Taguchi, T. Activation of STING requires palmitoylation at the Golgi. *Nat Commun.* 7, 11932, 2016.
53. Ablasser, A., Schmid-Burgk, J.L., Hemmerling, I., Horvath, G.L., Schmidt, T., Latz, E., Hornung, V. Cell intrinsic immunity spreads to bystander cells via the intercellular transfer of cGAMP. *Nature* 503, 530–4, 2013.

54. Ma, Z., Jacobs, S.R., West, J.A., Stopford, C., Zhang, Z., Davis, Z., Barber, G.N., Glaunsinger, B.A., Dittmer, D.P., Damania, B. Modulation of the cGAS-STING DNA sensing pathway by gammaherpesviruses. *Proc Natl Acad Sci*. 112, E4306–15, 2015.
55. Zhu, Y., An, X., Zhang, X., Qiao, Y., Zheng, T., Li, X. STING: a master regulator in the cancer-immunity cycle. *Mol Cancer.* 18, 152, 2019.
56. Zhang, Z. et al. The helicase DDX41 senses intracellular DNA mediated by the adaptor STING in dendritic cells. *Nat. Immunol.*12, 959–965, 2011.
57. Unterholzner, L. et al. IFI16 is an innate immune sensor for intracellular DNA. *Nat. Immunol.* 11, 997–1004, 2010.
58. Ferguson, B. J., Mansur, D. S., Peters, N. E., Ren, H. W. & Smith, G. L. DNA-PK is a DNA sensor for IRF-3-dependent innate immunity. *elife*1, e00047, 2012.
59. Wang, L., Wen, M. & Cao, X. Nuclear hnRNPA2B1 initiates and amplifies the innate immune response to DNA viruses. *Science* 365, eaav0758, 2019.
60. Orzalli, M. H., DeLuca, N. A. & Knipe, D. M. Nuclear IFI16 induction of IRF-3 signaling during herpesviral infection and degradation of IFI16 by the viral ICP0 protein. *Proc. Natl Acad. Sci.* 109, E3008–E3017, 2012.
61. Zhang, Y., Liang, C. Innate recognition of microbial-derived signals in immunity and inflammation. *Sci China Life Sci* 59, 1210-1217, 2016.
62. Yu, L., Feng, Z. The role of toll-like receptor signaling in the progression of heart failure. *Mediators Inflamm* 8, 9874109, 2018.
63. Wang, Y., Song, E., Bai, B., Vanhoutte, P.M. Toll-like receptors mediating vascular malfunction: lessons from receptor subtypes. *Pharm & Therap.* 158, 91-100, 2016.
64. Kawasaki, T., Kawai, T. Toll-like receptor signaling pathways. *Front Immunol.* 5, 461, 2014.
65. Gao, W., Xiong, Y., Li, Q., Yang, H. Inhibition of Toll-like receptor signaling as a promising therapy for inflammatory diseases: a journey from molecular to nano therapeutics. *Front physiol.* 8, 508-517, 2017.
66. Jin, M. S. and Lee, J.O. Structures of the Toll-like receptor family and its ligand complexes. *Immunity* 29, 182–191, 2008.
67. Choe, J., Kelker, M. S. and Wilson, I. A. Structural biology: crystal structure of human toll-like receptor 3 (TLR3) ectodomain. *Science* 309, 5734, 581–585, 2005.
68. Kim, H. M., Park, B. S., Kim, J.I. et al. Crystal structure of the TLR4-MD-2 complex with bound endotoxin antagonist Eritoran. *Cell* 130, 906–917, 2007.

69. Jin, M. S., Kim, S. E., Heo, J. Y. et al. Crystal structure of the TLR1-TLR2 heterodimer induced by binding of a tri-acylated lipopeptide. *Cell* 130, 1071–1082, 2007.
70. Kang, J. Y., Nan, X., Jin, M. S. et al. Recognition of lipopeptide patterns by Toll-like receptor 2-Toll-like receptor 6 heterodimer. *Immunity* 31, 873–848, 2009.
71. Akira, S., & Takeda, K. Toll-like receptor signaling. *Nat Rev Immunol* 4, 499-511, 2004.
72. Bernard, N. J., O'Neill, L.A. Mal, more than a bridge to MyD88. IUBMB Life 65, 777-786, 2013.
73. Bryant, C.E., Symmons, M., Gay, N. J. Toll-like receptor signaling through macromolecular protein complexes. *Mol Immunol* 63, 162-165, 2015.
74. McGettrick, A.F., Brint, E. K., Palsson-McDermott, E.M., *et al*. TRIF-related adaptor molecule is phosphorylated by PKCε during Toll-like receptor 4 signaling. Proc Natl Acad Sci 103, 9196-9201, 2006.
75. Kollewe, C., Mackensen, A.C., Neumann, D., Knop, J., Cao, P., Li, S., et al. Sequential autophosphorylation steps in the interleukin-1 receptor-associated kinase-1 regulate its availability as an adapter in interleukin-1 signaling. *J Biol Chem* 279, 5227–36, 2004.
76. Jiang, Z., Ninomiya-Tsuji, J., Qian, Y., Matsumoto, K., Li, X. Interleukin-1 (IL-1) receptor-associated kinase-dependent IL-1-induced signaling complexes phosphorylate TAK1 and TAB2 at the plasma membrane and activate TAK1 in the cytosol. *Mol Cell Biol* 22, 7158–67, 2002.
77. Chen, Z.J. (2005) Ubiquitin signalling in the NF-kappaB pathway. *Nat. Cell Biol.* 7, 758–765, 2005.
78. Kumar, H., Kawai, T., Akira, S. Pathogen recognition bythe innate immune system. *Int Rev Immunol* 30, 16-34, 2011.
79. Kawai, T., Akira, S. The role of pattern-recognition receptors in innate immunity: update on toll-like receptors. *Nat Immunol* 11, 373–84, 2010.
80. Sato, S., Sugiyama, M., Yamamoto, M., Watanabe, Y., Kawai, T., Takeda, K., & Akira, S. Toll/IL-1 receptor domain-containing adaptor inducing IFN-*β*(TRIF) associates with TNF receptor-associated factor 6 and TANK-binding kinase 1, and activates two distinct transcription factors, NF-*κ*B and IFN-regulatory factor-3, in the Toll-like receptor signaling. *Journal of Immunology*171, 4304–4310, 2003.
81. Li, Z., Yuan, W., Lin, Z. Functional roles in cell signaling of adaptor protein TRADD from a structural perspective. *Comput Struct Biotechnol J*. 18, 2867-2876, 2020.
82. H. Hacker, H., Redecke, V., Blagoev, B., Kratchmarova, I., Hsu, L.C, Wang, G.G., Kamps, M.P., Raz, E, Wagner, H., Hacker, G.,*et al.* Specificity in Toll-like receptor

signalling through distinct effector functions of TRAF3 and TRAF6. *Nature*, 439, 204-207, 2006.

83. Oganesyan, G., Saha, B., Guo, S.K., He, J.Q., Shahangian, A., Zarnegar, B., Perry, G., Cheng, A. Critical role of TRAF3 in the Toll-like receptor-dependent and -independent antiviral response. *Nature* 439, 208-211, 2006.
84. Tenoever, B.R., Ng, S.L., Chua, M.A., McWhirter, S.M., Garcia-Sastre, A., Maniatis, T. Multiple functions of the IKK-related kinase IKKepsilon in interferon-mediated antiviral immunity. *Science* 315, 1274-1278, 2007.
85. Emsley, J. Nature's Building Blocks. *Oxford: Oxford University Press* 506-510, 2001.
86. Teal, G. K. Single Crystals of Germanium and Silicon-Basic to the Transistor and Integrated Circuit. *IEEE Transactions on Electron Devices*. *ED-23* 7, 621–639, 1976.
87. Rieke, G.H. Infrared Detector Arrays for Astronomy. *Annual Review of Astronomy and Astrophysics* 45, 77-115, 2007.
88. Wada, T., Hanyu, T., Nozaki, K., Kataoka, K., Kawatani, T., Asahi, T., and Sawamura N. Antioxidant Activity of Ge-132, a Synthetic Organic Germanium, on Cultured Mammalian Cells. *Biol. Pharm. Bull.* 41, 749–753, 2018.
89. Tao, S.H., Bolger, P.M. Hazard assessment of germanium supplements. *Regul. Toxicol. Pharm.* 25, 211–219, 1997.
90. Kolesnikov, S. P. and Nefedov, O. M. *Zh. Obshch. Khim.* 37, 746, 1967.
91. Menchikov, L.G and Ignateko, M.A. Biological Activity of Organogermanium Compounds (A Review). *Pharmaceutical Chemistry Journal* 46, 2013.
92. Tsutsui, M., Kakimoto, N., Axtell, D., Oikawa, H., Asai, K. ChemInform Abstract: Crystal structure of ′carboxyethylgermanium sesquioxide. *Chemischer Informationsdienst* 1977.
93. Tsutsui, M., Kakimoto, N., Axtell, D.D., Oikawa, H., Asai, K. Crystal structure of "carboxyethylgermanium sesquioxide". *J. Am. Chem. Soc. 98*, 8287–8289, 1976.
94. Shimada, Y., Sato, K., Tokuji, Y., Nakamura, T. Nuclear magnetic resonance studies of the interactions between the organic germa- nium compound Ge-132 and saccharides. *Carbohydr Res* 407,10– 15, 2015.
95. Nagasawa, T., Sato, K., Shimada, Y., Kasumi, T. Efficient con- version of D-glucose to D-fructose in the presence of organogermanium compounds. *J Appl Glycosci* 63, 39–45, 2016.

96. Shimada, Y., Sato, K., Takeda, T., Tokuji Y. The Organogermanium Compound Ge-132 Interacts with Nucleic Acid Components and Inhibits the Catalysis of Adenosine Substrate by Adenosine Deaminase. *Biol Trace Elem Res.* 181, 164-17, 2018.

97. Nakamura, T., Shimada, Y., Takeda, T., Sato, K., Akiba, M., Fukaya, H. Organogermanium compound, Ge-132, forms complexes with adrenaline, ATP and other physiological cis-diol compounds. *Future Med Chem* 7, 1233–1246, 2015.

98. Azumi, J., Takeda, T., Shimada, Y., Aso, H., Nakamura, T. The Organogermanium Compound THGP Suppresses Melanin Synthesis via Complex Formation with L-DOPA on Mushroom Tyrosinase and in B16 4A5 Melanoma Cell. *Int J Mol Sci.* 20, 4785-4798, 2019.

99. Miyao, K. Toxicology and phase I studies on a novel organogermanium compound, Ge-132. *Curr. Chemother. Infec. Dis.* 2, 1527–1529, 1979.

100. Sugiya, Y., Sakamaki, S., Sugita, T., Abo, Y., Sato, H. Subacute oral toxicity of carboxyethylgermanium sesquioxide (Ge-132) in rats. *Ouyou Yakuri.* 31, 1181–1190, 1986.

101. Iwadate, K., Yamaguchi, Y., Sasaki, M., Nakatani, M., Doi, Y., Imai, N., Tamano, S., Nishihori, Y. Carcinogenicity study of poly-trans-[(2-carboxyethyl) germasesquioxane] (Ge-132) in F344 rats. *Fundam. Toxicol. Sci.* 5, 127–140, 2018.

102. Doi, Y., Imai, N., Suguro, M., Numano, T., Furukawa, F. No carcinogenicity of poly-trans-[(2-carboxyethyl) germasesquioxane] (Ge-132): 26-week feeding study using rasH2 mice. *Fundam. Toxicol. Sci.* 4, 137–150, 2017.

103. Ikemoto, K., Kobayashi, M. Fukumoto, T. *et al*. 2-Carboxyethylgermanium sesquioxide, a syntrhetic organogermanium compound, as an inducer of contra-suppressor T cells. *Experientia* 52, 159-166, 1996.

104. Kuwabara, M., Ohba, S., Yukawa, M. Effect of germanium, poly- *trans*-[2-carboxyethyl] germasesquioxane on natural killer (NK) activity in dogs. *J. Vet. Med. Sci.*, 64, 719–721, 2002.

105. Kobayashi, H., Aso, H., Ishida, N., Maeda, H., Schmitt, D.A., Pollard, R.B., Suzuki, F. Preventive effect of a synthetic immunomodulator, 2-car- boxyethylgermanium sesquioxide, on the generation of suppressor macrophages in mice immunized with allogeneic lymphocytes. *Immunopharmacol. Immunotoxicol.* 14, 841–864, 1992.

106. Aso, H., Suzuki, F., Ebina, T., Ishida, N. Antiviral activity of carboxy- ethylgermanium sesquioxide (Ge-132) in mice infected with influ- enza virus. *J. Biol. Response Mod.* 8, 180–189, 1989.

107. Sijpesteijn, A.K., Rijkens, F., Van Der Kerk, G.J., Manten, A. Antimicrobial activity of organogermanium derivatives. *Nature* 201, 736, 1964.

108. Hachisu, M., Takahashi, H., Koeda, T., Sekizawa, Y. Analgesic effect of novel organogermanium compound, GE-132. *J. Pharmacobiodyn.* 6, 814–820, 1983.

109. Kumano, N., Ishikawa, T., Koinumaru, S., Kikumoto, T., Suzuki, S., Nakai, Y., Konno, K. Antitumor effect of the organogermanium com- pound Ge-132 on the Lewis lung carcinoma (3LL) in C57BL/6 (B6) mice. *Tohoku J. Exp. Med.*, 146, 97–104, 1985.

110. Mainwaring, M.G., Poor, C., Zander, D.S., Harman, E. Complete remis- sion of pulmonary spindle cell carcinoma after treatment with oral germanium sesquioxide. *Chest*, 117, 591–593, 2000.

111. Nakamura, T., Saito, M., Aso, H. Effects of a lactobacilli, oligosaccharide, and organic germanium intake on the immune responses of mice. *Biosci. Biotechnol. Biochem.* 76, 375–377, 2012.

112. Nakamura, T., Takeda, T., Tokuji, Y. The Oral Intake of Organic Germanium, Ge-132, Elevates α-Tocopherol Levels in the Plas-ma and Modulates Hepatic Gene Expression Profiles to Promote Immune Activation in Mice. *Int. J. Vitam. Nutr. Res.* 84,183–195, 2014.

113. Aso, H., Shibuya, E., Suzuki, F., Nakamura, T., Inoue, H., Ebina, T., Ishida, N. Antitumor effect in mice of an organic germanium compound (Ge-132) when different administration methods are used. *Gan Kagaku Ryoho. Cancer Chemother.* 12, 2345–2351, 1985.

114. Suzuki, F., Brutkiewicz, R.R., Pollard, R.B. Ability of sera from mice treated with Ge-132, an organic germanium compound, to inhibit experimental murine ascites tumours. *Br. J. Cancer.* 52, 757, 1985.

115. Shiwata, Y., Yokochi, S., Suzuki, E., Michishita, H., Tashita, A., Asano, K., Mitani, T., Kurono, M. Effects of proxigermanium on interferon production and 2',5'-oligoadenylate synthetase activity in the lung of influenza virus-infected mice and in virus-infected human peripheral blood mononuclear cell cultures. *Arzneimittelforschung* 40, 896-9, 1990.

116. Hirayama, C., Suzuki, H., Ito, M., Okumura, M., Oda, T. Propagermanium: a nonspecific immune modulator for chronic hepatitis B. *J Gastroenterol* 38, 525-32, 2003.

117. Ishiwata, Y., Suzuki, E., Yokochi, S., Otsuka, T., Tasaka, F., Usuda, H., Mitani, T. Studies on the antiviral activity of propagermanium with immunostimulating action. *Arzneimittelforschung*. 44, 357-61, 1994. PMID: 8192703.

118. Bernard, J.J., Cowing-Zitron, C., Nakatsuji, T., Muehleisen, B., Muto, J., Borkowski, A.W., et al. Ultraviolet radiation damages self-noncoding RNA and is detected by TLR3. *Nat Med* 18,1286–90, 2012.

119. Takemura, N., Kawasaki, T., Kunisawa, J., Sato, S., Lamichhane, A., Kobiyama, K., et al. Blockade of TLR3 protects mice from lethal radiation-induced gastrointestinal syndrome. *Nat Commun* 5, 3492, 2014.

120. Akira, S., Uematsu, S., Takeuchi, O. Pathogen recognition and innate immunity. *Cell* 124, 783–801, 2006.

121. Guiducci, C., Gong, M., Cepika, A.M., Xu, Z., Tripodo, C., Bennett, L., et al. RNA recognition by human TLR8 can lead to autoimmune inflammation. *J Exp Med* 210, 2903–19, 2013.

122. Andrade, W.A., Souza Mdo, C., Ramos-Martinez, E., Nagpal, K., Dutra, M.S., Melo, M.B., et al. Combined action of nucleic acid-sensing toll-like receptors and TLR11/TLR12 heterodimers imparts resistance to *Toxoplasma gondii* in mice. *Cell Host Microbe* 13, 42–53, 2013.

123. Li, X.D., Chen, Z.J. Sequence specific detection of bacterial 23S ribosomal RNA by TLR13. *eLife* 1, e00102, 2012.

124. Oldenburg, M., Kruger, A., Ferstl, R., Kaufmann, A., Nees, G., Sigmund, A., et al. TLR13 recognizes bacterial 23S rRNA devoid of erythromycin resistance-forming modification. *Science* 337,1111–5, 2012.

125. Schlee, M. Master sensors of pathogenic RNA-RIG-I like receptors. *Immunobiology* 218, 1322-1335, 2013.

126. Furr, S.R., Chauhan, V.S., Moerdyk-Schauwecker, M.J., and Marriott, I. A role for DNA-dependent activator of interferon regulatory factor in the recognition of herpes simplex virus type 1 by glial cells. *J Neuroinflammation* 8, 99, 2011.

127. DeFilippis, V.R., Alvarado, D., Sali, T., Rothenburg, S., and Fruh, K. Human cytomegalovirus induces the interferon response via the DNA sensor ZBP1. *J Virol* 84, 585-598, 2010.

128. Takaoka, A., Wang, Z., Choi, M.K., Yanai, H., Negishi, H., Ban, T., Lu, Y., Miyagishi, M., Kodama, T., Honda, K., Ohba, Y., and Taniguchi, T. DAI (DLM-1/ZBP1) is a cytosolic DNA sensor and an activator of innate immune response. *Nature* 448, 501-505, 2007.

129. Wang, Z., Choi, M.K., Ban, T., Yanai, H., Negishi, H., Lu, Y., Tamura, T., Takaoka, A., Nishikura, K., and Taniguchi, T. Regulation of innate immune responses by DAI

(DLM-1/ZBP1) and other DNA-sensing molecules. *Proc Natl Acad Sci* 105, 5477-5482 2008.

130. Rebsamen, M., Heinz, L.X., Meylan, E., Michallet, M.C., Schroder, K., Hofmann, K., Vazquez, J., Benedict, C.A., and Tschopp, J. DAI/ZBP1 recruits RIP1 and RIP3 through RIP homotypic interaction motifs to activate NF-kappaB. *EMBO Rep* 10, 916-922, 2009.

131. Sun, L., Wu, J., Du, F., Chen, X., and Chen, Z.J. Cyclic GMP-AMP synthase is a cytosolic DNA sensor that activates the type I interferon pathway. *Science* 339, 786-791, 2013.

132. Burdette, D.L., Monroe, K.M., Sotelo-Troha, K., Iwig, J.S., Eckert, B., Hyodo, M., Hayakawa, Y., and Vance, R.E. STING is a direct innate immune sensor of cyclic di-GMP. *Nature* 478, 515-518, 2011.

133. Zhang, X., Shi, H., Wu, J., Zhang, X., Sun, L., Chen, C., and Chen, Z.J. Cyclic GMP-AMP containing mixed phosphdiester linkages is an endogenous high-affinity ligand for STING. *Mol Cell* 51, 226-235, 2013.

134. Leonard, D., Eloranta, M.L., Hagberg, N., et al. Activated T cells enhance interferon-α production by plasmacytoid dendritic cells stimulated with RNA-containing immune complexes. *Ann Rheum Dis* 75, 1728–34, 2016.

135. Crouse, J., Kalinke, U., Oxenius, A. Regulation of antiviral T cell responses by type I interferons. *Nat Rev Immunol* 15, 231–42, 2015.

136. Kiefer, K., Oropallo, M.A., Cancro, M.P., et al. Role of type I interferons in the activation of autoreactive B cells. *Immunol Cell Biol* 90, 498–504, 2012.

137. Fabre, A., Bourgeois, P., Coste, M.E., Roman, C., Barlogis, V., Badens, C. Management of syndromic diarrhea/tricho-hepato-enteric syndrome: A review of the literature. *Intractable Rare Dis Res*. 6, 152-157, 2017.

138. Fabre, A., Martinez-Vinson, C., Goulet, O., Badens, C. Syndromic diarrhea/Tricho-hepato-enteric syndrome. *Orphanet J Rare Dis.* 8, 5, 2013.

139. Stankler, L., Lloyd, D., Pollitt, R.J., Gray, E.S., Thom, H.A., Russell, G.E. Unexplained diarrhea and failure to thrive in 2 siblings with unusual facies and abnormal scalp hair shafts: A new syndrome. *Arch. Dis. Child.* 57, 212–216, 1982.

140. Goulet, O., Vinson, C., Roquelaure, B., Brousse, N., Bodemer, C., Cézard, J. Syndromic (phenotypic) diarrhea in early infancy. *Orphanet J. Rare Dis.* 3, 6, 2008.

141. Fabre, A., Charroux, B., Martinez-Vinson, C., Roquelaure, B., Odul, E., Sayar, E., Smith, H., Colomb, V., Andre, N., Hugot, J.P., et al. SKIV2L Mutations Cause Syndromic Diarrhea, or Trichohepatoenteric Syndrome. *Am. J. Hum. Genet*. 90, 689–692, 2012.

142. Eckard, S.C., Rice, G.I., Fabre, A., Badens, C., Gray, E.E., Hartley, J.L., Crow, Y.J., Stetson, D.B. The SKIV2L RNA exosome limits activation of the RIG-I-like receptors. *Nat Immunol.* 15, 839-845, 2014.

143. Reid, A. H., & Tautenberger, J. K. The origin of the 1918 pandemic influenza virus: A continuing enigma. *Journal of General Virology* 84, 2285–2292, 2003.

144. te Velthuis, A.J., Fodor, E. Influenza virus RNA polymerase: Insights into the mechanisms of viral RNA synthesis. *Nature Reviews Microbiology* 14, 479-493, 2016.

145. Palese, P., Shaw, M.L. Orthomyxoviridae: The Viruses and their Replication. In. *Fields Virology* Philadelphia: Lippincott Williams & Wilkins, 2007.

146. Lamb, R.A., Lai, C.J., Choppin, P.W. Sequences of mRNAs derived from genome RNA segment 7 of influenza virus: colinear and interrupted mRNAs code for overlapping proteins. *Proc Natl Acad Sci.* 78, 4170-4, 1981.

147. Kochs, G., García-Sastre, A., Martínez-Sobrido, L. Multiple anti-interferon actions of the influenza A virus NS1 protein. *J Virol*. 81, 7011-21, 2007.

148. Briedis, D.J., Lamb, R.A. Influenza B virus genome: sequences and structural organization of RNA segment 8 and the mRNAs coding for the NS1 and NS2 proteins. *J Virol.* 42, 186-93, 1982.

149. Wandzik, J.M., Kouba, T., Karuppasamy, M., Pflug, A., Drncova, P., Provaznik, J., Azevedo, N., Cusack, S. A structure-based model for the complete transcription cycle of influenza polymerase. *Cell 181*, 877–893.e21, 2020.

150. Pflug, A., Guilligay, D., Reich, S., Cusack, S. Structure of influenza A polymerase bound to the viral RNA promoter. *Nature 516*, 355–360, 2014.

151. Gultyaev, A.P., Fouchier, R.A.M., Olsthoorn, R.C.L. Influenza virus RNA structure: Unique and common features. *Int. Rev. Immunol. 29*, 533–556, 2010.

152. Zhang, X., Green, T.J., Tsao, J., Qiu, S., Luo, M. Role of intermolecular interactions of vesicular stomatitis virus nucleoprotein in RNA encapsidation. *J Virol* 82, 674–682, 2008.

153. Ball, L.A., White, C.N. Order of transcription of genes of vesicular stomatitis virus. *Proc. Natl. Acad. Sci. 73*, 442–446, 1976.

154. Pattnaik, A.K., et al. Phosphorylation within the amino-terminal acidic domain I of the phosphoprotein of vesicular stomatitis virus is required for transcription but not for replication. *J Virol.* 71, 8167–8175, 1997.

155. Ogino, T., Banerjee, A.K. Unconventional mechanism of mRNA capping by the RNA-dependent RNA polymerase of vesicular stomatitis virus. *Mol. Cell 25*, 85–97, 2007.

156. Qanungo, K.R., Shaji, D., Mathur, M., Banerjee, A.K. Two RNA polymerase complexes from vesicular stomatitis virus-infected cells that carry out transcription and replication of genome RNA. *Proc. Natl. Acad. Sci.* 101, 5952–5957, 2004.

157. Carocci, M., Bakkali-Kassimi, L. The encephalomyocarditis virus. *Virulence* 3, 351-67, 2012.

158. Hruby, D.E., Roberts, W.K. Encephalomyocarditis virus RNA. III. Presence of a genome-associated protein. *J Virol.* 25, 413-5, 1978.

159. Palmenberg, A.C., Kirby, E.M., Janda, M.R., Drake, N.L., Duke, G.M., Potratz, K.F., et al. The nucleotide and deduced amino acid sequences of the encephalomyocarditis viral polyprotein coding region. *Nucleic Acids Res.* 12, 2969–85, 1984.

160. Wu, F., Zhao, S., Yu, B., Chen, Y.M., Wang, W., Song, Z.G., Hu, Y., Tao, Z.W., Tian, J.H., Pei, Y.Y., Yuan, M.L., Zhang, Y.L., Dai, F.H., Liu, Y., Wang, Q.M., Zheng, J.J., Xu, L., Holmes, E.C., Zhang, Y.Z. A new coronavirus associated with human respiratory disease in China. *Nature* 579, 265–269, 2020.

161. Naqvi, A., Fatima, K., Mohammad, T., Fatima, U., Singh, I. K., Singh, A., Atif, S. M., Hariprasad, G., Hasan, G. M., & Hassan, M. I. (2020). Insights into SARS-CoV-2 genome, structure, evolution, pathogenesis and therapies: Structural genomics approach. *Biochimica et biophysica acta. Molecular basis of disease 1866*, 165878, 2020.

162. Zhu, N., Zhang, D., Wang, W., Li, X., Yang, B., Song, J., Zhao, X., Huang, B., Shi, W., Lu, R., et al. A novel coronavirus from patients with pneumonia in China, 2019. *N Engl J Med.* 382, 727–33, 2020.

163. Wu, A., Peng, Y., Huang, B., Ding, X., Wang, X., Niu, P., Meng, J., Zhu, Z., Zhang, Z., Wang, J., et al. Genome composition and divergence of the novel coronavirus (2019-nCoV) originating in China. *Cell Host Microbe*. 27, 325–8, 2020.

164. Gordon, D.E., Jang, G.M., Bouhaddou, M. *et al.* A SARS-CoV-2 protein interaction map reveals targets for drug repurposing. *Nature* 583, 459–468, 2020.

165. Kim, D., Lee, J.Y., Yang, J.S., Kim, J.W., Kim, V.N., Chang, H. The Architecture of SARS-CoV-2 Transcriptome. *Cell* 181, 914-921.e10, 2020.

166. Walls, A.C., Park, Y.J., Tortorici, M.A., Wall, A., McGuire, A.T., Veesler, D. Structure, function, and antigenicity of the SARS-CoV-2 spike glycoprotein. *Cell* 180, 1-12, 2020.

167. Maio, D. F., Cascio, L. E., Babini, G., Sali, M., Della, L. S., Tilocca, B., Roncada, P., Arcovito, A., Sanguinetti, M., Scambia, G., Urbani, A. Improved binding of SARS-CoV-2 envelope protein to tight junction-associated PALS1 could play a key role in COVID-19 pathogenesis. *Microbes Infect* 2020.

168. Lucchese, G. Epitopes for a 2019-nCoV vaccine. *Cell Mol Immunol.* 17, 539–40, 2020.

169. McBride, R., Van, Z. M., Fielding, B.C. The coronavirus nucleocapsid is a multifunctional protein. *Viruses* 6, 2991–3018, 2014.

170. Uchida, L., Espada-Murao, L.A., Takamatsu, Y., Okamoto, K., Hayasaka, D., Yu, F., Nabeshima, T., Buerano, C.C., Morita, K. The dengue virus conceals double-stranded RNA in the intracellular membrane to escape from an interferon response. *Sci Rep.* 4, 7395, 2014.

171. Neufeldt, C.J., Joyce, M.A., Van Buuren, N., Levin, A., Kirkegaard, K., Gale, M., Jr., Tyrrell, D.L., Wozniak, R.W. The hepatitis C virus-induced membranous web and associated nuclear transport machinery limit access of pattern recognition receptors to viral replication sites. *PLoS Pathog.* 12, e1005428, 2016.

172. Decroly, E., Debarnot, C., Ferron, F. *et al.* Crystal structure and functional analysis of the SARS-Coronavirus RNA cap 2′-O-methyltransferase nsp10/nsp16 complex. *PLOS Pathog*. 7, e 1002059, 2011.

173. Deng, X., Hackbart, M., Mettelman, R.C. *et al.* Coronavirus nonstructural protein 15 mediates evasion of dsRNA sensors and limits apoptosis in macrophages. *Proc Natl Acad Sci* USA, 114, 4251-60, 2017.

174. Shih, S.R., Krug, R.M. Surprising function of the three influenza viral polymerase proteins: selective protection of viral mRNAs against the cap-snatching reaction catalyzed by the same polymerase proteins. *Virology* 226, 430-435, 1996.

175. Pathak, H.B., Arnold, J.J., Wiegand, P.N., Hargittai, M.R., and Cameron, C.E. Picornavirus genome replication: assembly and organization of the VPg uridylylation ribonucleoprotein (initiation) complex. *J Biol Chem* 282, 16202-16213, 2007.

176. Habjan, M., Andersson, I., Klingström, J., Schümann, M., Martin, A., Zimmermann, P., Wagner, V., Pichlmair, A., Schneider, U., Mühlberger, E., Mirazimi, A., and Weber, F. Processing of genome 5’ termini as a strategy of negative-strand RNA viruses to avoid RIG-I-dependent interferon induction. *PLoS One* 3, e2032, 2008.

177. Y an, N., Regalado-Magdos, A.D., Stiggelbout, B., Lee-Kirsch, M.A., and Lieberman, J. The cytosolic exonuclease TREX1 inhibits the innate immune response to human immunodeficiency virus type 1. *Nat Immunol* 11, 1005-1013, 2010.

178. Hastie, K.M., Kimberlin, C.R., Zandonatti, M.A., MacRae, I.J., and Saphire, E.O. Structure of the Lassa virus nucleoprotein reveals a dsRNA-specific 3′ to 5′ exonuclease activity essential for immune suppression. *Proc Natl Acad Sci U S A* 108, 2396-2401, 2011.

179. Feng, Q., Langereis ,M.A., Lork, M., Nguyen ,M., Hato, S.V., Lanke, K., Emdad, L., Bhoopathi, P., Fisher ,P.B., Lloyd, R.E. Enterovirus 2Apro targets MDA5 and MAVS in infected cells. *J Virol.* 88, 3369–3378, 2014.

180. Meylan, E., Curran, J., Hofmann, K., Moradpour, D., Binder, M., Bartenschlager, R., Tschopp, J. Cardif is an adaptor protein in the RIG-I antiviral pathway and is targeted by hepatitis C virus. *Nature.*437,1167–1172, 2005.

181. Li, K., Foy, E., Ferreon, J.C., Nakamura, M., Ferreon, A.C., Ikeda, M., Ray, S.C., Gale, M., Jr., Lemon, S.M. Immune evasion by hepatitis C virus NS3/4A protease-mediated cleavage of the Toll-like receptor 3 adaptor protein TRIF. *Proc Natl Acad Sci U S A.* 102,2992–2997,2005.

182. Pan, S., Liu, X., Ma, Y., Cao, Y. & He, B. Herpes simplex virus 1 gamma134.5 protein inhibits STING activation that restricts viral replication. *J. Virol.* 92, 2018.

183. Thomsen, M.K., Nandakumar, R., Stadler, D. *et al.* Lack of immunological DNA sensing in hepatocytes facilitates hepatitis B virus infection. Hepatology, 64, 746-459, 2016.

184. Zheng, Y., Liu, Q., Wu, Y., *et al. Z*ika virus elicits inflammation to evade antiviral response by cleaving cGAS via NS1-caspase-1 axis. *EMBO.J,* 37 e99347, 2018.

185. Biolatti, M., Oste, D., Pautasso, S., Gugliesi, F., Von Einem, J., Krapp, C., Jakobsen, M.R., Borgogna, C., Gariglio, M., Andrea De, M., *et al.* Human cytomegalovirus tegument protein pp65 (pUL83) Dampens type I interferon production by inactivating the DNA sensor cGAS without affecting STING. *J Virol,* 92, 1-18, 2018.

186. Gack, M.U., Albrecht, R.A., Urano, T., Inn, K.S., Huang, I.C., Carnero, E., Farzan, M., Inoue, S., Jung, J.U., Garcia-Sastre, A. Influenza A virus NS1 targets the ubiquitin ligase TRIM25 to evade recognition by the host viral RNA sensor RIG-I. *Cell Host Microbe.* 5, 439–449, 2009.

187. Yu, C.Y., Liang, J.J., Li, J.K., Lee, Y.L., Chang, B.L., Su, C.I., Huang, W.J., Lai, M.M., Lin, Y.L. Dengue virus impairs mitochondrial fusion by cleaving mitofusins. *PLoS Pathog.* 11, e1005350, 2015.

188. Prins, K.C., Cardenas, W.B., Basler, C.F. Ebola virus protein VP35 impairs the function of interferon regulatory factor-activating kinases IKKepsilon and TBK-1. *J Virol.* 83,3069–3077, 2009.

189. Xiang, Z., Liu, L., Lei, X., Zhou, Z., He, B., Wang, J. 3C protease of enterovirus D68 inhibits cellular defense mediated by interferon regulatory factor 7. *J Virol.* 90,1613–1621, 2015.

190. Stone, A.E., Mitchell, A., Brownell, J., Miklin, D.J., Golden-Mason, L., Polyak S.J., Gale M.J., Jr., Rosen H.R. Hepatitis C virus core protein inhibits interferon production by a human plasmacytoid dendritic cell line and dysregulates interferon regulatory factor-7 and signal transducer and activator of transcription (STAT) 1 protein expression. *PLoS One.* 9, e95627, 2014.

191. Gambaryan, A.S., Tuzikov, A.B., Piskarev, V.E., Yamnikova, S.S., Lvov, D.K., Robertson, J.S., Bovin, N.V., Matrosovich, M.N. Specification of receptor-binding phenotypes of influenza virus isolates from different hosts using synthetic sialylglycopolymers: non-egg-adapted human H1 and H3 influenza A and influenza B viruses share a common high binding affinity for 6′-sialyl(N-acetyllactosamine). *Virology* 232, 345-350, 1997.

192. Ito, T., Kawaoka, Y. Host-range barrier of influenza A viruses. *Vet Microbiol.* 74, 71-75, 2000.

193. Matrosovich, M., Tuzikov, A., Bovin, N., Gambaryan, A., Klimov, A., Castrucci, M.R., Donatelli, I., Kawaoka, Y. Early alterations of the receptor-binding properties of H1, H2, and H3 avian influenza virus hemagglutinins after their introduction into mammals. *J Virol.* 74, 8502-8512, 2000.

194. Connor, R.J., Kawaoka, Y., Webster, R.G., Paulson, J.C. Receptor specificity in human, avian, and equine H2 and H3 influenza virus isolates. *Virology* 205, 17-23, 1994.

195. Skehel, J.J., Wiley, D.C. Receptor binding and membrane fusion in virus entry: the influenza hemagglutinin. *Annu Rev Biochem.* 69, 531-569, 2000.

196. Martin K, Helenius A: Transport of incoming influenza virus nucleocapsids into the nucleus. J Virol. 1991, 65 (1): 232-244.

197. Martin, K., Helenius, A. Nuclear transport of influenza virus ribonucleoproteins: the viral matrix protein (M1) promotes export and inhibits import. *Cell* 67, 117-130, 1991.

198. Whittaker, G., Bui, M., Helenius, A. Nuclear trafficking of influenza virus ribonuleoproteins in heterokaryons. *J Virol*. 70, 2743-2756, 1996.

199. Wang, P., Palese, P., O'Neill, R.E. The NPI-1/NPI-3 (karyopherin alpha) binding site on the influenza a virus nucleoprotein NP is a nonconventional nuclear localization signal. *J Virol*. 71, 1850-1856, 1997.

200. Neumann, G., Brownlee, G.G., Fodor, E., Kawaoka, Y. Orthomyxovirus replication, transcription, and polyadenylation. *Curr Top Microbiol Immunol.* 283, 121-143, 2004.

201. Li, M.L., Rao, P., Krug, R.M. The active sites of the influenza cap-dependent endonuclease are on different polymerase subunits. *EMBO J.* 20, 2078–2086, 2001.

202. Poon, L.L., Pritlove, D.C., Fodor, E., Brownlee, G.G. Direct evidence that the poly(A) tail of influenza A virus mRNA is synthesized by reiterative copying of a U track in the virion RNA template. *J Virol.* 73, 3473-3476, 1999.

203. Katze, M.G., DeCorato, D., Krug, R.M. Cellular mRNA translation is blocked at both initiation and elongation after infection by influenza virus or adenovirus. *J Virol.* 60, 1027-1039, 1986.

204. Wagner, R., Matrosovich, M., Klenk, H.D. Functional balance between haemagglutinin and neuraminidase in influenza virus infections. *Rev Med Virol*. 12, 59-166, 2002.

205. Leser, G.P., Lamb, R.A. Influenza virus assembly and budding in raft-derived microdomains: a quantitative analysis of the surface distribution of HA, NA and M2 proteins. *Virology* 342, 215-227, 2005.

206. Hutchinson, E.C., von Kirchbach, J.C., Gog, J.R., Digard, P. Genome packaging in influenza A virus. *J Gen Virol*. 91, 313-328, 2010.

207. Webster, R.G., Braciale, T.J., Monto, A.S., Lamb, R.A. Textbook of influenza. 2nd edition. ed. *Chichester, West Sussex, UK; Hoboken, NJ: Wiley-Blackwell* 502, 2013.

208. Zangrillo, A., Biondi-Zoccai, G., Landoni, G., Frati, G., Patroniti, N., Pesenti, A., et al. Extracorporeal membrane oxygenation (ECMO) in patients with H1N1 influenza infection: a systematic review and meta-analysis including 8 studies and 266 patients receiving ECMO. *Crit Care.* 17, R30, 2013.

209. Kadoglou, N.P.E., Bracke, F., Simmers, T., Tsiodras, S., Parissis, J. Influenza infection and heart failure-vaccination may change heart failure prognosis? *Heart Fail Rev.* 22, 329–36, 2017.

210. Kwong, J.C., Schwartz, K.L., Campitelli, M.A. Acute myocardial infarction after laboratory-confirmed influenza infection. *N Engl J Med*. 378, 2540–1, 2018.

211. Cardani, A., Boulton, A., Kim, T.S., Braciale, T.J. Alveolar macrophages prevent lethal influenza pneumonia by inhibiting infection of type-1 alveolar epithelial cells. *PLoS Pathog.* 13, e1006140, 2017.

212. Teijaro, J.R., Walsh, K.B., Cahalan, S., Fremgen, D.M., Roberts, E., Scott, F., et al. Endothelial cells are central orchestrators of cytokine amplification during influenza virus infection. *Cell* 146, 980–91, 2011.

213. Boyd, D.F., Thomas, P.G. Towards integrating extracellular matrix and immunological pathways. *Cytokine* 98, 79–86, 2017.

214. Florescu, D.F., Kalil, A.C. The complex link between influenza and severe sepsis. *Virulence* 5, 137–42, 2014.

215. Okuno, H., Yahata, Y., Tanaka-Taya, K., Arai, S., Satoh, H., Morino, S., et al. Characteristics and outcomes of Influenza-associated encephalopathy cases among children and adults in Japan, 2010-2015. *Clin Infect Dis.* 66, 1831–7, 2018.

216. Sellers, S.A., Hagan, R.S., Hayden, F.G., Fischer, W.A. The hidden burden of influenza: a review of the extra-pulmonary complications of influenza infection. *Influenza Other Respir Viruses* 11, 372–93, 2017.

217. Krammer, F., Smith, G.J.D., Fouchier, R.A.M. *et al.* Influenza. *Nat Rev Dis Primers* 4, 3, 2018.

218. Yan, N., Chen, Z.J. Intrinsic antiviral immunity. *Nature Immunol*. 13, 214-222, 2012.

219. Le Goffic, R., Balloy, V., Lagranderie, M., Alexopoulou, L., Escriou, N., Flavell, R., Chignard, M., Si-Tahar, M. Detrimental contribution of the Toll-like receptor (TLR)3 to influenza A virus-induced acute pneumonia. *PLoS Pathog*. 2, e53, 2006.

220. Guillot, L., Le Goffic, R., Bloch, S., Escriou, N., Akira, S., Chignard, M, Si-Tahar, M. Involvement of toll-like receptor 3 in the immune response of lung epithelial cells to double-stranded RNA and influenza A virus. *J Biol Chem.* 280, 5571-5580, 2005.

221. Diebold, S.S., Kaisho, T., Hemmi, H., Akira, S., Reis e Sousa, C. Innate antiviral responses by means of TLR7-mediated recognition of single-stranded RNA. *Science* 303, 1529-1531, 2004.

222. Lund, J.M., Alexopoulou, L., Sato, A., Karow, M., Adams, N.C., Gale, N.W., Iwasaki, A., Flavell, R.A. Recognition of single-stranded RNA viruses by Toll-like receptor 7. *Proc Natl Acad Sci USA* 101, 5598-5603, 2004.

223. Kato, H., Takeuchi, O., Sato, S., Yoneyama, M., Yamamoto, M., Matsui, K., Uematsu, S., Jung, A., Kawai, T., Ishii, K.J. Differential roles of MDA5 and RIG-I helicases in the recognition of RNA viruses. *Nature* 441, 101-105, 2006.

224. Opitz, B., Rejaibi, A., Dauber, B., Eckhard, J., Vinzing, M., Schmeck, B., Hippenstiel, S., Suttorp, N., Wolff, T. IFNbeta induction by influenza A virus is mediated by RIG-I which is regulated by the viral NS1 protein. *Cell Microbiol.* 9, 930-938, 2007.

225. Le Goffic, R., Pothlichet, J., Vitour, D., Fujita, T., Meurs, E., Chignard, M., Si-Tahar, M. Cutting Edge: Influenza A virus activates TLR3-dependent inflammatory and RIG-I-dependent antiviral responses in human lung epithelial cells. *J Immunol.* 178, 3368-3372, 2007.

226. Ichinohe, T., Pang, I.K., Iwasaki, A. Influenza virus activates inflammasomes via its intracellular M2 ion channel. *Nature Immunol.* 11, 404-410, 2010.

227. Thomas, P.G., Dash, P., Aldridge, J.R., Ellebedy, A.H., Reynolds, C., Funk, A.J., Martin, W.J., Lamkanfi, M., Webby, R.J., Boyd, K.L. The intracellular sensor NLRP3 mediates key innate and healing responses to influenza A virus via the regulation of caspase 1. *Immunity* 30, 566-575, 2009.

228. Ichinohe, T., Lee, H.K., Ogura, Y., Flavell, R., Iwasaki, A. Inflammasome recognition of influenza virus is essential for adaptive immune responses. *J Exp Med.* 206, 79-87, 2009.

229. Allen, I.C., Scull, M.A., Moore, C.B., Holl, E.K., McElvania-TeKippe, E., Taxman, D.J., Guthrie, E.H., Pickles, R.J., Ting, J.P. The NLRP3 inflammasome mediates in vivo innate immunity to influenza A virus through recognition of viral RNA. *Immunity* 30, 556-565, 2009.

230. Li, S., Min, J. Y., Krug, R. M. & Sen, G. C. Binding of the influenza A virus NS1 protein to PKR mediates the inhibition of its activation by either PACT or double-stranded RNA. *Virology* 349, 13–2, 2006.

231. Min, J. Y. & Krug, R. M. The primary function of RNA binding by the influenza A virus NS1 protein in infected cells: Inhibiting the 2′-5′ oligo (A) synthetase/RNase L pathway. *Proc. Natl Acad. Sci. USA* 103, 7100–7105, 2006.

232. Zhao, C., Hsiang, T.Y., Kuo, R.L., Krug, R.M. ISG15 conjugation system targets the viral NS1 protein in influenza A virus-infected cells. *Proc Natl Acad Sci USA.* 107, 2253-2258, 2010.

233. Conenello, G. M. & Palese, P. Influenza A virus PB1-F2: a small protein with a big punch. *Cell Host Microbe* 2, 207–209, 2007.

234. Varga, Z.T., Ramos, I., Hai, R., Schmolke, M., Garcia-Sastre, A., Fernandez-Sesma, A., Palese, P. The influenza virus protein PB1-F2 inhibits the induction of type I interferon at the level of the MAVS adaptor protein. *PLoS Pathog.* 7, e1002067, 2011.

235. Graef, K. M. et al. The PB2 subunit of the influenza virus RNA polymerase affects virulence by interacting with the mitochondrial antiviral signaling protein and inhibiting expression of beta interferon. *J. Virol.* 84, 8433–8445, 2010.

236. Sato, S., Li, K., Kameyama, T., Hayashi, T., Ishida, Y., Murakami, S., Watanabe, T., Iijima, S., Sakurai, Y., Watashi, K., Tsutsumi, S., Sato, Y., Akita, H., Wakita, T., Rice, C.M., Harashima, H., Kohara, M., Tanaka, Y., Takaoka, A. The RNA Sensor RIG-I Dually Functions as an Innate Sensor and Direct Antiviral Factor for Hepatitis B Virus. *Immunity* 42, 123–132, 2015.

237. Yamada, T., Horimoto, H., Kameyama, T., Hayakawa, S., Yamato, H., Dazai, M., Takada, A., Kida, H., Bott, D., Zhou, A.C., Hutin, D., Watts, T.H., Asaka, M., Matthews, J., Takaoka, A. (2016). Constitutive aryl hydrocarbon receptor signaling constrains type I interferon-mediated antiviral innate defense. *Nat Immunol.* 17, 687-694, 2016.

238. Suzuki, H., Kameyama, T., Takaoka, A. BinCARD2 as a positive regulator of interferon response in innate immunity. *Biochem Biophys Res Commun*. 511, 287-293, 2019.

239. Sato, S., Li, K., Sakurai, N., Hashizume, M.., Baidya, S., Nonaka, H., Noguchi, K., Ishikawa, K., Obuse, C., Takaoka, A. Regulation of an adaptor protein STING by Hsp90β to enhance innate immune responses against microbial infections. *Cell Immunol.* 356, 104188, 2020.

240. Kubota, T. et al. Virus infection triggers SUMOylation of IRF3 and IRF7, leading to the negative regulation of type I interferon gene expression. *J.Biol.Chem.* 283, 25660–25670, 2008.

241. Ozawa, M., Fujii, K., Muramoto, Y., Yamada, S., Yamayoshi, S., Takada, A., Goto, H., Horimoto, T., Kawaoka, Y. Contributions of two nuclear localization signals of influenza A virus nucleoprotein to viral replication. *J. Virol.* 81, 30–41, 2007.

242. Cong, L., Ran, F.A., Cox, D., Lin, S., Barretto, R., Habib, N., Hsu, P.D., Wu, X., Jiang, W., Marraffini, L.A., Zhang, F. Multiplex genome engineering using CRISPR/Cas systems. *Science* 339, 819-823, 2013.

243. Onomoto, K., Onoguchi, K. & Yoneyama, M. Regulation of RIG-I-like receptor-mediated signaling interaction between host and viral factors. *Cell Mol Immunol* 18**,** 539–555, 2021.

244. Rehwinkel, J., Gack, M.U. RIG-I-like receptors: their regulation and roles in RNA sensing. *Nat Rev Immunol* 20, 537–551, 2020.

245. Muramoto, Y., Noda, T., Kawakami, E., Akkina, R., & Kawaoka, Y. Identification of novel influenza A virus proteins translated from PA mRNA. *Journal of virology* 87, 2455–2462, 2013.

246. Lee, M. T., Bishop, K., Medcalf, L., Elton, D., Digard, P., & Tiley, L. Definition of the minimal viral components required for the initiation of unprimed RNA synthesis by influenza virus RNA polymerase. *Nucleic acids research* 30, 429–438, 2002.

247. Yoneyama, M., Kikuchi, M., Natsukawa, T., Shinobu, N., Imaizumi, T., Miyagishi, M., Taira, K., Akira, S., Fujita, T. The RNA helicase RIG-I has an essential function in double-stranded RNA-induced innate antiviral responses. *Nat Immunol*. 5, 730-737, 2004.

248. Yoneyama, M., Kikuchi, M., Matsumoto, K., Imaizumi, T., Miyagishi, M., Taira, K., Foy, E., Loo, Y.M., Gale, M. Jr, Akira, S., Yonehara, S., Kato, A., Fujita, T. Shared and unique functions of the DExD/H-box helicases RIG-I, MDA5, and LGP2 in antiviral innate immunity. *J Immunol.* 175, 2851-2858, 2005.

249. Romano, M., Ruggiero, A., Squeglia, F., Maga, G., & Berisio, R. A Structural View of SARS-CoV-2 RNA Replication Machinery: RNA Synthesis. *Cells* 9, 1267, 2020.

250. Matsuoka, Y., Matsumae, H., Katoh, M. *et al.* A comprehensive map of the influenza A virus replication cycle. *BMC Syst Biol* 7, 97, 2013.

251. Tisoncik, J. R., Korth, M. J., Simmons, C. P., Farrar, J., Martin, T. R., & Katze, M. G. Into the eye of the cytokine storm. *Microbiology and molecular biology reviews* 76, 16–32, 2012.

252. Weber, M., Gawanbacht, A., Habjan, M., Rang, A., Borner, C., Schmidt, A. M., Veitinger, S., Jacob, R., Devignot, S., Kochs, G., García-Sastre, A., & Weber, F. Incoming RNA virus nucleocapsids containing a 5'-triphosphorylated genome activate RIG-I and antiviral signaling. *Cell host & microbe*, 13, 336–346, 2013.

253. Verbruggen, P., Ruf, M., Blakqori, G., Overby, A.K., Heidemann, M., Eick, D., Weber, F. Interferon antagonist NSs of La Crosse virus triggers a DNA damage response-like degradation of transcribing RNA polymerase II. *J Biol Chem.* 286, 3681–3692, 2011.

254. Santhakumar, D., Rohaim, M., Hussein, H. A., Hawes, P., Ferreira, H. L., Behboudi, S., Iqbal, M., Nair, V., Arns, C. W., & Munir, M. Chicken Interferon-induced Protein with Tetratricopeptide Repeats 5 Antagonizes Replication of RNA Viruses. *Scientific reports*, 8, 6794, 2018.

255. Alison, M. K. and Michael, G. Jr. RIG-I in RNA virus recognition. *Virology*, 479, 110–121, 2015.

256. Kolakofsky, D. Isolation and characterization of Sendai virus DI-RNAs. *Cell,* 8:547–555, 1976.

257. Rehwinkel, J. et al. RIG-I Detects Viral Genomic RNA during Negative-Strand RNA Virus Infection. *Cell,* 140, 397–408, 2010.